# Technical Reference Material to:
# An urban ecohydrological model to quantify the effect of vegetation on urban climate and hydrology (UT&C v1.0)

Naika Meili[1,2], Gabriele Manoli[2,13], Paolo Burlando[2], Elie Bou-Zeid[3], Winston T.L. Chow[4], Andrew M. Coutts[5,6], Edoardo Daly[7], Kerry A. Nice[5,6,8], Matthias Roth[9], Nigel J. Tapper[5,6], Erik Velasco[10], Enrique R. Vivoni[11,12], and Simone Fatichi[2]

[1]ETH Zurich, Future Cities Laboratory, Singapore-ETH Centre, Singapore
[2]Institute of Environmental Engineering, ETH Zurich, Zurich, Switzerland
[3]Department of Civil and Environmental Engineering, Princeton University, NJ, USA
[4]School of Social Sciences, Singapore Management University, Singapore
[5]School of Earth, Atmosphere and Environment, Monash University, Clayton, Australia
[6]Cooperative Research Centre for Water Sensitive Cities, Melbourne, Australia
[7]Department of Civil Engineering, Monash University, Clayton, Australia
[8]Transport, Health, and Urban Design Hub, Faculty of Architecture, Building, and Planning, University of Melbourne, Victoria, Australia
[9]Department of Geography, National University of Singapore, Singapore
[10]Centre for Urban Greenery and Ecology, National Parks Board, Singapore
[11]School of Sustainable Engineering and the Built Environment, Arizona State University, Tempe, Arizona, USA
[12]School of Earth and Space Exploration, Arizona State University, Tempe, Arizona, USA
[13]Department of Civil, Environmental and Geomatic Engineering, University College London, London WC1E 6BT, UK

**Correspondence:** Naika Meili (meili@ifu.baug.ethz.ch)

# Contents

# 1 Radiation

## 1.1 Shortwave radiation

The direct $S_{net,i}^{dir}$ and diffuse $S_{net,i}^{diff}$ solar shortwave radiation absorbed by each urban surface i [W m$^{-2}$] are calculated as a function of urban geometry and albedo. The urban geometry provides shade by blocking part of the incoming direct beam solar radiation. It further decreases the sky-view factor, which reduces the incoming diffuse solar radiation and traps reflected solar radiation within the urban canyon. UT&C calculates the absorbed solar shortwave radiation with the following steps:

1. (a) The direct shortwave radiation received by each urban surface is calculated as a function of solar position and shade provided by buildings and trees (Sect. 1.1.2, 1.1.3, 1.1.4).

    (b) The diffuse shortwave radiation received by each urban surface is calculated as a function of its sky-view factor (Sect. 1.1.5).

2. Infinite radiation reflections within the urban canyon are calculated using view factors and the total absorbed shortwave radiation of each urban surface i is consequently calculated (Sect. 1.1.6).

It is assumed that all urban surfaces are Lambertian with isotropic scattering and reflections. The view factors are calculated analytically (Sect. 1.3.1) if there are no trees in the urban environment and with a Monte Carlo ray tracing algorithm (Sect. 1.3.2) if trees are present. UT&C assumes no obstruction of the roof surface and the absorbed shortwave radiation is only influenced by the solar position and surface albedo (Sect. 1.1.1). UT&C further calculates the absorbed shortwave radiation due to direct beam radiation and diffuse radiation (Sect. 1.1.7) which allows to investigate the effects of shade and albedo in more detail. The energy associated with shortwave radiation is perfectly conserved (Sect. 1.1.8).

### 1.1.1 Absorbed shortwave radiation: Roof

The direct $S_{net,i}^{dir}$, diffuse $S_{net,i}^{diff}$, and total $S_{net,i}$ absorbed shortwave radiation of each roof surface fraction i [W m$^{-2}$] are calculated as:

$$S_{net,i}^{dir} = (1 - \alpha_i)\, S\!\downarrow^{dir}, \tag{1}$$

$$S_{net,i}^{diff} = (1 - \alpha_i)\, S\!\downarrow^{diff}, \tag{2}$$

$$S_{net,i} = (1 - \alpha_i)\, (S\!\downarrow^{dir} + S\!\downarrow^{diff}), \tag{3}$$

where $\alpha_i$ [$-$] is the surface albedo of roof surface fraction i, $S\!\downarrow^{dir}$ [W m$^{-2}$] the incoming direct, and $S\!\downarrow^{diff}$ [W m$^{-2}$] the incoming diffuse shortwave radiation from the sky.

### 1.1.2 Incoming direct shortwave radiation: Ground and wall without trees

In the absence of trees, the direct solar radiation received by the ground facets $S_{in,g}^{dir}$, sunlit wall $S_{in,wsun}^{dir}$, and shaded wall $S_{in,wshd}^{dir}$ [W m$^{-2}$], are calculated according to Kusaka et al. (2001), Wang et al. (2013), and Ryu et al. (2016). The shade

positions on the ground $x_0$, and on the wall $y_0$ $[-]$ (Fig. 1) are:

$$x_0 = \max[1 - h_{can}\xi,\, 0] \,, \tag{4}$$

$$y_0 = \max[h_{can} - 1/\xi,\, 0] \,, \tag{5}$$

where $h_{can}$ $[-]$ is the canyon height normalized by canyon width $w_{can}$ (often referred to as height-to-width ratio), and $\xi$ $[-]$ summarizes the influence of solar position in relation to canyon position as (Kusaka et al., 2001; Wang et al., 2013; Ryu et al., 2016):

$$\xi = \tan\theta_z \,|\sin\theta_a| \,, \tag{6}$$

where $\theta_z$ [rad] is the solar zenith angle, and $\theta_a$ [rad] the difference between solar azimuth angle and canyon orientation ($\theta_{azimuth}$ [rad] - $\theta_{canyon}$ [rad]). The shadow length on the ground $\chi_{shadow}$ $[-]$, and on the wall $\eta_{shadow}$ $[-]$, are calculated as (Kusaka et al., 2001; Wang et al., 2013; Ryu et al., 2016):

$$\chi_{shadow} = 1 - x_0 \,, \tag{7}$$

$$\eta_{shadow} = y_0\, h_{can}^{-1} \,, \tag{8}$$

The direct solar radiation received by the ground $S_{in,g}^{dir}$, the sunlit wall $S_{in,wsun}^{dir}$, and the shaded wall $S_{in,wshd}^{dir}$ [W m$^{-2}$] are calculated as (Kusaka et al., 2001; Wang et al., 2013; Ryu et al., 2016):

$$S_{in,g}^{dir} = S\downarrow^{dir} [1 - \chi_{shadow}] \,, \tag{9}$$

$$S_{in,wsun}^{dir} = S\downarrow^{dir} \xi [1 - \eta_{shadow}] \,, \tag{10}$$

$$S_{in,wshd}^{dir} = 0 \,, \tag{11}$$

where $S\downarrow^{dir}$ [W m$^{-2}$] is the incoming direct shortwave radiation from the sky. The shaded wall does not receive any direct solar radiation.

### 1.1.3 Incoming direct shortwave radiation: Ground and wall with trees

In the presence of trees, the direct solar radiation received by the ground $S_{in,g}^{dir}$, the sunlit wall $S_{in,wsun}^{dir}$, and the shaded wall $S_{in,wshd}^{dir}$ [W m$^{-2}$] are calculated according to Ryu et al. (2016) as:

$$S_{in,g}^{dir} = S\downarrow^{dir} [1 - \chi_{shadow} + \tau\chi_{tree}] \,, \tag{12}$$

$$S_{in,wsun}^{dir} = S\downarrow^{dir} \xi [h_{can} - \eta_{shadow} + \tau\eta_{tree}] \,, \tag{13}$$

$$S_{in,wshd}^{dir} = 0 \,, \tag{14}$$

where $S\downarrow^{dir}$ [W m$^{-2}$] is the direct incoming solar radiation, $\chi_{shadow}$ $[-]$ the total shadow length on the ground, $\chi_{tree}$ $[-]$ the shadow length on the ground due to tree shading alone, $\eta_{shadow}$ $[-]$ the total shadow length on the wall, and $\eta_{tree}$ $[-]$ the
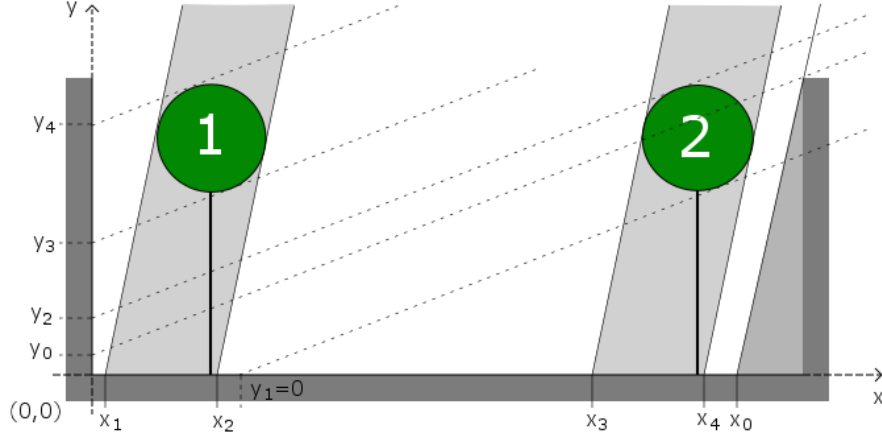
**Figure 1.** Shadow location on the ground and wall cast by trees and opposite wall according to Ryu et al. (2016). $x_0$, $x_1$, $x_2$, $x_3$, $x_4$ are the shadow locations on the ground and $y_0$, $y_1$, $y_2$, $y_3$, $y_4$ on the wall as described in Sect. 1.1.3.

shadow length on the wall due to tree shading alone. The variable $\tau$ [$-$] is the tree canopy transmittance as a function of leaf area index, LAI [$-$], and optical trasmittance factor $K_{opt}$ [$-$], calculated according to Maass et al. (1995) as:

$$\tau = e^{-K_{opt}\ LAI}\ , \tag{15}$$

The shaded wall does not receive any direct solar radiation. The shadow lengths $\chi_{shadow}$ [$-$], $\eta_{shadow}$ [$-$], $\chi_{tree}$ [$-$], and $\eta_{tree}$
130 [$-$] are calculated according to Ryu et al. (2016) who computes the shadow location coordinates (Fig. 1) as:

$$x_0 = \max[1 - h_{can}\xi,\ 0]\ , \tag{16}$$

$$y_0 = \max[h_{can} - 1/\xi,\ 0]\ , \tag{17}$$

$$x_1 = \max[d_t - h_t\xi - r_t\sqrt{1+\xi^2},\ 0]\ , \tag{18}$$

$$x_2 = \max[d_t - h_t\xi + r_t\sqrt{1+\xi^2},\ 0]\ , \tag{19}$$

135 $$x_3 = \max[1 - d_t - h_t\xi - r_t\sqrt{1+\xi^2},\ 0]\ , \tag{20}$$

$$x_4 = \max[1 - d_t - h_t\xi + r_t\sqrt{1+\xi^2},\ 0]\ , \tag{21}$$

$$y_1 = \max[h_t - (1-d_t)\xi^{-1} - r_t\sqrt{1+\xi^{-2}},\ 0]\ , \tag{22}$$

$$y_2 = \max[h_t - (1-d_t)\xi^{-1} + r_t\sqrt{1+\xi^{-2}},\ 0]\ , \tag{23}$$

$$y_3 = \max[h_t - d_t\xi^{-1} - r_t\sqrt{1+\xi^{-2}},\ 0]\ , \tag{24}$$

140 $$y_4 = \max[h_t - d_t\xi^{-1} + r_t\sqrt{1+\xi^{-2}},\ 0]\ , \tag{25}$$

where $x_1 < x_2 < x_3 < x_4$ and $y_1 < y_2 < y_3 < y_4$, $h_t$ $[-]$ is the normalized tree height, $r_t$ $[-]$ the normalized tree radius, and $d_t$ $[-]$ the normalized tree-to-wall distance (Fig. 2). The shadow length caused by tree 1 and tree 2 on the ground, $\chi_{tree1}$ $[-]$ and $\chi_{tree2}$ $[-]$, and on the wall, $\eta_{tree1}$ $[-]$ and $\eta_{tree2}$ $[-]$, are:

$$\chi_{tree1} = x_2 - x_1 \, , \tag{26}$$

$$\chi_{tree2} = x_4 - x_3 \, , \tag{27}$$

$$\eta_{tree1} = y_4 - y_3 \, , \tag{28}$$

$$\eta_{tree2} = y_2 - y_1 \, , \tag{29}$$

The total shadow length caused by trees and wall on the ground $\chi_{shadow}$ $[-]$, and wall $\eta_{shadow}$ $[-]$, are (Ryu et al., 2016):

$$\chi_{shadow} = \begin{cases} 1 - \min[x_0, \, x_3] + \chi_{tree1} - \max[x_2 - x_0, \, 0] & \text{if } x_0 < x_4 \\ 1 - x_0 + \chi_{tree1} + \chi_{tree2} & \text{if } x_0 \geq x_4 \end{cases} \, , \tag{30}$$

$$\eta_{shadow} = \begin{cases} \max[y_0, \, y_1, \, y_2, \, y_3, \, y_4] & \text{if } y_3 \leq \max[y_0, \, y_2] \\ \eta_{Tree1} + \max[y_0, \, y_2] & \text{if } y_3 > \max[y_0, \, y_2] \end{cases} \, , \tag{31}$$

The total shadow length caused by trees only on the ground $\chi_{tree}$ $[-]$, and wall $\eta_{tree}$ $[-]$, are (Ryu et al., 2016):

$$\chi_{tree} = \begin{cases} \chi_{tree1} - \max[x_2 - x_0, \, 0] & \text{if } x_0 < x_3 \\ \chi_{tree1} + x_0 - x_3 & \text{if } x_3 \leq x_0 < x_4 \\ \chi_{tree1} + \chi_{tree2} & \text{if } x_0 \geq x_4 \end{cases} \, , \tag{32}$$

$$\eta_{tree} = \begin{cases} \eta_{tree1} + y_2 - y_0 & \text{if } y_3 > \max[y_0, \, y_2] \ \& \ y_2 > y_0 \\ \eta_{tree1} & \text{if } y_3 > \max[y_0, \, y_2] \ \& \ y_2 \leq y_0 \\ \eta_{tree1} + \eta_{tree2} & \text{if } y_3 > \max[y_0, \, y_2] \ \& \ y_1 > y_0 \\ \\ y_4 - y_0 & \text{if } y_3 \leq \max[y_0, \, y_2] \ \& \ y_2 > y_0 \\ 0 & \text{if } y_3 \leq \max[y_0, \, y_2] \ \& \ y_2 \leq y_0 \end{cases} \, , \tag{33}$$

### 1.1.4 Incoming direct shortwave radiation: Trees

The direct shortwave radiation received by the tree canopy $S_{in,t}^{dir}$ [W m$^{-2}$ circle area] is calculated according to Ryu et al. (2016) as:

$$S_{in,t}^{dir} = (1 - \tau)\left(S_{in,t1}^{dir} + S_{in,t2}^{dir}\right)/2 \, , \tag{34}$$
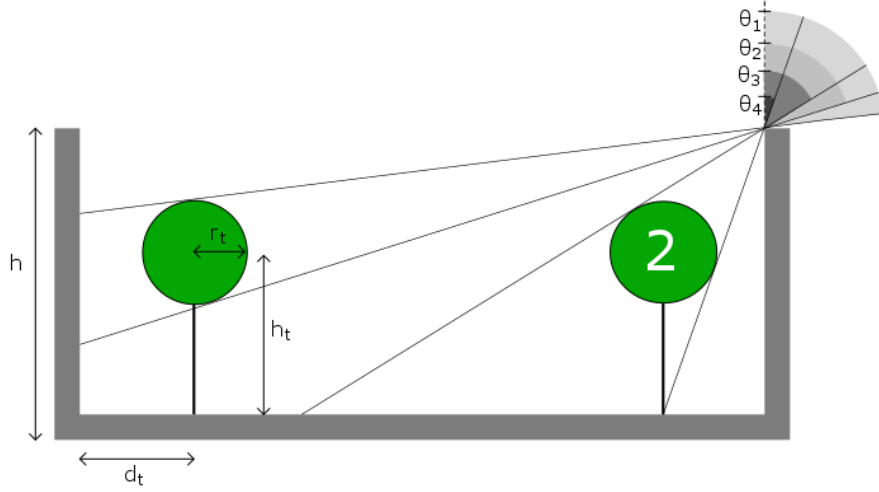
**Figure 2.** Urban geometry and its interaction with direct beam solar radiation according to Ryu et al. (2016). $h$ is the normalized building height, $h_t$ the normalized tree height, $r_t$ the normalized tree radius, and $d_t$ the normalized distance of tree trunk from the wall. $\theta_1, \theta_2, \theta_3, \theta_4$ are reference angles used to calculate radiation-tree interaction as described in Sect. 1.1.4.

where $S^{dir}_{in,t1}$ and $S^{dir}_{in,t2}$ [W m$^{-2}$ circle area] are the direct shortwave radiation received by tree 1 and tree 2, $\tau$ [$-$] is the tree canopy transmittance (Eq. (15)). $S^{dir}_{in,t1}$ and $S^{dir}_{in,t2}$ [W m$^{-2}$ circle area] are calculated as follows (Ryu et al., 2016):

$$
S^{dir}_{in,t1} = \begin{cases} 0 & \text{if } \xi \geq \tan\theta_1 \\ S{\downarrow}^{dir} \left[r_t\sqrt{1+\xi^2} + (1-d_t) - (h_{can}-h_t)\xi\right]/(2\pi r_t) & \text{if } \tan\theta_2 \leq \xi < \tan\theta_1 \\ S{\downarrow}^{dir} \left[2r_t\sqrt{1+\xi^2}\right]/(2\pi r_t) & \text{if } \xi < \tan\theta_2 \end{cases}
$$

$$
S^{dir}_{in,t2} = \begin{cases} 0 & \text{if } \xi \geq \tan\theta_3 \\ S{\downarrow}^{dir} \left[r_t\sqrt{1+\xi^2} + d_t - (h_{can}-h_t)\xi\right]/(2\pi r_t) & \text{if } \tan\theta_4 \leq \xi < \tan\theta_3 \\ S{\downarrow}^{dir} \left[2r_t\sqrt{1+\xi^2}\right]/(2\pi r_t) & \text{if } \xi < \tan\theta_4 \end{cases} \tag{35}
$$

where $S{\downarrow}^{dir}$ [W m$^{-2}$] is the incoming direct shortwave radiation from the sky, and $d_t$ [$-$] the normalized tree-to-wall distance (Fig. 2).

The four reference angles $\theta_1$, $\theta_2$, $\theta_3$, and $\theta_4$ (Fig. 2) are calculated as (Ryu et al., 2016):

$$\tan\theta_1 = \frac{(1-d_t)\,(h_{can}-h_t)+r_t\sqrt{(1-d_t)^2+\left(h_{can}-h_t\right)^2-r_t^2}}{\left(h_{can}-h_t\right)^2-r_t^2}\,,\tag{36}$$

$$\tan\theta_2 = \frac{(1-d_t)\,(h_{can}-h_t)-r_t\sqrt{(1-d_t)^2+\left(h_{can}-h_t\right)^2-r_t^2}}{\left(h_{can}-h_t\right)^2-r_t^2}\,,\tag{37}$$

$$\tan\theta_3 = \frac{d_t\,(h_{can}-h_t)+r_t\sqrt{d_t^2+\left(h_{can}-h_t\right)^2-r_t^2}}{\left(h_{can}-h_t\right)^2-r_t^2}\,,\tag{38}$$

$$\tan\theta_4 = \frac{d_t\,(h_{can}-h_t)-r_t\sqrt{d_t^2+\left(h_{can}-h_t\right)^2-r_t^2}}{\left(h_{can}-h_t\right)^2-r_t^2}\,,\tag{39}$$

The relationships developed by Ryu et al. (2016) and applied in UT&C does not account for tree-on-tree shading. Hence, energy conservation is only met when trees do not shade each other. In the case of tree on tree shading, the excess or deficit of energy is added to the tree surfaces.

### 1.1.5   Incoming diffuse shortwave radiation: Ground, wall, trees

The diffuse shortwave radiation received by each urban surface i $S_{in,i}^{diff}$ [W m$^{-2}$] is a function of sky-view factors (Masson, 2000; Kusaka et al., 2001; Wang et al., 2013; Ryu et al., 2016) and is calculated as:

$$S_{in,i}^{diff} = S\!\downarrow^{diff} F_{is}^{(t)}\,,\tag{40}$$

where $S\!\downarrow^{diff}$ [W m$^{-2}$] is the incoming diffuse solar radiation from the sky, and $F_{is}^{(t)}$ [$-$] the respective sky-view factor of surface i either without trees ($F_{is}$) or with trees ($F_{is}^t$). In the absence of trees, the sky-view factors $F_{is}$ are calculated with the analytically derived equations (Masson, 2000; Kusaka et al., 2001; Oleson et al., 2007; Park and Lee, 2008; Ryu et al., 2011; Wang et al., 2013) described in Sect. 1.3.1. In the presence of trees, the sky-view factors $F_{is}^t$ are calculated with the Monte Carlo ray tracing algorithm once at the beginning of the simulation period (Hoff and Janni, 1989; Wang, 2014; Frank et al., 2016) described in Sect. 1.3.2.

### 1.1.6   Radiation reflection and total absorbed shortwave radiation

UT&C calculates infinite reflections of shortwave radiation within the urban canyon according to the method developed by Sparrow and Cess (1970), and applied by Harman (2003), and Wang (2010, 2014).

The infinite reflection theory and its step by step application to the longwave radiative transfer in an urban canyon without trees are described in Sect. 1.2.2 and 1.2.3. The solution of shortwave radiation reflections can be derived identically under the following assumptions:

- There is no shortwave radiation generated: $\Omega_i = 0$.

- The incoming direct shortwave radiation $S_{in,i}^{dir}$ is added to each surface i.

- The reflectivity term $(1 - \varepsilon_i)$ for longwave radiation is replaced by the albedo $\alpha_i$.

Applying these changes and following the step by step derivation described in Sect. 1.2.3 leads to the following equation:

$$T_{ij} B_i = C_i , \tag{41}$$

Where $B_i$ [W m$^{-2}$] is the vector of outgoing shortwave radiation from surface i, $C_i$ [W m$^{-2}$] the vector of incoming direct and diffuse shortwave radiation from the sky to surface i, and $T_{ij}$ [$-$] the matrix describing the geometric relationship between the different surfaces with their view factors. In the absence of trees, $T_{ij}$, $B_i$, and $C_i$ are:

$$C_i = \begin{bmatrix} C_{gv}\alpha_{gv}(S_{in,g}^{dir} + F_{gs}S\downarrow^{diff}) \\ C_{gb}\alpha_{gb}(S_{in,g}^{dir} + F_{gs}S\downarrow^{diff}) \\ C_{gi}\alpha_{gi}(S_{in,g}^{dir} + F_{gs}S\downarrow^{diff}) \\ \alpha_w(S_{wsun}^{dir} + F_{ws}S\downarrow^{diff}) \\ \alpha_w F_{ws}S\downarrow^{diff} \end{bmatrix} , \qquad B_i = \begin{bmatrix} B_{gv} \\ B_{gb} \\ B_{gi} \\ B_{wsun} \\ B_{wshd} \end{bmatrix} , \tag{42}$$

$$T_{ij} = \begin{bmatrix} 1 & 0 & 0 & -C_{gv}\alpha_{gv}F_{gw} & -C_{gv}\alpha_{gv}F_{gw} \\ 0 & 1 & 0 & -C_{gb}\alpha_{gb}F_{gw} & -C_{gb}\alpha_{gb}F_{gw} \\ 0 & 0 & 1 & -C_{gi}\alpha_{gi}F_{gw} & -C_{gi}\alpha_{gi}F_{gw} \\ -C_{gv}f_{gv}\alpha_w F_{wg} & -C_{gb}f_{gb}\alpha_w F_{wg} & -C_{gi}f_{gi}\alpha_w F_{wg} & 1 & -\alpha_w F_{ww} \\ -C_{gv}f_{gv}\alpha_w F_{wg} & -C_{gb}f_{gb}\alpha_w F_{wg} & -C_{gi}f_{gi}\alpha_w F_{wg} & -\alpha_w F_{ww} & 1 \end{bmatrix} , \tag{43}$$

In the presence of trees, $T_{ij}$, $B_i$, and $C_i$ are:

$$C_i = \begin{bmatrix} C_{gv}\alpha_{gv}(S_{in,g}^{dir} + F_{gs}^t S\downarrow^{diff}) \\ C_{gb}\alpha_{gb}(S_{in,g}^{dir} + F_{gs}^t S\downarrow^{diff}) \\ C_{gi}\alpha_{gi}(S_{in,g}^{dir} + F_{gs}^t S\downarrow^{diff}) \\ \alpha_w(S_{wsun}^{dir} + F_{ws}^t S\downarrow^{diff}) \\ \alpha_w F_{ws}^t S\downarrow^{diff} \\ \alpha_t(S_{in,t}^{dir} + F_{ts}^t S\downarrow^{diff}) \end{bmatrix} , \qquad B_i = \begin{bmatrix} B_{gv} \\ B_{gb} \\ B_{gi} \\ B_{wsun} \\ B_{wshd} \\ B_t \end{bmatrix} , \tag{44}$$

$$T_{ij} = \begin{bmatrix} 1 & 0 & 0 & -C_{gv}\alpha_{gv}F_{gw}^t & -C_{gv}\alpha_{gv}F_{gw}^t & -C_{gv}\alpha_{gv}F_{gt}^t \\ 0 & 1 & 0 & -C_{gb}\alpha_{gb}F_{gw}^t & -C_{gb}\alpha_{gb}F_{gw}^t & -C_{gv}\alpha_{gv}F_{gt}^t \\ 0 & 0 & 1 & -C_{gi}\alpha_{gi}F_{gw}^t & -C_{gi}\alpha_{gi}F_{gw}^t & -C_{gv}\alpha_{gv}F_{gt}^t \\ -C_{gv}f_{gv}\alpha_w F_{wg}^t & -C_{gb}f_{gb}\alpha_w F_{wg}^t & -C_{gi}f_{gi}\alpha_w F_{wg}^t & 1 & -\alpha_w F_{ww}^t & -\alpha_w F_{wt}^t \\ -C_{gv}f_{gv}\alpha_w F_{wg}^t & -C_{gb}f_{gb}\alpha_w F_{wg}^t & -C_{gi}f_{gi}\alpha_w F_{wg}^t & -\alpha_w F_{ww}^t & 1 & -\alpha_w F_{wt}^t \\ -C_{gv}f_{gv}\alpha_t F_{tg}^t & -C_{gb}f_{gb}\alpha_t F_{tg}^t & -C_{gi}f_{gi}\alpha_t F_{tg}^t & -\alpha_t F_{tw}^t & -\alpha_t F_{tw}^t & 1 - \alpha_t F_{tt}^t \end{bmatrix} , \tag{45}$$

where $C_{gv}$, $C_{gb}$, and $C_{gi}$ are logical factors accounting for the presence ($C_{gi} = 1$) or absence ($C_{gi} = 0$) of vegetated, bare, or impervious ground cover. $\alpha_i$ [−] is the albedo of surface i, $S_{in,i}^{dir}$ [W m$^{-2}$] the direct incoming radiation of surface i, $F_{ij}^{(t)}$ [−] the view factor from surface i to surface j, $S\downarrow^{diff}$ [W m$^{-2}$] the incoming diffuse shortwave radiation from the sky, $f_{gv}$, $f_{gb}$, and $f_{gi}$ are the fraction of vegetated, bare and impervious ground, respectively. $B_i$ [W m$^{-2}$] is the outgoing solar shortwave radiation from surface i. The subscripts $gv$, $gb$, $gi$, $wsun$, $wshd$, and $t$ denote vegetated ground, bare ground, impervious ground, sunlit wall, shaded wall, and trees, respectively.

The outgoing shortwave radiation of surface i, $B_i$ [W m$^{-2}$], is calculated with matrix inversion of Eq. (41):

$$B_i = [T_{ij}]^{-1} C_i , \tag{46}$$

Subsequently, the incoming shortwave radiation of surface i, $\Lambda_i$ [W m$^{-2}$], and net absorbed shortwave radiation of surface i $S_{net,i}$ [W m$^{-2}$] are calculated according to Eq. (58) and (59).

### 1.1.7 Absorbed direct and diffuse shortwave radiation

The direct absorbed shortwave radiation of each surface $S_{net,i}^{dir}$ [W m$^{-2}$] is calculated as a function of the direct incoming solar radiaton to surface i $S_{in,i}^{dir}$ [W m$^{-2}$] and its albedo $\alpha_i$ [−] as:

$$S_{net,i}^{dir} = (1 - \alpha_i) S_{in,i}^{dir} , \tag{47}$$

The diffuse absorbed shortwave radiation of each surface i $S_{net,i}^{diff}$ [W m$^{-2}$] is calculated afterwards subtracting the absorbed direct solar radiation $S_{net,i}^{dir}$ [W m$^{-2}$] from the total absorbed solar radiation of surface i $S_{net,i}$ [W m$^{-2}$]:

$$S_{net,i}^{diff} = S_{net,i} - S_{net,i}^{dir} , \tag{48}$$

### 1.1.8 Energy conservation

UT&C is designed to conserve shortwave radiation energy. View factors are direction specific and need to fulfill a reciprocity criterion in order to conserve radiation energy. Monte Carlo Ray tracing algorithms do generally not result in reciprocal view factors due to the finite number of rays. Hence, the view factors used in UT&C are post processed to fulfill reciprocity.

Taking the directionality of the view factors into account, the shortwave radiation energy balance can be calculated from the perspective of the urban surface $EB_{surf}$ [W m$^{-2}$] and from the perspective of the urban canyon $EB_{can}$ [W m$^{-2}$] as:

$$EB_{surf} = \sum_i S_{in,i} \frac{f_i A_i}{A_g} - \sum_i S_{net,i} \frac{f_i A_i}{A_g} - \sum_i S_{out,i} \frac{f_i A_i}{A_g} , \tag{49}$$

$$EB_{can} = S\downarrow^{dir} + S\downarrow^{diff} - \sum_i S_{net,i} \frac{f_i A_i}{A_g} - \sum_i S_{out,i} f_i F_{si}^{(t)} , \tag{50}$$

where $S_{in,i}$ [$W\ m^{-2}$] is the incoming, $S_{out,i}$ [$W\ m^{-2}$] the outgoing, and $S_{net,i}$ [$W\ m^{-2}$] the net absorbed shortwave radiation of surface i. $A_i$ is the surface area i, $A_g$ the total ground area equal to the canyon width, $f_i$ the ground cover fraction ($f_i = 1$ for wall or tree), $F_{si}^{(t)}$ [−] the sky-view factor, $S\downarrow^{dir}$ [W m$^{-2}$] the direct, and $S\downarrow^{diff}$ [W m$^{-2}$] the diffuse incoming shortwave radiation from the sky.

## 1.2 Longwave radiation

The absorbed longwave radiation of surface i $L_{net,i}$ [W m$^{-2}$] is calculated as the difference between incoming $L_{in,i}$ and emitted outgoing longwave radiation $L_{out,i}$, which is dependent on the surface temperature. As with shortwave radiation, UT&C calculates infinite reflections of longwave radiation within the urban canyon (Sparrow and Cess, 1970; Harman, 2003; Wang, 2010, 2014). Sect. 1.2.2 describes the infinite radiation reflection theory (Harman, 2003) between multiple surfaces, which is applied step by step to the urban canyon (Sect. 1.2.3). UT&C assumes no obstruction of roof surface in the calculation of longwave radiation transfer (Sect. 1.2.1). The air within the canyon does not interact in the radiative exchange. UT&C is designed to fully conserve the energy budget of longwave radiation (Sect. 1.2.4).

### 1.2.1 Absorbed longwave radiation: Roof

The absorbed longwave radiation of each roof surface i $L_{net,i}$ [W m$^{-2}$] is calculated as:

$$L_{net,i} = \varepsilon_i (L\downarrow - \sigma T_i^4) \,, \tag{51}$$

where $L\downarrow$ [W m$^{-2}$] is the incoming longwave radiation from the atmosphere, $\varepsilon_i$ [−] the emissivity and $(1 - \epsilon_i)$ the reflectivity of surface i for longwave radiation, $\sigma = 5.67 * 10^{-8}$ [W m$^{-2}$ K$^{-4}$] the Stefan-Boltzmann constant, and $T_i$ [K] the temperature of surface i.

### 1.2.2 Infinite radiation reflections: Theory

The incoming $\Lambda_i$ [W m$^{-2}$], outgoing $B_i$ [W m$^{-2}$], emitted $\Omega_i$ [W m$^{-2}$], and net absorbed $Q_i$ [W m$^{-2}$] longwave radiation flux of each surface i can be described as (Sparrow and Cess, 1970; Harman, 2003; Wang, 2010, 2014) :

$$\Lambda_i = \sum_j F_{ij} B_j \,, \tag{52}$$

$$B_i = \Omega_i + (1 - \varepsilon_i)\Lambda_i \,, \qquad \Omega_i = \begin{cases} \varepsilon_i \sigma T_i^4 & \text{for } i = g, w, t \\ L\downarrow & \text{for } i = s \end{cases} \,, \tag{53}$$

$$Q_i = \Lambda_i - B_i \,, \tag{54}$$

where $F_{ij}$ [−] is the view factor from surface i to surface j, $\varepsilon_i$ [−] the emissivity and $(1 - \varepsilon_i)$ the longwave reflectivity of surface i, and $T_i$ [K] the temperature of surface i.

Equations (52) and (53) are combined and solved for the emitted radiation of surface i $\Omega_i$ [W m$^{-2}$] as:

$$B_i = \Omega_i + (1 - \varepsilon_i) \sum_j F_{ij} B_j \,, \tag{55}$$

$$\Omega_i = B_i - (1 - \varepsilon_i) \sum_j F_{ij} B_j = \sum_j \Gamma_{ij} B_j \,, \tag{56}$$

$$\Gamma_{ij} = \delta_{ij} - (1 - \varepsilon_i) F_{ij} \,, \tag{57}$$

Equation (56) shows recurrence of outgoing radiation $B_i$ [W m$^{-2}$]. The geometric relationship between the surfaces is described by the view factors $F_{ij}$ [$-$] in matrix $\Gamma_{ij}$. $\Gamma_{ij}$ always has an inverse $[\Gamma_{ij}]^{-1}$ and the outgoing $B_i$ [W m$^{-2}$], incoming $\Lambda_i$ [W m$^{-2}$], and net absorbed longwave radiation flux $Q_i$ [W m$^{-2}$] are calculated as:

$$B_i = \sum_j [\Gamma_{ij}]^{-1}\Omega_j , \qquad \Lambda_i = \frac{B_i - \Omega_i}{1 - \varepsilon_i} , \tag{58}$$

$$Q_i = \begin{cases} \sum_j F_{ij}B_j - \Omega_i, & \text{if } \varepsilon_i = 1 \\ (\varepsilon_i B_i - \Omega_i)/(1 - \varepsilon_i) & \text{otherwise} \end{cases} , \tag{59}$$

UT&C applies the above described solution for infinite reflections to the computation of longwave and shortwave radiation transfer.

### 1.2.3 Infinite longwave radiation reflections: Step by step

The following equations show the step by step derivation and application of the infinite reflection theory described in Sect. 1.2.2 to calculate the net absorbed longwave radiation in an urban canyon without trees.

The outgoing longwave radiation of surface i, $B_i$ [W m$^{-2}$], is the sum of emitted $\Omega_i = \varepsilon_i \sigma T_i^4$ [W m$^{-2}$] and reflected $\Lambda_i$ [W m$^{-2}$] longwave radiation (Eq. (53)):

$$B_{gv} = \varepsilon_{gv}\sigma T_{gv}^4 + (1 - \varepsilon_{gv})\Lambda_{gv} , \tag{60}$$

$$B_{gb} = \varepsilon_{gb}\sigma T_{gb}^4 + (1 - \varepsilon_{gb})\Lambda_{gb} , \tag{61}$$

$$B_{gi} = \varepsilon_{gi}\sigma T_{gi}^4 + (1 - \varepsilon_{gi})\Lambda_{gi} , \tag{62}$$

$$B_{wsun} = \varepsilon_w\sigma T_{wsun}^4 + (1 - \varepsilon_w)\Lambda_{wsun} , \tag{63}$$

$$B_{wshd} = \varepsilon_w\sigma T_{wshd}^4 + (1 - \varepsilon_w)\Lambda_{wshd} , \tag{64}$$

Similarly, the incoming longwave radiation to surface i, $\Lambda_i$ [W m$^{-2}$], can be written as (Eq. (52)):

$$\Lambda_{gv} = F_{gs}L\downarrow + F_{gw}B_{wsun} + F_{gw}B_{wshd} , \tag{65}$$

$$\Lambda_{gb} = F_{gs}L\downarrow + F_{gw}B_{wsun} + F_{gw}B_{wshd} , \tag{66}$$

$$\Lambda_{gi} = F_{gs}L\downarrow + F_{gw}B_{wsun} + F_{gw}B_{wshd} , \tag{67}$$

$$\Lambda_{wsun} = F_{ws}L\downarrow + f_{gv}F_{wg}B_{gv} + f_{gb}F_{wg}B_{gb} + f_{gi}F_{wg}B_{gi} + F_{ww}B_{wshd} , \tag{68}$$

$$\Lambda_{wshd} = F_{ws}L\downarrow + f_{gv}F_{wg}B_{gv} + f_{gb}F_{wg}B_{gb} + f_{gi}F_{wg}B_{gi} + F_{ww}B_{wsun} , \tag{69}$$

where $B_j$ [W m$^{-2}$] is the outgoing longwave radiation from the surrounding surfaces j, and $F_{ij}$ [$-$] the view factor from surface i to surface j. Equations (65) to (69) show that there is no direct radiative exchange between different ground covers fractions. The walls receive a weighted average of the emitted ground radiation according to the surface cover fractions ($f_{gv}$, $f_{gb}$, $f_{gi}$). UT&C assumes homogeneous distribution of ground cover and hence, the view factors are not ground cover specific.

Combining Eq. (60) to (64) with Eq. (65) to (69) leads to:

$$B_{gv} = \varepsilon_{gv}\sigma T_{gv}^4 + (1-\varepsilon_{gv})\left(F_{gs}L\downarrow + F_{gw}B_{wsun} + F_{gw}B_{wshd}\right), \tag{70}$$

$$B_{gb} = \varepsilon_{gb}\sigma T_{gb}^4 + (1-\varepsilon_{gb})\left(F_{gs}L\downarrow + F_{gw}B_{wsun} + F_{gw}B_{wshd}\right), \tag{71}$$

$$B_{gi} = \varepsilon_{gi}\sigma T_{gi}^4 + (1-\varepsilon_{gi})\left(F_{gs}L\downarrow + F_{gw}B_{wsun} + F_{gw}B_{wshd}\right), \tag{72}$$

$$B_{wsun} = \varepsilon_w\sigma T_{wsun}^4 + (1-\varepsilon_w)\left(F_{ws}L\downarrow + f_{gv}F_{wg}B_{gv} + f_{gb}F_{wg}B_{gb} + f_{gi}F_{wg}B_{gi} + F_{ww}B_{wshd}\right), \tag{73}$$

$$B_{wshd} = \varepsilon_w\sigma T_{wshd}^4 + (1-\varepsilon_w)\left(F_{ws}L\downarrow + f_{gv}F_{wg}B_{gv} + f_{gb}F_{wg}B_{gb} + f_{gi}F_{wg}B_{gi} + F_{ww}B_{wsun}\right), \tag{74}$$

Rearranging Eq. (70) to (74) leads to:

$$B_{gv} - (1-\varepsilon_{gv})(F_{gw}B_{wsun} + F_{gw}B_{wshd}) = \varepsilon_{gv}\sigma T_{gv}^4 + (1-\varepsilon_{gv})F_{gs}L\downarrow, \tag{75}$$

$$B_{gb} - (1-\varepsilon_{gb})(F_{gw}B_{wsun} + F_{gw}B_{wshd}) = \varepsilon_{gb}\sigma T_{gb}^4 + (1-\varepsilon_{gb})F_{gs}L\downarrow, \tag{76}$$

$$B_{gi} - (1-\varepsilon_{gi})(F_{gw}B_{wsun} + F_{gw}B_{wshd}) = \varepsilon_{gi}\sigma T_{gi}^4 + (1-\varepsilon_{gi})F_{gs}L\downarrow, \tag{77}$$

$$B_{wsun} - (1-\varepsilon_w)(f_{gv}F_{wg}B_{gv} + f_{gb}F_{wg}B_{gb} + f_{gi}F_{wg}B_{gi} + F_{ww}B_{wshd}) = \varepsilon_w\sigma T_{wsun}^4 + (1-\varepsilon_w)F_{ws}L\downarrow, \tag{78}$$

$$B_{wshd} - (1-\varepsilon_w)(f_{gv}F_{wg}B_{gv} + f_{gb}F_{wg}B_{gb} + f_{gi}F_{wg}B_{gi} + F_{ww}B_{wsun}) = \varepsilon_w\sigma T_{wshd}^4 + (1-\varepsilon_w)F_{ws}L\downarrow, \tag{79}$$

The system of equations (Eq. (75) to (79)) can be written in matrix notation as:

$$T_{ij}B_i = C_i, \tag{80}$$

where:

$$C_i = \begin{bmatrix} C_{gv}(\varepsilon_{gv}\sigma T_{gv}^4 + (1-\varepsilon_{gv})F_{gs}L\downarrow) \\ C_{gb}(\varepsilon_{gb}\sigma T_{gb}^4 + (1-\varepsilon_{gb})F_{gs}L\downarrow) \\ C_{gi}(\varepsilon_{gi}\sigma T_{gi}^4 + (1-\varepsilon_{gi})F_{gs}L\downarrow) \\ \varepsilon_w\sigma T_{wsun}^4 + (1-\varepsilon_w)F_{ws}L\downarrow \\ \varepsilon_w\sigma T_{wshd}^4 + (1-\varepsilon_w)F_{ws}L\downarrow \end{bmatrix}, \qquad B_i = \begin{bmatrix} B_{gv} \\ B_{gb} \\ B_{gi} \\ B_{wsun} \\ B_{wshd} \end{bmatrix}, \tag{81}$$

$$T_{ij} = \begin{bmatrix} 1 & 0 & 0 \\ 0 & 1 & 0 \\ 0 & 0 & 1 \\ -C_{gv}f_{gv}(1-\varepsilon_w)F_{wg} & -C_{gb}f_{gb}(1-\varepsilon_w)F_{wg} & -C_{gi}f_{gi}(1-\varepsilon_w)F_{wg} \\ -C_{gv}f_{gv}(1-\varepsilon_w)F_{wg} & -C_{gb}f_{gb}(1-\varepsilon_w)F_{wg} & -C_{gi}f_{gi}(1-\varepsilon_w)F_{wg} \end{bmatrix} \tag{82}$$

$$\begin{bmatrix} -C_{gv}(1-\varepsilon_{gv})F_{gw} & -C_{gv}(1-\varepsilon_{gv})F_{gw} \\ -C_{gb}(1-\varepsilon_{gb})F_{gw} & -C_{gb}(1-\varepsilon_{gb})F_{gw} \\ -C_{gi}(1-\varepsilon_{gi})F_{gw} & -C_{gi}(1-\varepsilon_{gi})F_{gw} \\ 1 & -(1-\varepsilon_w)F_{ww} \\ -(1-\varepsilon_w)F_{ww} & 1 \end{bmatrix}, \tag{83}$$

$C_{gv}$, $C_{gb}$, and $C_{gi}$ are logical factors accounting for the presence ($C_{gi} = 1$) or absence ($C_{gi} = 0$) of a ground cover fraction.

310 The outgoing longwave radiation of surface i, $B_i$ [W m$^{-2}$], is calculated with matrix inversion as:

$$B_i = [T_{ij}]^{-1} C_i \,, \tag{84}$$

Subsequently, the incoming $\Lambda_i$ [W m$^{-2}$] and net absorbed $Q_i$ [W m$^{-2}$] longwave radiation are calculated according to Eq. (58) and (59).

The matrices used to describe the system of equations solving infinite longwave reflections in an urban canyon with trees are:

315 $$T_{ij} B_i = C_i \,, \tag{85}$$

where:

$$C_i = \begin{bmatrix} C_{gv}(\varepsilon_{gv}\sigma T_{gv}^4 + (1-\varepsilon_{gv})F_{gs}^t L\downarrow) \\ C_{gb}(\varepsilon_{gb}\sigma T_{gb}^4 + (1-\varepsilon_{gb})F_{gs}^t L\downarrow) \\ C_{gi}(\varepsilon_{gi}\sigma T_{gi}^4 + (1-\varepsilon_{gi})F_{gs}^t L\downarrow) \\ \varepsilon_w\sigma T_{wsun}^4 + (1-\varepsilon_w)F_{ws}^t L\downarrow \\ \varepsilon_w\sigma T_{wshd}^4 + (1-\varepsilon_w)F_{ws}^t L\downarrow \\ \varepsilon_t\sigma T_t^4 + (1-\varepsilon_t)F_{ts}^t L\downarrow \end{bmatrix}, \qquad B_i = \begin{bmatrix} B_{gv} \\ B_{gb} \\ B_{gi} \\ B_{wsun} \\ B_{wshd} \\ B_t \end{bmatrix}, \tag{86}$$

$$T_{ij} = \begin{bmatrix} 1 & 0 & 0 \\ 0 & 1 & 0 \\ 0 & 0 & 1 \\ -C_{gv}f_{gv}(1-\varepsilon_w)F_{wg}^t & -C_{gb}f_{gb}(1-\varepsilon_w)F_{wg}^t & -C_{gi}f_{gi}(1-\varepsilon_w)F_{wg}^t \\ -C_{gv}f_{gv}(1-\varepsilon_w)F_{wg}^t & -C_{gb}f_{gb}(1-\varepsilon_w)F_{wg}^t & -C_{gi}f_{gi}(1-\varepsilon_w)F_{wg}^t \\ -C_{gv}f_{gv}(1-\varepsilon_t)F_{tg}^t & -C_{gb}f_{gb}(1-\varepsilon_t)F_{tg}^t & -C_{gi}f_{gi}(1-\varepsilon_t)F_{tg}^t \end{bmatrix} \tag{87}$$

320
$$\begin{bmatrix} -C_{gv}(1-\varepsilon_{gv})F_{gw}^t & -C_{gv}(1-\varepsilon_{gv})F_{gw}^t & -C_{gv}(1-\varepsilon_{gv})F_{gt}^t \\ -C_{gb}(1-\varepsilon_{gb})F_{gw}^t & -C_{gb}(1-\varepsilon_{gb})F_{gw}^t & -C_{gv}(1-\varepsilon_{gv})F_{gt}^t \\ -C_{gi}(1-\varepsilon_{gi})F_{gw}^t & -C_{gi}(1-\varepsilon_{gi})F_{gw}^t & -C_{gv}(1-\varepsilon_{gv})F_{gt}^t \\ 1 & -(1-\varepsilon_w)F_{ww}^t & -(1-\varepsilon_w)F_{wt}^t \\ -(1-\varepsilon_w)F_{ww}^t & 1 & -(1-\varepsilon_w)F_{wt}^t \\ -(1-\varepsilon_t)F_{tw}^t & -(1-\varepsilon_t)F_{tw}^t & 1-(1-\varepsilon_t)F_{tt}^t \end{bmatrix}, \tag{88}$$

where $F_{ij}^t$ [$-$] is the view factor from surface i to surface j for an urban canyon with trees. The subscripts $_{gv,\ gb,\ gi,\ wsun,\ wshd,}$ $_t$ denote vegetated ground, bare ground, impervious ground, sunlit wall, shaded wall, and trees, respectively.

#### 1.2.4 Energy conservation

The longwave radiation energy conservation can be calculated from the perspective of the urban surfaces $EB_{L,surf}$ [W m$^{-2}$] and from the perspective of the urban canyon $EB_{L,can}$ [W m$^{-2}$]. This directionality is important as explained in Sect. 1.1.8.

$$EB_{L,surf} = \sum_i L_{in,i} \frac{f_i A_i}{A_g} - \sum_i L_{net,i} \frac{f_i A_i}{A_g} - \sum_i L_{out,i} \frac{f_i A_i}{A_g} \,, \tag{89}$$

$$EB_{L,can} = L\downarrow - \sum_i L_{net,i} \frac{f_i A_i}{A_g} - \sum_i L_{out,i} f_i F_{si}^{(t)} \,, \tag{90}$$

where $L_{in,i}$ [W m$^{-2}$] is the incoming, $L_{out,i}$ [W m$^{-2}$] the outgoing, and $L_{net,i}$ [W m$^{-2}$] the net absorbed longwave radiation of surface i. $A_i$ is the area of surface i, $A_g$ the total ground area equal to the canyon width, $f_i$ the ground cover fraction ($f_i = 1$ if i is wall or tree), $F_{si}^{(t)}$ [$-$] the sky-view factor, and $L\downarrow$ [W m$^{-2}$] the incoming longwave radiation from the atmosphere to the urban canyon.

### 1.3 View factor calculation

#### 1.3.1 Analytical solution

The view factors $F_{ij}$ [$-$] for an infinite urban canyon without trees can be calculated with the following analytically derived equations (Sparrow and Cess, 1970; Masson, 2000; Harman, 2003; Oleson et al., 2007; Park and Lee, 2008; Ryu et al., 2011; Wang et al., 2013):

$$F_{sg} = F_{gs} = \sqrt{1 + \left(\frac{h_{can}}{w_{can}}\right)^2} - \frac{h_{can}}{w_{can}} \,, \tag{91}$$

$$F_{ww} = \sqrt{1 + \left(\frac{w_{can}}{h_{can}}\right)^2} - \frac{w_{can}}{h_{can}} \,, \tag{92}$$

$$F_{wg} = F_{ws} = 0.5\left(1 - F_{ww}\right) \,, \tag{93}$$

$$F_{gw} = 0.5\left(1 - F_{gs}\right) \,, \tag{94}$$

where $w_{can} = 1$ [$-$] is the normalized canyon width. The subscripts $s$, $g$, $w$ denote sky, ground, and wall, respectively. The view factors $F_{ij}$ [$-$] are directional so that the incoming flux density onto surface i $\Lambda_{i(j)}$ [$W\ m^{-2}$] originating from surface j $B_j$ [W m$^{-2}$] is (Harman, 2003):

$$\Lambda_{i(j)} = F_{ij} B_j \,, \tag{95}$$
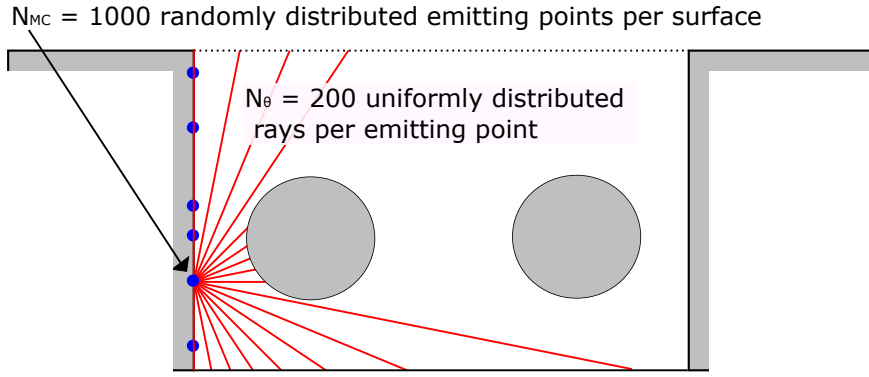
**Figure 3.** Representation of a 2 dimensional Monte Carlo ray tracing algorithm in an urban canyon with 2 trees.

345    The view factors $F_{ij}$ $[-]$ fulfill the following three conditions (Wang, 2014): The self-view factor of a flat surface $F_{ii}$ $[-]$ must be zero (Eq. (96)), energy must be conserved (Eq. (97)), and view factors are reciprocal (Eq. (98)).

$$F_{ii} = 0 \, , \tag{96}$$

$$\sum_{j=1}^{N} F_{ij} = 1 \, , \tag{97}$$

$$A_i F_{ij} = A_j F_{ji} \, , \tag{98}$$

350    $A_i$ and $A_j$ are the area of surface i and surface j.

### 1.3.2    Monte Carlo Ray Tracing

The view factors $F_{ij}^t$ $[-]$ for an urban canyon with trees are calculated with a Monte Carlo ray tracing algorithm (Fig. 3). UT&C includes a simplified two dimensional Monte Carlo ray tracing code similar to the methods described by Wang (2014) and Frank et al. (2016). The Monte Carlo ray tracing algorithm does a probabilistic sampling of all rays emitted by surface i.

355    The relative frequency of rays emitted by surface i that hit surface j is an estimation of the view factor $F_{ij}$ (Frank et al., 2016). On each surface i, a large number $N_{MC}$, of randomly distributed emitting points are selected. The emitting coordinates on each canyon surface are defined as:

$$x_{g,e} = w_{can} \, R_{N_{MC}} \, , \tag{99}$$

$$z_{w,e} = h_{can} \, R_{N_{MC}} \, , \tag{100}$$

360    $$x_{t,e} = r_{tree} \, cos(2\pi R_{N_{MC}}) \, , \tag{101}$$

$$z_{t,e} = r_{tree} \, sin(2\pi R_{N_{MC}}) \, , \tag{102}$$

where $x_{g,e}$ is the x-coordinate of the emitting points on the ground and sky surfaces, $z_{w,e}$ the z-coordinate of the emitting points on the wall, and $x_{t,e}$ and $z_{t,e}$ are the (x,z)-coordinates of the emitting points on the circular tree surface, and $R_{N_{MC}}$ are

$N_{MC}$ uniformly distributed random variables in the intervall [0,1]. The direction of the emitted ray at the emitting point can be defined with the polar angle $\theta_{MC}$ [rad] as:

$$\theta_{MC} = \arcsin R_{N_\theta} \, , \tag{103}$$

where $R_{N_\theta}$ are $N_\theta$ uniformely distributed variables in the intervall [0,1]. The polar angle $\theta_{MC}$ [rad] is defined to be zero perpendicular to the emitting surface for the ground, sky and wall and perpendicular to the tangent of the emitting point on the tree circle. The intersection of an emitted ray with a canyon surface can be calculated as the line intersection between ray and surface defining a maximum ray distance. The first surface hit by a ray is counted towards the view factor calculation. Subsequently, the view factor $F_{ij}^t$ is calculated as:

$$F_{ij}^t = \frac{N_{rays,j}}{N_{rays,tot}} \, , \tag{104}$$

$$F_{ii}^t = 0 \, , \tag{105}$$

where $N_{rays,j}$ are the number of rays hitting surface j, and $N_{rays,tot}$ the total number of rays emitted. The self view factor is corrected to be 0 (Eq. (105)). The view factors do not necessarily fulfill the reciprocity criterion (Eq. (98)) right after the Monte Carlo ray tracing, due to the finite number of rays emitted in the algorithm. In a subsequent step, the computed view factors are corrected to be reciprocal as to meet energy conservation in the infinite reflection scheme. The corrections applied in UT&C are as follows:

Urban canyon without trees

$$F_{gs} = f(Monte\ Carlo\ ray\ tracing) \, , \tag{106}$$

$$F_{gw} = 0.5(1 - F_{gs}) \, , \tag{107}$$

$$F_{sg} = F_{gs} \, , \tag{108}$$

$$F_{sw} = F_{gw} \, , \tag{109}$$

$$F_{wg} = F_{gw} w_{can}/h_{can} \, , \tag{110}$$

$$F_{ws} = F_{sw} w_{can}/h_{can} \, , \tag{111}$$

$$F_{ww} = 1 - F_{wg} - F_{ws} \, , \tag{112}$$

Urban canyon with trees

$$F_{gs}^t = f(Monte\ Carlo\ ray\ tracing)\ , \tag{113}$$

$$F_{gt}^t = f(Monte\ Carlo\ ray\ tracing)\ , \tag{114}$$

$$F_{gw}^t = 0.5(1 - F_{gs}^t - F_{gt}^t)\ , \tag{115}$$

$$F_{st}^t = f(Monte\ Carlo\ ray\ tracing)\ , \tag{116}$$

$$F_{sg}^t = F_{gs}^t\ , \tag{117}$$

$$F_{sw}^t = 0.5(1 - F_{sg}^t - F_{st}^t)\ , \tag{118}$$

$$F_{wt}^t = f(Monte\ Carlo\ ray\ tracing)\ , \tag{119}$$

$$F_{wg}^t = F_{gw}^t w_{can}/h_{can}\ , \tag{120}$$

$$F_{ws}^t = F_{sw}^t w_{can}/h_{can}\ , \tag{121}$$

$$F_{ww}^t = 1 - F_{wg}^t - F_{ws}^t - F_{wt}^t\ , \tag{122}$$

$$F_{ts}^t = F_{st}^t w_{can}/A_{tree}\ , \tag{123}$$

$$F_{tg}^t = F_{gt}^t w_{can}/A_{tree}\ , \tag{124}$$

$$F_{tw}^t = F_{wt}^t h_{can}/A_{tree}\ , \tag{125}$$

$$F_{tt}^t = 1 - F_{ts}^t - 2F_{tw}^t - F_{tg}^t\ , \tag{126}$$

where $A_{tree} = 2(2\pi r_{tree})\ [-]$ is the normalized tree surface area. The Monte Carlo ray tracing algorithm implemented in UT&C is able to reproduce the analytical view factors for an urban canyon without trees (Fig. 4). The number of emitting points $N_{MC} = 1000$ and the number of emitted rays per emitting point $N_{rays} = 200$ show a sufficient approximation to the analytical solution (Fig. 4). Note that the tree canopy is assumed impermeable in the view factor calculation as well as in the calculation of infinite reflections within the urban canyon. This could lead to a slight overestimation of absorbed radiation by the tree canopy.

## 2 Turbulent fluxes

The total flux of sensible $H_{urb}$ [W m$^{-2}$] and latent $\lambda E_{urb}$ [W m$^{-2}$] heat from the urban environment is calculated as the area weighted average of turbulent roof and canyon fluxes:

$$H_{urb} = f_r H_r + f_{can} H_{can}\ , \tag{127}$$

$$\lambda E_{urb} = f_r \lambda E_r + f_{can} \lambda E_{can}\ , \tag{128}$$
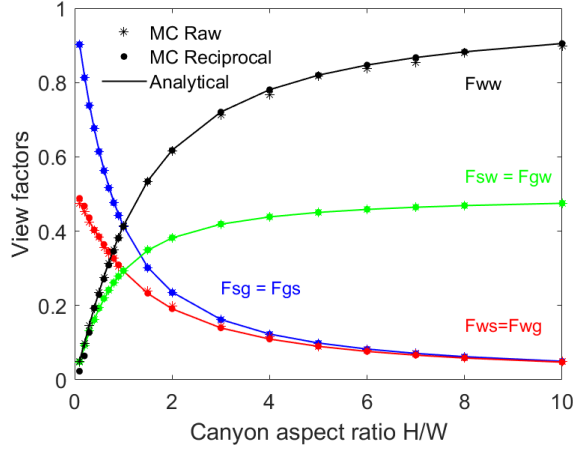
**Figure 4.** View factors calculated with the Monte Carlo ray tracing algorithm implemented in UT&C (MC Raw) corrected for reciprocity (MC Reciprocal) and compared with the analytical solution (Analytical) of the different canyon surfaces as a function of canyon aspect ratio H/W. The subscripts g, w and s denote ground, wall and sky, respectively.

where $f_r$ $[-]$ is the roof plan area fraction and $f_{can}$ $[-]$ the canyon plan area fraction. The total sensible and latent roof heat flux is calculated as:

$$H_r = f_{r,imp}H_{r,imp} + f_{r,veg}H_{r,veg} \, , \tag{129}$$

$$\lambda E_r = f_{r,imp}\lambda E_{r,imp} + f_{r,veg}\lambda E_{r,veg} \, , \tag{130}$$

where $f_{r,imp}$ $[-]$ is the impervious and $f_{r,veg}$ $[-]$ the vegetated roof fraction. The total sensible and latent canyon heat flux is calculated as:

$$H_{can} = w_{can}H_g + h_{can}H_{w,sun} + h_{can}H_{w,shd} + 4r_{tree}H_{tree} + Q_f \, , \tag{131}$$

$$\lambda E_{can} = w_{can}\lambda E_g + h_{can}\lambda E_{w,sun} + h_{can}\lambda E_{w,shd} + 4r_{tree}\lambda E_{tree} \, , \tag{132}$$

where $Q_f$ $[\mathrm{W\ m^{-2}}]$ is the anthropogenic heat input. The sensible and latent heat fluxes of the tree, $H_{tree}$ and $\lambda E_{tree}$, are calculated as Watts per horizontal tree area. Therefore, $H_{tree}$ and $\lambda E_{tree}$ need to be multiplied by $4r_{tree}$ to rescale to the canyon extent. The total sensible and latent ground heat flux is calculated as:

$$H_g = f_{g,imp}H_{g,imp} + f_{g,bare}H_{g,bare} + f_{g,veg}H_{g,veg} \, , \tag{133}$$

$$\lambda E_g = f_{g,imp}\lambda E_{g,imp} + f_{g,bare}\lambda E_{g,bare} + f_{g,veg}\lambda E_{g,veg} \, , \tag{134}$$

where $f_{g,imp}$ $[-]$ is the impervious, $f_{g,bare}$ $[-]$ the bare, and $f_{g,veg}$ $[-]$ the vegetated ground fraction. The calculation of the individual sensible and latent heat fluxes are described in Sect. 2.1.1 to 2.1.5 and 2.2.1 to 2.2.5.

## 2.1 Sensible heat

The sensible heat flux from any surface i to a generic air mass near the surface, $H_i$ [W m$^{-2}$], is calculated as (Shuttleworth, 2012):

$$H_i = \rho_a C_p \frac{(T_i - T_a)}{\sum r_j} \,,$$ (135)

where $\rho_a$ [kg m$^{-3}$] is the air density (Eq. (137)), $C_p$ [J kg$^{-1}$ K$^{-1}$] the specific heat capacity of air at constant pressure (Eq. (136)), $T_i$ [K] the temperature of surface i, $T_a$ [K] the air temperature, and $\sum r_j$ [s m$^{-1}$] the sum of resistances j to the turbulent transport of sensible heat from the surface i to the air layer. A detailed description of the resistance calculations is described in Sect. 3.3 to 3.6. The specific heat capacity of air at constant pressure $C_p$ [J kg$^{-1}$ K$^{-1}$] is calculated as:

$$C_p = 1005 + \frac{(T_a + 23.15)^2}{3364} \,,$$ (136)

The air density $\rho_a$ [$kg m^{-3}$] is calculated as:

$$\rho_a = \frac{P_a}{287.04 T_a} \left(1 - \frac{e_a}{P_a}(1 - 0.622)\right) \,,$$ (137)

where $P_a$ [Pa] is the air pressure, and $e_a$ [Pa] the vapour pressure.

### 2.1.1 Sensible heat: Roof

The sensible heat flux from the impervious $H_{r,imp}$ [W m$^{-2}$], and vegetated roof fraction $H_{r,veg}$ [W m$^{-2}$] to the air at atmospheric reference level is calculated as:

$$H_{r,imp} = \rho_a C_p \frac{(T_{r,imp} - T_{atm})}{r_{ah,r}} \,,$$ (138)

$$H_{r,veg} = \rho_a C_p \frac{(T_{r,veg} - T_{atm})}{r_{ah,r} + \frac{r_{b,r}}{2(LAI_r + SAI_r)}} \,,$$ (139)

where $T_{r,imp}$ [K], $T_{r,veg}$ [K], and $T_{atm}$ [K] are the surface temperatures of the impervious and vegetated roof fraction, and the air temperature at atmospheric reference height. The resistance $r_{ah,r}$ [s m$^{-1}$] denotes the aerodynamic resistance from the roof to the atmospheric reference height (Sect. 3.3.1), and $r_{b,r}$ [s m$^{-1}$] the leaf boundary resistance of the roof vegetation (Sect. 3.4). The term $LAI_r$ [−] and $SAI_r$ [−] are, respectively, the leaf and stem area index of the roof vegetation. Note, both leaf sides interact in the sensible heat exchange (Fatichi et al., 2012a, b, c).

### 2.1.2 Sensible heat: Ground

The sensible heat flux from the impervious $H_{g,imp}$ [W m$^{-2}$], bare $H_{g,bare}$ [W m$^{-2}$], and vegetated ground fraction $H_{g,veg}$ [W m$^{-2}$] to the canyon air is calculated as:

$$H_{g,imp} = \rho_a C_p \frac{(T_{g,imp} - T_{can})}{r_{ah,g}} \ , \tag{140}$$

$$H_{g,bare} = \rho_a C_p \frac{(T_{g,bare} - T_{can})}{r_{ah,g}} \ , \tag{141}$$

$$H_{g,veg} = \rho_a C_p \frac{(T_{g,veg} - T_{can})}{r_{ah,g} + \frac{r_{b,g,veg}}{2(LAI_{g,veg} + SAI_{g,veg})}} \ , \tag{142}$$

where $T_{g,imp}$ [K], $T_{g,bare}$ [K], $T_{g,veg}$ [K], and $T_{can}$ [K] are the surface tempertures of the impervious, bare and vegetated ground fraction, and the air temperature at canyon calculation height ($Z_{calc} = h_{disp,can} + z_{0m,can}$, see Sect. 3.2). The resistance $r_{ah,g}$ [s m$^{-1}$] denotes the aerdoynamic resistance from the ground to the canyon calculation height (Sect. 3.3.2), and $r_{b,g,veg}$ [s m$^{-1}$] the leaf boundary resistance of the ground vegetation (Sect. 3.4). $LAI_{g,veg}$ [$-$] is the leaf and $SAI_{g,veg}$ [$-$] the stem area index of the ground vegetation. Note, both leave sides contribute to the sensible heat exchange (Fatichi et al., 2012a, b, c).

### 2.1.3 Sensible heat: Trees

The sensible heat flux from the trees $H_{tree}$ [W m$^{-2}$ horizontal tree area] to the canyon air is calculated as:

$$H_{tree} = \rho_a C_p \frac{(T_{tree} - T_{can})}{r_{ah,tree} + \frac{r_{b,tree}}{2(LAI_{tree} + SAI_{tree})}} \ , \tag{143}$$

where $T_{tree}$ [K] and $T_{can}$ [K] are the tree surface temperature and the air temperature at canyon calculation height ($Z_{calc} = h_{disp,can} + z_{0m,can}$, Sect. 3.2). $LAI_{tree}$ [$-$] is the leaf and $SAI_{tree}$ [$-$] the stem area index of the trees. The resistance $r_{ah,tree}$ [s m$^{-1}$] denotes the aerdoynamic resistance from the tree to the canyon calculation height (Sect. 3.3.2), and $r_{b,tree}$ [s m$^{-1}$] the leaf boundary resistance of the tree (Sect. 3.4).

### 2.1.4 Sensible heat: Wall

The canyon air is divided into two layers and the sensible heat flux from the wall contributing to the canyon air temperature at height $Z_p = 2$ m and at height $Z_{calc} = h_{disp,can} + z_{0m,can}$ ($h_{disp,can}$ [m] is the canyon displacement height and $z_{0m,can}$ [m] the canyon roughness length, see Sect. 3.2) are calculated individually (Fig. 5). The height of the first layer is $2Z_p$ and the height of the second layer $H_{can} - 2Z_p$. The total sensible heat flux from the sunlit wall $H_{w,sun}$ [W m$^{-2}$], and shaded wall $H_{w,shd}$ [W m$^{-2}$] to the canyon air is calculated as the area weighted average of the sensible heat fluxes from wall layer 1 and wall layer 2.

$$H_{w,sun} = \frac{2Z_p}{H_{can}} H_{w1,sun} + \frac{H_{can} - 2Z_p}{H_{can}} H_{w2,sun} \ , \tag{144}$$

$$H_{w,shd} = \frac{2Z_p}{H_{can}} H_{w1,shd} + \frac{H_{can} - 2Z_p}{H_{can}} H_{w2,shd} \ , \tag{145}$$
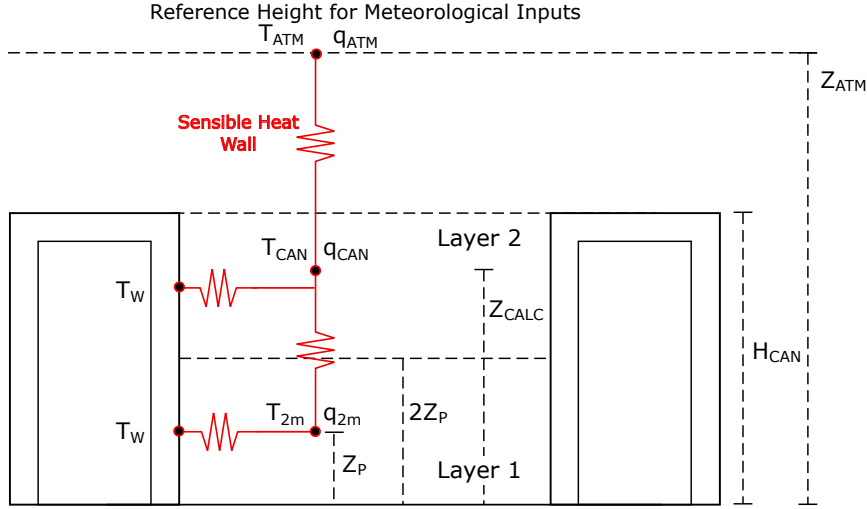
**Figure 5.** Sensible wall heat fluxes and canyon air layers. $T_{2m}$ and $q_{2m}$ are the 2 m air temperature and humidity calculated at height $Z_p = 2$ m. $T_{can}$ and $q_{can}$ are the air temperature and humidity at canyon calculation height $Z_{calc}$. The thickness of the first wall layer is $2Z_p$ and the thickness of the second wall layer is $H_{can} - 2Z_p$. The variables $T_{2m}$ and $q_{2m}$ are calculated at mid height of the first wall layer while $T_{can}$ and $q_{can}$ do not necessarily correspond to the mid height of the second wall layer. The horizontal resistances from wall to canyon air for both canyon air layers are calculated at their mid heights and their subsequent vertical aerodynamic resistance is applied to reach $Z_{calc}$.

where $Z_p = 2$ [m] and $H_{can}$ [m] is the canyon height. $H_{w1,sun}$ and $H_{w2,sun}$ [W m$^{-2}$] denote the sensible heat flux from sunlit wall layer 1 and layer 2. Similarly, $H_{w1,shd}$ and $H_{w2,shd}$ [W m$^{-2}$] denote the sensible heat flux from shaded wall layer 1 and layer 2. The sensible heat fluxes $H_{w1,sun}$, $H_{w2,sun}$, $H_{w1,shd}$, and $H_{w2,shd}$ are calculated as follows:

$$H_{w1,sun} = \rho_a C_p \frac{(T_{w,sun} - T_{can})}{r_{w1} + r_{ah1,w}} \ , \tag{146}$$

$$H_{w1,shd} = \rho_a C_p \frac{(T_{w,shd} - T_{can})}{r_{w1} + r_{ah1,w}} \ , \tag{147}$$

$$H_{w2,sun} = \rho_a C_p \frac{(T_{w,sun} - T_{can})}{r_{w2} + r_{ah2,w}} \ , \tag{148}$$

$$H_{w2,shd} = \rho_a C_p \frac{(T_{w,shd} - T_{can})}{r_{w2} + r_{ah2,w}} \ , \tag{149}$$

where $T_{w,sun}$ [K], $T_{w,shd}$ [K], and $T_{can}$ [K] are the sunlit and shaded wall surface temperatures and the air temperature at canyon calculation height ($Z_{calc} = h_{disp,can} + z_{0m,can}$, Sect. 3.2). The resistances $r_{w1}$ and $r_{w2}$ [s m$^{-1}$] are the horizontal aerodynamic resistance from the wall surface to the canyon air at mid height of layer 1 and layer 2 (Sect. 3.3.3). The resistances $r_{ah1,w}$ and $r_{ah2,w}$ [s m$^{-1}$] are the vertical aerodynamic resistance from the mid height of layer 1 and layer 2 to the canyon air at calculation height (Sect. 3.3.2).

### 2.1.5 Sensible heat: Canyon

The total sensible heat flux from canyon air to atmospheric reference height $H_{can}$ [W m$^{-2}$] is calculated as:

$$H_{can} = \rho_a C_p \frac{(T_{can} - T_{atm})}{r_{ah,c}} \, , \tag{150}$$

where $T_{can}$ [K] is the canyon air temperature, $T_{atm}$ [K] the temperature at atmospheric reference height, and $r_{ah,c}$ [s m$^{-1}$] the aerodynamic resistance from canyon air at calculation height to the atmospheric reference height (Sect. 3.3.1).

## 2.2 Latent heat

The latent heat flux from any surface i to a generic mass of air above/near the surface $\lambda E_i$ [W m$^{-2}$] is calculated as (Shuttleworth, 2012):

$$\lambda E_i = \lambda \rho_a \frac{(q_{sat,(T_i)} - q_a)}{\sum r_j} \, , \tag{151}$$

where $\lambda$ [J kg$^{-1}$] is the latent heat of vaporization (Eq. (152)), $\rho_a$ [kg m$^{-3}$] the dry air density (Eq. (137)), $q_{sat,(T_i)}$ [−] the specific humidity of surface i at saturation (Eq. (153)), $q_a$ [−] the specific humdity of the air (Eq. (155)), and $\sum r_j$ [s m$^{-1}$] the sum of resistances j to the turbulent transport of latent heat from the surface i to the air layer. The latent heat of vaporization $\lambda$ [J kg$^{-1}$] is calculated as (Shuttleworth, 2012):

$$\lambda = 1000(2501.3 - 2.351 T_a) \, , \tag{152}$$

where $T_a$ [°C] is the air temperature. The specific humidity of surface i at saturation $q_{sat,(T_i)}$ [−] is calculated as a function of surface temperature $T_i$ (Shuttleworth, 2012):

$$q_{sat,(T_i)} = \frac{0.622 e_{sat,(T_i)}}{P_a - 0.378 e_{sat,(T_i)}} \, , \tag{153}$$

where $P_a$ [Pa] is the air pressure, and $e_{sat,(T_i)}$ [Pa] the saturation vapour pressure at temperature $T_i$ [°C]. The saturation vapour pressure is calculated as (Shuttleworth, 2012):

$$e_{sat,(T_i)} = 611 e^{\frac{17.27 T_i}{237.3 + T_i}} \, , \tag{154}$$

The specific humidity of the air $q_a$ [−] is calculated as a function of vapour pressure $e_a$ [Pa] (Shuttleworth, 2012):

$$q_a = \frac{0.622 e_a}{P_a - 0.378 e_a} \, , \tag{155}$$

### 2.2.1 Latent heat: Roof

UT&C calculates evaporation from ponding water on impervious roof $E_{r,imp}$, evaporation from intercepted water on vegetation canopy $E_{r,veg,in}$, soil evaporation $E_{r,veg,soil}$, and transpiration from sunlit $TE_{r,veg,sun}$ and shaded $TE_{r,veg,shd}$ roof

vegetation canopy. All roof evapotranspiration fluxes have the unit of $[\text{kg m}^{-2}\,\text{s}^{-1}]$ and are calculated from the roof level to the atmospheric reference height as:

$$E_{r,imp} = \frac{\rho_a\big(q_{sat,(T_{r,imp})} - q_{atm}\big)}{r_{ah,r}} \;,\tag{156}$$

$$E_{r,veg} = E_{r,veg,int} + E_{r,veg,soil} + TE_{r,veg}\;,\tag{157}$$

$$E_{r,veg,int} = \frac{\rho_a\big(q_{sat,(T_{r,veg})} - q_{atm}\big)}{r_{ah,r} + \frac{r_{b,r}}{(LAI_r + SAI_r)d_{w,r}}}\;,\tag{158}$$

$$E_{r,veg,soil} = \frac{\rho_a\big(\hat{\alpha}_{soil,r}\,q_{sat,(T_{r,veg})} - q_{atm}\big)}{r_{ah,r} + r_{soil,r}}\;,\tag{159}$$

$$TE_{r,veg,sun} = \frac{\rho_a\big(q_{sat,(T_{r,veg})} - q_{atm}\big)}{r_{ah,r} + \frac{r_{b,r}}{LAI_r F_{sun,r}(1 - d_{w,r})} + \frac{r_{s,r,sun}}{LAI_r F_{sun,r}(1 - d_{w,r})}}\;,\tag{160}$$

$$TE_{r,veg,shd} = \frac{\rho_a\big(q_{sat,(T_{r,veg})} - q_{atm}\big)}{r_{ah,r} + \frac{r_{b,r}}{LAI_r F_{shd,r}(1 - d_{w,r})} + \frac{r_{s,r,shd}}{LAI_r F_{shd,r}(1 - d_{w,r})}}\;,\tag{161}$$

$$TE_{r,veg} = TE_{r,veg,sun} + TE_{r,veg,shd}\;,\tag{162}$$

where $q_{atm}$ $[-]$ is the specific humidity at atmospheric reference height, $r_{ah,r}$ $[\text{s m}^{-1}]$ the aerodynamic resistance from roof to atmospheric reference height (Sect. 3.3.1), $r_{b,r}$ $[\text{s m}^{-1}]$ the leaf boundary layer resistance of roof vegetation (Sect. 3.4), $r_{soil,r}$ $[\text{s m}^{-1}]$ the soil resistance (Sect. 3.5), and $r_{s,r,sun}$ and $r_{s,r,shd}$ $[\text{s m}^{-1}]$ the stomata resistance of the sunlit and shaded vegetation canopy fraction (Sect. 3.6). The sunlit $F_{sun}$ $[-]$ and shaded $F_{shd}$ $[-]$ canopy fractions are calculated assuming exponential decay of direct beam radiation within the vegetation canopy where the light transmission coefficient $K_{opt} = 0.5$ is assumed constant for simplicity rather than calculated with more complex canopy radiation transfer models (Fatichi et al., 2012a, b, c):

$$F_{sun} = \frac{1}{LAI}\frac{1 - e^{(-K_{opt}LAI)}}{K_{opt}}\;,\tag{163}$$

$$F_{shd} = 1 - F_{sun}\;,\tag{164}$$

Evapotraspiration from canopy interception is calculated for the canopy fraction covered by intercepted water $d_w$ $[-]$, whereas transpiration is calculated for the canopy fraction free of intercepted water $(1 - d_w)$ $[-]$. The canopy fraction covered by intercepted water $d_w$ $[-]$ is calculated according to Deardorff (1978) as:

$$d_w = min\big[1, (In/In_{max})^{2/3}\big]\;,\tag{165}$$

where $In$ [mm] is the intercepted water and $In_{max}$ [mm] the maximum canopy interception capacity. The evaporation from canopy interception and ponding is eventually limited by the amount of water intercepted and ponding. The canopy transpiration and the evaporation from the first soil layer are controlled by stomata resistance and soil resistance, respectively.

## 2.2.2 Latent heat: Ground

UT&C calculates evaporation from ponding water on impervious ground $E_{g,imp}$, soil evaporation from bare soil $E_{g,bare,soil}$, evaporation from intercepted water on vegetation canopy $E_{g,veg,in}$, soil evaporation from vegetated soil $E_{r,veg,soil}$, and transpiration from sunlit $TE_{g,veg,sun}$ and shaded $TE_{g,veg,shd}$ ground vegetation canopy. All evapotranspiration fluxes have the unit of $[\mathrm{kg\ m^{-2}\ s^{-1}}]$ and are calculated from the ground to the canyon calculation height ($Z_{calc} = h_{disp,can} + z_{0m,can}$, Sect. 3.2) as follows:

$$E_{g,imp} = \frac{\rho_a\left(q_{sat,(T_{g,imp})} - q_{can}\right)}{r_{ah,g}} \ , \tag{166}$$

$$E_{g,bare} = \frac{\rho_a\left(\hat{\alpha}_{soil,g}\, q_{sat,(T_{g,bare})} - q_{can}\right)}{r_{ah,g} + r_{soil}} \ , \tag{167}$$

$$E_{g,veg} = E_{g,veg,int} + E_{g,veg,soil} + TE_{g,veg} \ , \tag{168}$$

$$E_{g,veg,int} = \frac{\rho_a\left(q_{sat,(T_{g,veg})} - q_{can}\right)}{r_{ah,g} + \frac{r_{b,g,veg}}{(LAI_g + SAI_g)d_{w,g,veg}}} \ , \tag{169}$$

$$E_{g,veg,soil} = \frac{\rho_a\left(\hat{\alpha}_{soil}\, q_{sat,(T_{g,veg})} - q_{can}\right)}{r_{ah,g} + r_{soil,g}} \ , \tag{170}$$

$$TE_{g,veg} = TE_{g,veg,sun} + TE_{g,veg,shd} \ , \tag{171}$$

$$TE_{g,veg,sun} = \frac{\rho_a\left(q_{sat,(T_{g,veg})} - q_{can}\right)}{r_{ah,g} + \frac{r_{b,g}}{LAI_g F_{sun,g}(1-d_{w,g})} + \frac{r_{s,g,sun}}{LAI_g F_{sun,g}(1-d_{w,g})}} \ , \tag{172}$$

$$TE_{g,veg,shd} = \frac{\rho_a\left(q_{sat,(T_{g,veg})} - q_{can}\right)}{r_{ah,g} + \frac{r_{b,g}}{LAI_g F_{shd,g}(1-d_{w,g})} + \frac{r_{s,g,shd}}{LAI_g F_{shd,g}(1-d_{w,g})}} \ , \tag{173}$$

where $q_{can}$ $[-]$ is the specific humidity at canyon calculation height, $r_{ah,g}$ $[\mathrm{s\ m^{-1}}]$ the aerodynamic resistance from ground to canyon calculation height (Sect. 3.3.2), $r_{b,g}$ $[\mathrm{s\ m^{-1}}]$ the leaf boundary layer resistance (Sect. 3.4), $r_{soil,g}$ $[\mathrm{s\ m^{-1}}]$ the soil resistance (Sect. 3.5), and $r_{s,g,sun}$ and $r_{s,g,shd}$ $[\mathrm{s\ m^{-1}}]$ the stomata resistance of sunlit and shaded canopy fraction (Sect. 3.6), $\hat{\alpha}_{soil,g}$ $[-]$ the relative humidity in the soil pores (Sect. 3.5), $d_{w,g}$ $[-]$ the vegetation fraction covered by intercepted water (Eq. (165)), and $F_{sun,g}$ $[-]$ and $F_{shd,g}$ $[-]$ the sunlit and shaded vegetation canopy fraction (Eq. (163) and (164)). The evaporative fluxes from interception and ponding are eventually limited by the amount of water intercepted on the canopy and ponding on the ground. In the case of ponding water, there is no soil resistance and the relative humidity $\hat{\alpha}$ $[-]$ is one.

## 2.2.3 Latent heat: Trees

UT&C calculates evaporation from intercepted water on the tree canopy $E_{tree,in}$, and transpiration from the sunlit $TE_{r,veg,sun}$ and shaded $TE_{r,veg,shd}$ tree canopy fraction. All evapotranspiration fluxes have the unit of $[\mathrm{kg\ m^{-2}\ horizontal\ tree\ area\ s^{-1}}]$

and are calculated from tree height to canyon calculation height ($h_{disp,can} + z_{0m,can}$, Sect. 3.2) as follows:

$$E_{tree} = E_{tree,int} + TE_t ,\qquad(174)$$

$$E_{tree,int} = \frac{\rho_a\big(q_{sat,(T_{tree})} - q_{can}\big)}{r_{ah,t} + \frac{r_{b,t}}{(LAI_t + SAI_t)d_{w,t}}} ,\qquad(175)$$

$$TE_t = TE_{t,sun} + TE_{t,shd} ,\qquad(176)$$

$$TE_{t,sun} = \frac{\rho_a\big(q_{sat,(T_t)} - q_{can}\big)}{r_{ah,t} + \frac{r_{b,t}}{LAI_t F_{sun,t}(1 - d_{w,t})} + \frac{r_{s,t,sun}}{LAI_t F_{sun,t}(1 - d_{w,t})}} ,\qquad(177)$$

$$TE_{t,shd} = \frac{\rho_a\big(q_{sat,(T_t)} - q_{can}\big)}{r_{ah,t} + \frac{r_{b,t}}{LAI_t F_{shd,t}(1 - d_{w,t})} + \frac{r_{s,t,shd}}{LAI_t F_{shd,t}(1 - d_{w,t})}} ,\qquad(178)$$

where $q_{can}$ [$-$] is the specific humidity at canyon calculation height, $r_{ah,t}$ [s m$^{-1}$] the aerodynamic resistance from tree to canyon calculation height (Sect. 3.3.2), $r_{b,t}$ [s m$^{-1}$] the leaf boundary layer resistance (Sect. 3.4), and $r_{s,t,sun}$ and $r_{s,t,shd}$ [s m$^{-1}$] the stomata resistance of the sunlit and shaded tree canopy fraction (Sect. 3.6), $d_{w,t}$ [$-$] the canopy fraction covered by intercepted water (Eq. (165)), and $F_{sun,t}$ [$-$] and $F_{shd,t}$ [$-$] the sunlit and shaded canopy fraction (Eq. (163) and (164)). The evaporative flux from interception is eventually limited by the amount of water intercepted on the tree canopy.

### 2.2.4 Latent heat: Wall

The latent heat fluxes from sunlit and shaded wall, $E_{w,sun}$ and $E_{w,sun}$, are assumed to be negligible and equal to zero ($E_{w,sun} = 0$ and $E_{w,shd} = 0$). This means that the current version of UT&C does not include green walls.

### 2.2.5 Latent heat: Canyon

The total latent heat flux from canyon air to atmospheric reference height $E_{can}$ [kg m$^{-1}$ s$^{-1}$] is calculated as follows:

$$E_{can} = \frac{\rho_a(q_{can} - q_{atm})}{r_{ah,c}} ,\qquad(179)$$

where $q_{can}$ [$-$] is the specific humidity at canyon calculation height, $q_{atm}$ [$-$] the specific humidity at atmospheric reference height, and $r_{ah,c}$ [s m$^{-1}$] the aerodynamic resistance from canyon air to the atmospheric reference height (Sect. 3.3.1).

### 2.3 2 m air temperature and humidity

The air temperature and canyon humidity are calculated at two heights, $Z_p = 2$ m and $Z_{calc} = h_{disp,can} + z_{0m,can}$ (Sect. 3.2). The variables $T_{can}$ [°C] and $q_{can}$ [$-$] refer to the air temperature and specific humidity at canyon calculation height $Z_{calc}$. The variables $T_{can,2m}$ [°C] and $q_{can,2m}$ [$-$] refer to the air temperature and specific humidity at a height of 2 m above the ground. A height of 2 m is often used for urban meteorological measurements and corresponds to the temperature and humidity felt by pedestrians.

$T_{can}$ and $q_{can}$ are calculated solving the following equations:

$$H_{can} = f_{g,imp}H_{g,imp} + f_{g,bare}H_{g,bare} + f_{g,veg}H_{g,veg} + h_1(H_{w1,sun} + H_{w1,shd}) + h_2(H_{w2,sun} + H_{w2,shd})$$

$$+ 4r_{tree}H_{tree} + Q_f , \tag{180}$$

$$LE_{can} = f_{g,imp}LE_{g,imp} + f_{g,bare}LE_{g,bare} + f_{g,veg}LE_{g,veg} + 4r_{tree}LE_{tree} , \tag{181}$$

$Q_f$ [W m$^{-2}$] denotes the anthropogenic heat flux which is directly added to the energy balance of the canyon air. The calculation of $T_{can}$ and $q_{can}$ considers all sensible and latent heat fluxes from ground fractions, trees, and wall layer 1 and 2.

The variables $T_{can,2m}$ and $q_{can,2m}$ are calculated solving the following equations:

$$H_{can,2m} = f_{g,imp}H_{g,imp,2m} + f_{g,bare}H_{g,bare,2m} + f_{g,veg}H_{g,veg,2m} + h_1(H_{w1,sun} + H_{w1,shd}) , \tag{182}$$

$$LE_{can,2m} = f_{g,imp}LE_{g,imp,2m} + f_{g,bare}LE_{g,bare,2m} + f_{g,veg}LE_{g,veg,2m} , \tag{183}$$

$H_{i,2m}$ and $LE_{i,2m}$ are calculated as described in Sect.2.1.2 to 2.1.5 and 2.2.2 to 2.2.5 replacing aerodynamic resistance $r_{ah,can} : f(h_{disp,can} + z_{0m,can})$ with aerodynamic resistance $r_{ah,2m} : f(2\,m)$, and $T_{can}$ and $q_{can}$ with $T_{can,2m}$ and $q_{can,2m}$. The heat fluxes from wall layer 2 and trees are not directly considered in the calculation of $T_{can,2m}$ and $q_{can,2m}$ but they play an indirect role through $T_{can}$ and $q_{can}$.

## 3 Energy and mass transfer resistances

The turbulent mass and energy fluxes described in Sect. 2 to 2.3 are calculated with a set of resistances. These resistances parameterize different processes influencing the turbulent transport of water vapour and energy from the urban surface to the planetary boundary layer at reference height, $Z_{atm}$ [m]. UT&C accounts for aerodynamic resistance $r_{ah}$ above and within the canyon (Sect. 3.3, 3.3.1, 3.3.2 and 3.3.3), leaf boundary resistance $r_b$ (Sect. 3.4), soil resistance $r_{soil}$ (Sect. 3.5), and stomata resistance of sunlit and shaded leaves $r_{s,sun}$ and $r_{s,shd}$ (Sect. 3.6). The unit of resistance is the inverse of velocity [s m$^{-1}$].

### 3.1 Wind profile

The wind speed profile $u(z)$ is assumed to be logarithmic above the urban canopy ($Z_{atm} \geq z \geq H_{can}$), exponential within the urban canyon ($H_{can} \geq z \geq Z_{can,ref}$), and logarithmic again close to the ground surface ($Z_{can,ref} \geq z$) (Masson, 2000; Mahat et al., 2013) and is calculated as (Fig. 6):

$$u(z) = \frac{1}{k}u^*_{atm} \ln\left(\frac{z - h_{d,can}}{z_{om,can}}\right) \qquad \text{for } Z_{atm} \geq z \geq H_{can} , \tag{184}$$

$$u(z) = u_{H_{can}} \exp\left(-\hat{\beta}(1 - \frac{z}{H_{can}})\right) \quad \text{for } H_{can} \geq z \geq Z_{can,ref} , \tag{185}$$

$$u(z) = \frac{1}{k}u^*_{Z_{can,ref}} \ln\left(\frac{z}{z_{om,g}}\right) \qquad \text{for } Z_{can,ref} \geq z , \tag{186}$$

where $k = 0.4$ is the von Karman constant, $\hat{\beta}$ [$-$] an attenuation coefficient, $h_{d,can}$ [m] the urban canopy displacement height (Sect. 3.2), $z_{om,can}$ [m] the urban canopy roughness length (Sect. 3.2), $z_{om,g}$ [m] the ground roughness length (Sect. 3.2),
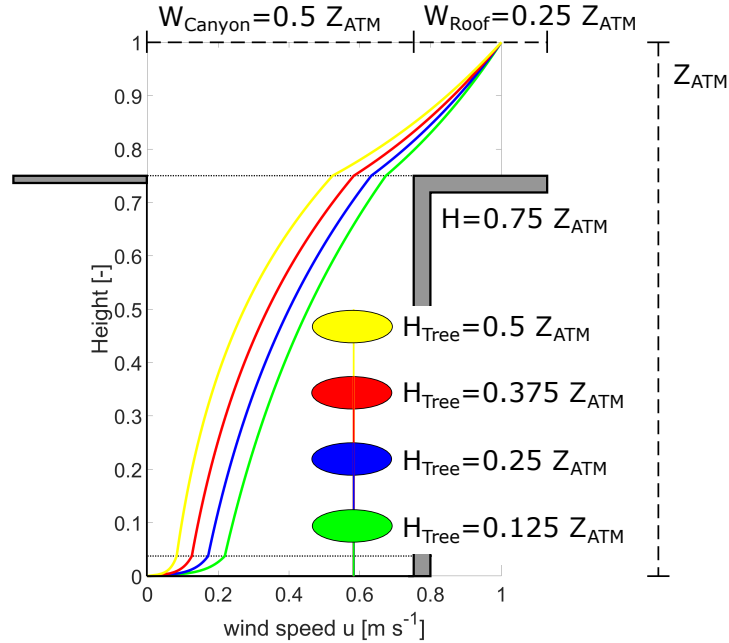
**Figure 6.** Vertical wind speed profile: Logarithmic above the urban canopy, exponential within the urban canyon, and logarithmic close to the canyon ground. The displayed wind speed profiles are calculated from the atmospheric reference level $Z_{ATM}$ to the canyon ground with a canyon height of $H = 0.75\ Z_{ATM}$, a canyon width of of $W_{Canyon} = 0.5\ Z_{ATM}$, a roof width of $W_{Roof} = 0.25\ Z_{ATM}$, and varying tree heights of $H_{Tree} = 0.125\ Z_{ATM}$ to $0.5\ Z_{ATM}$.

$u^*$ [m s$^{-1}$] the friction velocity, $u_{H_{can}} = \frac{1}{k} u^*_{atm} \ln\left(\frac{H_{can} - h_{d,can}}{z_{om,can}}\right)$ [m s$^{-1}$] the wind velocity at canyon height, $Z_{atm}$ [m] the atmospheric reference height, $H_{can}$ [m] the canyon height, and $Z_{can,ref}$ [m] a reference height close to the ground where the exponential wind profile changes to a logarithmic wind profile. The friction velocities $u^*_{atm}$ and $u^*_{Z_{can,ref}}$ are calculated as:

$$u^*_{atm} = \frac{k\, u_{atm}}{\ln(Z_{atm} - h_{d,can})/(z_{om,can}))} \ , \tag{187}$$

$$u^*_{Z_{can,ref}} = \frac{k\, u_{Z_{can,ref}}}{\ln(Z_{can,ref})/(z_{om,g}))} \ , \tag{188}$$

where $u_{atm}$ [m s$^{-1}$] is the wind velocity at atmospheric reference height, and $u_{Z_{can,ref}} = \frac{1}{k} u^*_{Z_{can,ref}} \ln\left(\frac{Z_{can,ref}}{z_{om,g}}\right)$ [m s$^{-1}$] the wind speed at the canyon reference height $Z_{can,ref}$. The attenuation coefficient $\hat{\beta}$ controls the vertical gradient of wind speed within the urban canyon. UT&C applies the approach developed by Fatichi et al. (2012a, b, c) for vegetated canopy which is based on a point equivalence between logarithmic and exponential wind speed profile at reference height $Z_{atm}$ [m] and canopy height $H_{can}$ [m]:

$$\hat{\beta} = \frac{\ln[u_{atm}/u_{H_{can}}]}{Z_{atm}/H_{can} - 1} \ , \tag{189}$$
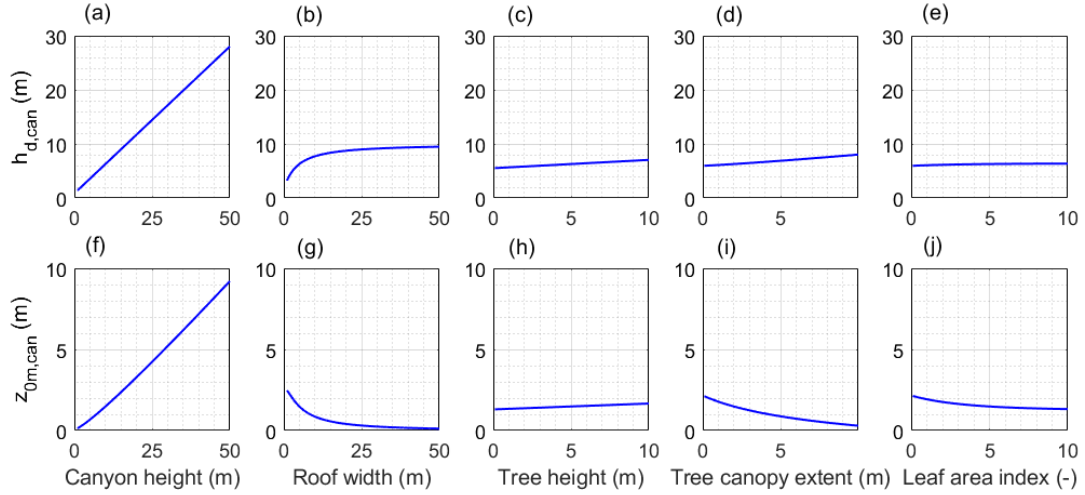
**Figure 7.** Sensitivity of canyon displacement height $h_{d,can}$ (Eq. (190)) and canyon roughness height $z_{0m,can}$ (Eq. (191)) as a function of canyon height, roof width, tree height, tree canopy extent, and leaf area index. The baseline scenario is a canyon height of 10 m, a canyon width of 10 m, a roof width of 5 m, a tree height of 5 m, a tree extend of 2 m, and a leaf area index of 5.

The mean vertical wind speed $w(z)$ $[\text{m s}^{-1}]$ is assumed to be negligible since we do not consider three-dimensional effects. The presence of trees modifying the wind profile is considered in the canyon displacement height $h_{d,can}$ and roughness length
630 $z_{om,can}$ as described in Sect. 3.2. The effect of ground vegetation is considered in the ground roughness length $z_{om,g}$ as described in Sect. 3.2, however displacement height of ground vegetation is considered negligible in the overall roughness parameterization of the ground, which typically include large fractions of smooth impervious surfaces.

## 3.2 Roughness length and zero displacement height

The urban canopy displacement height $h_{d,can}$ [m] and roughness length $z_{om,can}$ [m] are calculated according to the approach
635 developed by Macdonald et al. (1998) which was modified by Kent et al. (2017) to include the effect of trees on the wind profile above the canyon (Fig. 7) as follows:

$$h_{d,can} = (1 + \alpha_A^{-\lambda_p}(\lambda_p - 1))\overline{H}_{urb} , \tag{190}$$

$$z_{om,can} = \overline{H}_{urb}\left(1 - \frac{h_{d,can}}{\overline{H}_{urb}}\right)\exp\left[-\left(\frac{1}{\kappa^2}0.5\beta_A C_{Db}\left(1 - \frac{h_{d,can}}{\overline{H}_{urb}}\right)\frac{\{A_{f,b} + (P_v)A_{f,v}\}}{A_{tot}}\right)^{-0.5}\right] , \tag{191}$$

where $\kappa = 0.4$ $[-]$ is the von Karman constant, and $\alpha_A = 4.43$ $[-]$, $\beta_A = 1$ $[-]$, and $C_{Db} = 1.2$ $[-]$ are parameter values for
640 staggered arrays (Macdonald et al., 1998). $\overline{H}_{urb}$ [m] is the average height of the urban roughness elements, $\lambda_p$ $[-]$ the plan area index of the urban roughness elements, $A_{f,b}$ [m] the actual frontal area of buildings, $A_{f,v}$ [m] the actual frontal area of vegetation, $A_{tot}$ [m] the total urban plan area, and $P_v$ $[-]$ the ratio between vegetation drag $C_{Dv}$ and building drag $C_{Db}$. The average height $\overline{H}_{urb}$ [m] and the plan area index of the urban roughness elements $\lambda_p$ $[-]$ are calculated as follows (Kent et al.,

2017):

$$\overline{H}_{urb} = \frac{H_{can} A_{p,b} + H_{tree} (1 - P_{3D}) A_{p,v}}{A_{p,b} + (1 - P_{3D}) A_{p,v}} , \tag{192}$$

$$\lambda_p = \frac{A_{p,b} + (1 - P_{3D}) A_{p,v}}{A_{tot}} , \tag{193}$$

where $H_{can}$ [m] is the urban canyon height, $H_{tree}$ [m] the tree height, $A_{p,b} = W_{roof}$ [m] the building plan area, $A_{p,v} = 4r_{tree}$ [m] the tree plan area, $A_{tot} = W_{roof} + W_{can}$ [m] the total urban plan area, and $P_{3D}$ [−] the volumetric/aerodynamic porosity. The volumetric/aerodynamic porosity $P_{3D}$ is calculated as a function of the optical porosity $P_{2D}$ (Guan et al., 2003):

$$P_{3D} = P_{2D}{}^{0.40} , \tag{194}$$

$$P_{2D} = exp(-K_{opt} LAI) , \tag{195}$$

The optical porosity $P_{2D}$ [−] is computed identically to the direct beam transmission through vegetation canopy (Sect. 1.1.3) where $K_{opt}$ [−] is the light extinction parameter, and LAI [−] the leaf area index. The ratio $P_v$ [−] between vegetation drag $C_{Dv}$ and building drag $C_{Db}$ is calculated as (Guan et al., 2000):

$$P_v = \frac{-1.251 P_{3D}^2 + 0.489 P_{3D} + 0.803}{C_{Db}} , \tag{196}$$

where $C_{Db} = 1.2$ [−] (Macdonald et al., 1998). The actual frontal area of buildings $A_{f,b}$ [m] and vegetation $A_{f,v}$ [m] is calculated as (Kent et al., 2017):

$$A_f = \frac{\overline{H}_{urb}}{\overline{H}_{urb} - h_{d,can}} A_f^* , \tag{197}$$

where $A_f^*$ [m] is the unsheltered frontal area of buildings $A_{f,b}^* = H_{can}$ [m] and trees $A_{f,v}^* = 2r_{tree}$ [m].

The total roughness length of roof $z_{om,r}$ [m] and ground $z_{om,g}$ [m] cover are calculated as the maximum of the individual patch roughness lengths $z_{om,i}$ [m]. It is assumed that the largest roughness elements of a surface will govern the wind profile.

$$z_{om,r} = max(z_{om,r,veg}, z_{om,r,imp}) , \tag{198}$$

$$z_{om,g} = max(z_{om,g,veg}, z_{om,g,bare}, z_{om,g,imp}) , \tag{199}$$

where $z_{om,r,veg}$ [m] is the roughness length of roof vegetation, $z_{om,r,imp}$ [m] of impervious roof, $z_{om,g,veg}$ [m] of ground vegetation, $z_{om,g,bare}$ [m] of bare ground, and $z_{om,g,imp}$ [m] of impervious ground. The vegetation roughness length $z_{om,veg}$ [m] and vegetation displacement height $h_{disp,veg}$ [m] are calculated as a function of the vegetation height $h_{veg}$ [m] (Brutsaert, 1982):

$$z_{om,veg} = 0.123 h_{veg} , \tag{200}$$

$$z_{oh,veg} = z_{ow,veg} = 0.1 z_{om,veg} , \tag{201}$$

$$h_{d,veg} = 0.67 h_{veg} , \tag{202}$$

where $h_{veg}$ [m] is the vegetation canopy height. The momentum roughness length of bare soil $z_{om,bare} = 0.003$ [m], road $z_{om,road} = 0.003$ [m], and impervious roof $z_{om,roof} = 0.01$ [m] are chosen according to values used by Wieringa (1993), Su (2002), and Wang et al. (2013). The roughness lengths for heat and water vapour are assumed to be one tenth of the momentum roughness length:

$$z_{oh,bare} = z_{ow,bare} = 0.1 z_{om,bare} \; , \tag{203}$$

$$z_{oh,road} = z_{ow,road} = 0.1 z_{om,road} \; , \tag{204}$$

$$z_{oh,roof} = z_{ow,roof} = 0.1 z_{om,roof} \; , \tag{205}$$

### 3.3 Aerodynamic resistance, $r_{ah}$

The aerodynamic resistance parametrizes the transport of sensible and latent heat caused by buoyancy and turbulence in the atmospheric surface layer and is based on the Monin-Obukhov similarity theory (Monin and Obukhov, 1954; Arya, 2001). Solving the complete Monin-Obukhov similarity theory is computationally demanding though and UT&C applies a simplified parametrization developed by Mascart et al. (1995) and applied by Noilhan and Mafhouf (1996), Masson (2000), Wang et al. (2013), and Fatichi et al. (2012a, b, c) (Sect. 3.3.1). The vertical aerodynamic resistance within the canyon is calculated similarly to an undercanopy resistance for a tree covered landsurface as described by Mahat et al. (2013) (Sect. 3.3.2). The horizontal aerodynamic resistance within the canyon describing the turbulent transport between wall surface and canyon air is calculated using the parametrization developed by Rowley et al. (1930) and Rowley and Eckley (1932) and applied by Masson (2000) and Wang et al. (2013) (Sect. 3.3.3). The aerodynamic resistances to the transport of heat and water vapour are assumed equal, i.e. $r_{ah} = r_{aw}$. This is a common approximation in land surface, hydrological, and urban canopy models (Viterbo and Beljaars, 1995; Sellers et al., 1996a; Noilhan and Mafhouf, 1996; Bertoldi et al., 2006; Ivanov et al., 2008a; Ryu et al., 2011; Wang et al., 2013; Ryu et al., 2016; Fatichi et al., 2012a, b, c).

### 3.3.1 Aerodynamic resistance: Above canyon $r_{ah_r}$, $r_{ah_c}$

The aerodynamic resistance from the roof surface $r_{ah_r}$ [m s$^{-1}$] and the canyon air $r_{ah_c}$ [m s$^{-1}$] to the atmospheric reference height $Z_{atm}$ [m] is calculated using the simplified parametrization developed by Mascart et al. (1995) as applied in the ecohydrological model T&C (Fatichi et al., 2012a, b, c).

The aerodynamic resistance $r_{ah}$ [s m$^{-1}$] is calculated as a function of the neutral transport coefficient $C_n$ and an empirical equation $F_h = f(Ri_B)$ accounting for atmospheric stability as follows:

$$r_{ah} = \frac{1}{C_n F_h(Ri_B) u_a} \; , \tag{206}$$

Where $u_a$ [m s$^{-1}$] is the wind speed at atmospheric reference height, and $C_n$ and $F_h = f(Ri_B)$ are calculated as:

$$C_n = \frac{k^2}{\ln\big[(z_{atm} - d)/z_{om}\big]^2} \; , \tag{207}$$

$$F_h(Ri_B) = \left[1 - \frac{15 Ri_B}{1 + c_h \sqrt{|Ri_B|}}\right] \left[\frac{\ln[(z_{atm} - d)/z_{om}]}{\ln[(z_{atm} - d)/z_{oh}]}\right] \quad \text{if } Ri_B \leq 0 \,,$$

$$F_h(Ri_B) = \left[\frac{1}{1 + 15 Ri_B \sqrt{1 + 5 Ri_B}}\right] \left[\frac{\ln[(z_{atm} - d)/z_{om}]}{\ln[(z_{atm} - d)/z_{oh}]}\right] \text{ if } Ri_B > 0 \,, \tag{208}$$

$c_h$ is calculated as:

$$c_h = 15 c_h{}^* C_n \left[(z_{atm} - d)/z_{oh}\right]^{p_h} \left[\frac{\ln[(z_{atm} - d)/z_{om}]}{\ln[(z_{atm} - d)/z_{oh}]}\right] \,, \tag{209}$$

$$c_h{}^* = 3.2165 + 4.3431\mu + 0.5360\mu^2 - 0.0781\mu^3 \,, \tag{210}$$

$$p_h = 0.5802 - 0.1571\mu + 0.0327\mu^2 - 0.0026\mu^3 \,, \tag{211}$$

$$\mu = \ln(z_{om}/z_{oh}) \,, \tag{212}$$

where $u_a$ [m s$^{-1}$] is the wind speed at the atmospheric reference height, k = 0.4 the von Karman constant, $z_{atm}$ [m] the atmospheric reference height, d [m] the zero plane displacement, and $z_{zoh}$ and $z_{zom}$ [m] the roughness lengths of heat and
 momentum, respecivley. The bulk Richardson number $Ri_B$ (Mascart et al., 1995; Abdella and McFarlane, 1996; van den Hurk and Holtslag, 1997) including the correction proposed by Kot and Song (1998) is calculated as:

$$Ri_B = f^2 \frac{g(\theta_a - \theta_s)(z_{atm} - d)}{0.5(\theta_a + \theta_s)u_a{}^2} \,, \tag{213}$$

$$f^2 = [1 - z_{om}/(z_{atm} - d)]^2/[1 - z_{oh}/(z_{atm} - d)] \,, \tag{214}$$

where $\theta_a$ and $\theta_s$ [K] are the potential air and surface temperature which are the temperatures corrected for the pressure gradient
 in the atmosphere. Note that using the potential temperature neglects the density stratification due to humidity gradients (Brutsaert, 2005). Hence, UT&C includes the option of using the virtual potential temperature which accounts for the influence of humidity on the boundary layer stability. This modification is proposed as high canyon humidity is observed during night times caused by stable boundary layer conditions. The bulk Richardson number describes the boundary layer stability condition. A stable boundary layer results in $Ri_B > 0$ and an unstable boundary layer in $Ri_B < 0$. Equation (208) for stable conditions is
 modified from its original form (Mascart et al., 1995) according to Noilhan and Mafhouf (1996) and van den Hurk and Holtslag (1997).

The aerodynamic resistance formulation of Mascart et al. (1995) reaches infinity ($r_{ah} = \infty$) and prohibits turbulent transport in completely windless conditions ($u_a = 0$). This is almost never observed in reality (Kondo and Ishida, 1997) and UT&C computes the aerodynamic resistance according to Beljaars (1994) at wind speeds $u_a < 0.05$:

$$\frac{1}{r_{ah}} = 0.15 \left[\frac{g\nu}{0.5(\theta_s + \theta_a)Pr^2}\right]^{1/3} (\theta_s - \theta_a)^{1/3} \,, \tag{215}$$

where g = 9.81 [m s$^{-2}$] is the gravitational acceleration, $\nu = 1.5^{-5}$ [m$^2$ s$^{-1}$] and $Pr = 0.71$.

The aerodynamic resistance above the roof $r_{ah_r}$ is cacluated from the roof level $H_{can}$ to the atmospheric reference height $Z_{atm}$. It is assumed that the area averaged roof temperature ($T_r = f_{r,veg} T_{r,veg} + f_{r,imp} T_{r,imp}$) determines boundary layer stability. The displacement height and roughness length of the roof cover is calculated as described in Sect.3.2. The aerodynamic

resistance above the canyon $r_{ah_c}$ is calculated from the canyon calculation height $Z_{calc}$ to the atmospheric reference height $Z_{atm}$. The canyon calculation height is $Z_{calc} = h_{disp,can} + z_{0m,can}$ [m] (Sect. 3.2) for simplicity.

### 3.3.2 Aerodynamic resistance: Within canyon $r_{ah_g}, r_{ah1_w}, r_{ah2_w}$

The vertical aerodynamic resistances within the urban canyon, $r_{ah_g}$, $r_{ah1_w}$, and $r_{ah2_w}$ [s m$^{-1}$], are calculated according to the formulation of vegetation undercanopy resistance as developed by Mahat et al. (2013) and applied by Fatichi et al. (2012a, b, c). Mahat et al. (2013) derived the vegetation undercanopy resistance applying a logarithmic wind profile above the canopy, an exponential wind profile within the canopy, and a logarithmic wind profile close to the ground surface. These wind profile assumptions match with the wind profiles commonly used in urban canopy parametrizations (Masson, 2000; Wang et al., 2013) as described in Sect. 3.1. Hence, the urban aerodynamic undercanopy resistance $r'_{ah}$ [s m$^{-1}$] is derived similarly to a vegetation undercanopy resistance and is calculated as follows (Mahat et al., 2013):

$$r'_{ah} = \frac{H_{can}e^{\hat{\beta}}}{\hat{\beta}K_{H_{can}}} \left( e^{-\hat{\beta}\frac{Z_{can,ref}}{H_{can}}} - e^{-\hat{\beta}\frac{h_{d,can}+z_{om,can}}{H_{can}}} \right) + \frac{1}{k^2 u_{Z_{can,ref}}} \ln\left(\frac{Z_{can,ref}}{z_{om,g}}\right)^2 , \tag{216}$$

where $H_{can}$ [m] is the canyon height, $\hat{\beta} = \frac{\ln[u_{atm}/u_{H_{can}}]}{Z_{atm}/H_{can}-1}$ the attenuation coefficient of the exponential wind profile (Sect. 3.1), $K_{H_{can}} = \kappa^2 u_{atm}\frac{H_{can}-h_{d,can}}{ln([Z_{atm}-h_{d,can}]/z_{om,can})}$ the eddy diffusion coefficient at canyon height (Mahat et al., 2013), $Z_{can,ref}$ [m] the selected reference height within the canyon close to the ground where exponential wind profile changes to logarithmic wind profile, $h_{d,can}$ [m] the urban canopy displacement height, $z_{om,can}$ [m] the urban canopy roughness length, $u_{Z_{can,ref}}$ [m s$^{-1}$] the wind speed at $Z_{can,ref}$, and $z_{om,g}$ [m] the ground roughness length. The undercanopy resistance depends on the turbulence and stability of the roughness sublayer. The following formulations are used to adjust for atmospheric stability (Choudhury and Monteith, 1988):

$$r'_{ah} = \frac{r'_{ah}}{(1-5Ri)^{3/4}} \qquad \text{if } Ri \leq 0 , \tag{217}$$

$$r'_{ah} = \frac{r'_{ah}}{(1-5Ri)^2} \qquad \text{if } Ri > 0 , \tag{218}$$

$$Ri = \frac{g(T_{can} - T_{s,av})Z_{can,ref}}{(0.5(T_a+T_s)+273.15)u^2_{Z_{can,ref}}} , \tag{219}$$

where Ri is the Richardson number within the canyon. $Ri = 0.16$ is used for $Ri > 0.16$ as Eq. (218) reaches infinity at $Ri = 0.2$. The superscript prime indicates the undercanopy quantities. The reference height within the urban canyon $Z_{can,ref}$ is assumed to be 1.5 m and the wind speed at $Z_{can,ref}$ is $u_{Z_{can,ref}} = u_{H_{can}} exp[-\hat{\beta}(1 - Z_{can,ref}/H_{can})]$. The canyon temperature $T_{can}$ [K] and the area averaged ground surface temperature including trees $T_{s,av}$ [K] are used to account for the atmospheric stability within the urban canyon. The effect of trees and ground vegetation in modifying the undercanopy resistance are taken into account in the canyon displacement heigth $h_{d,can}$, canyon roughness length $z_{om,can}$, and ground roughness length $z_{om,g}$ (Sect. 3.2).

The aerodynamic resistance $r_{ah_g}$ is calculated from the ground roughness length $z_{om,g}$ level to the canyon calculation height $Z_{calc}$. The aerodynamic resistances $r_{ah1_w}$ and $r_{ah2_w}$ are calculated from mid height of layer 1 and 2 to the canyon calculation

height as:

$$r_{ah1_w} = r_{ah}(z_{om,g} \rightarrow h_{d,can} + z_{om,can}) - r_{ah}(z_{om,g} \rightarrow Z_{p,w1,m}) \,, \tag{220}$$

$$r_{ah2_w} = r_{ah}(z_{om,g} \rightarrow h_{d,can} + z_{om,can}) - r_{ah}(z_{om,g} \rightarrow Z_{p,w2,m}) \,, \tag{221}$$

### 3.3.3 Aerodynamic resistance: Wall $r_w$

The horizontal aerodynamic resistance $r_w$ [s m$^{-1}$] to the turbulent transport of sensible and latent heat from the wall surface to the canyon air is calculated as (Rowley et al., 1930; Rowley and Eckley, 1932; Masson, 2000; Wang et al., 2013):

$$r_w = C_p \rho_a (11.8 + 4.2\sqrt{u(Z_{p,can})^2 + w(Z_{p,can})^2})^{-1} \,, \tag{222}$$

where $u(Z_{p,can})$ [m s$^{-1}$] is the horizontal, and $w(Z_{p,can})$ [m s$^{-1}$] the vertical wind speed within the urban canyon at height $Z_{p,can}$ (Sect. 3.1). The original formulation is multiplied by the air density $\rho_a$ [kg m$^{-3}$] and the specific heat capacity of air $C_p$ [J kg$^{-1}$ K$^{-1}$] to be consistent with the general resistance formulations and the apparent unit incongruence in Eq. (222) is due to the empirical coefficients used in Rowley et al. (1930) and Rowley and Eckley (1932). The effect of atmospheric stability on the aerodynamic resistance is not considered in the formulations of Rowley et al. (1930) and Rowley and Eckley (1932). The described horizontal aerodynamic resistance is calculated at the mid heights of layer 1 and 2.

### 3.4 Leaf boundary resistance, $r_b$

The leaf boundary resistance describes the resistance imposed by a thin layer of air around the leaf surface. UT&C calculates the one-sided leaf boundary resistance per unit leaf area $r_b$ [s m$^{-1}$] as a function of leaf boundary conductance at forced turbulence $g_{b,forc}$ [m s$^{-1}$] and leaf boundary conductance at free convection $g_{b,free}$ [m s$^{-1}$] (Fatichi et al., 2012a, b, c):

$$r_b = \frac{1}{g_{b,free} + g_{b,forc}} \,, \tag{223}$$

The leaf boundary conductance at free convection $g_{b,free}$ is calculated according to Monteith (1973) and Leuning et al. (1995) if $T_s > T_a$. The leaf boundary conductance at forced turbulence ($u_a > 0$) is calculated as follows (Jones, 1983; Choudhury and Monteith, 1988; Shuttleworth and Gurney, 1990; Fatichi et al., 2012a, b, c):

$$g_{b,free} = \frac{0.5 D_h G_r^{0.25}}{d_{leaf}} \,, \tag{224}$$

$$g_{b,forc} = \left(\frac{2a}{\hat{\beta}}\right)\left(\frac{u_{H_{veg}}}{d_{leaf}}\right)^{1/2}\left[1 - e^{-\hat{\beta}/2}\right] \,, \tag{225}$$

where $d_{leaf}$ [m] is the characteristic leaf dimension, $D_h = 1.9 \cdot 10^{-5}$ [m$^2$ s$^{-1}$] the molecular diffusivity of heat, $a = 0.01$ [m s$^{-1/2}$] an empirical coefficient (Choudhury and Monteith, 1988), $\hat{\beta}$ [$-$] the wind profile attenuation coefficient, and $G_r = 1.6 \cdot 10^8 (T_s - T_a) d_{leaf}^3$ [$-$] the Grashof number. The wind speed at vegetation canopy height $u_{H_{veg}}$ is calculated as described in Sect. 3.1. Equations (224) and (225) are derived under the assumption of a linear distribution of leaf area index over the vegetation height $L(z) = LAI/H_{veg}$ (Choudhury and Monteith, 1988) and the effects of atmospheric stability are not

considered. Note that $r_b$ is the leaf boundary resistance for one side of the leaf. Hence, the leaf boundary resistance has to be rescaled by a factor of two to account for both leaf sides and by the LAI to account for the whole vegetation canopy. Leaf

790 boundary resistance increases with larger leaf size and lower wind speed.

## 3.5 Soil resistance, $r_{soil}$

The soil resistance $r_{soil}$ $[\text{s m}^{-1}]$ describes the transport of water vapour from the soil pores to the air above the soil surface boundary layer. The transport of water vapour from the soil to the air is controlled by atmospheric conditions, diffusion in the soil boundary layer, moisture transport within the soil, and wetness of the surface soil layer. UT&C applies the expressions

795 derived by Haghighi et al. (2013) and implemented in the ecohydrological model T&C (Fatichi et al., 2012a, b, c). Haghighi et al. (2013) calculates the soil resistance $r_{soil}$ $[\text{s m}^{-1}]$ as a function of soil type, soil water content in the top layer, and soil boundary layer characteristics. The total soil resistance $r_{soil}$ $[\text{s m}^{-1}]$ is the sum of soil boundary layer resistance $r_{vbl}$ $[\text{s m}^{-1}]$ and internal capillary-viscous resistance $r_{sv}$ $[\text{s m}^{-1}]$:

$$r_{soil} = r_{vbl} + r_{sv} \,, \tag{226}$$

800 The soil internal capillary-viscous resistance $r_{sv}$ accounts for the water vapour transport within the porous media (soil) while the soil boundary layer resistance $r_{vbl}$ accounts for the presence of a boundary layer at the soil surface which poses a resistance to the transport of water vapour from the soil surface to the air just above the soil (Haghighi et al., 2013).

The soil internal capillary-viscous resistance $r_{sv}$ is calculated as a function of soil water content of the surface layer $\theta_S$ and a proportionality constant $\gamma$ (Haghighi et al., 2013):

805
$$r_{sv} = \frac{\gamma}{4K(\theta_S)} \,, \tag{227}$$

where $K$ $[\text{m s}^{-1}]$ is the soil hydraulic conductivity at soil water content $\theta_S$. The proportionality constant $\gamma$ $[-]$ transforms the unit of capillary liquid to the unit of vapor flux (Haghighi et al., 2013):

$$\gamma = \frac{\hat{\alpha} e_{sat} - e_a}{\rho_w R_d T_g} \,, \tag{228}$$

where $e_{sat}$ and $e_a$ $[\text{Pa}]$ are the saturation vapour pressure in the soil and the vapour pressure of the air, respectively, and $\hat{\alpha}$

810 is the relative humidity of air in the soil pores. $T_g$ $[\text{K}]$ is the soil surface temperture, $\rho_w$ $[\text{kg m}^{-3}]$ the water density, and $R_d$ $[\text{J kg}^{-1}\,\text{K}^{-1}]$ the water vapor gas constant. The relative humidity in the soil pores $\hat{\alpha}$ is calculated as Philip (1957):

$$\hat{\alpha} = \exp\left[-\frac{g\Psi_S}{R_d T_g}\right] \,, \tag{229}$$

where $\Psi_S$ $[\text{m}]$ is the water potential in the soil surface layer, and $g = 9.81$ $[\text{m s}^{-2}]$ the gravity acceleration constant.

The soil boundary layer resistance $r_{vbl}$ is calculated as (Haghighi et al., 2013):

815
$$r_{vbl} = \frac{\delta_m + P_{sz} f(\theta_S)}{Da} \,, \tag{230}$$

where $\delta_m$ [m] is the soil boundary layer thickness, $P_{sz}$ [m] the pore size, and $Da$ [m$^2$ s$^{-1}$] the molecular diffusivity of water vapour. The function $f(\theta_S)$ [−] describes the coupling of surface layer soil water content $\theta_S$ and diffusive resistance. The boundary layer thickness $\delta_m$ is calculated as (Shahraeeni et al., 2012):

$$\delta_m = 2.26\,10^{-3}u_a^{-0.5} , \tag{231}$$

where $u_{ref}$ [m s$^{-1}$] is the wind speed at reference height for bare and vegetated ground (2 m on the roof, 1.5 m on the ground). The soil pore size $P_{sz}$ [m] is correlated with the soil texture and can be computed as (Haghighi et al., 2013):

$$P_{sz} = 11.12\,n^{3.28}\,10^{-6} , \tag{232}$$

where n is the pore size distribution parameter of the van-Genuchten soil water retention curve (Mualem, 1976; van Genuchten, 1980). According to Haghighi et al. (2013), $f(\theta_S)$ is calculated as follows:

$$f(\theta_s) = \frac{2}{\pi} \frac{\left[\sqrt{\frac{\pi}{4\theta_S}} - 1\right]}{\sqrt{4\theta_S}} , \tag{233}$$

UT&C typically considers a top soil layer with a depth of 10 [mm]. The formulation of $r_{soil}$ proposed by Haghighi et al. (2013) and described here is mostly based on physical principles. Therefore, most uncertainty lays in the definition of soil texture and soil layer discretization (Fatichi et al., 2012a, b, c). Note that the soil resistance $r_{soil} = 0$ and the relative humidity $\hat{\alpha} = 1$ in the case of ponding water.

## 3.6   Stomata resistance, $r_s$

UT&C calculates the stomata resistance to the turbulent transport of water vapour from leaf interior to exterior air $r_s$ [s m$^{-1}$] as a function of plant photosynthetic activty. Plants open their stomata to allow the transfer of $CO_2$ from the atmosphere to their chloroplasts inside the leaves. The open stomata lead to an inevitable loss of water vapour from the water-saturated tissue within the plants (Sellers et al., 1997). The stomata resistance is calculated individually for roof vegetation, ground vegetation, and trees. Following a two-big leaf approach, the stomata resistance for sunlit and shaded leaf area is calculated separately to account for light limitation in the shaded vegetation fraction. One single leaf temperature for sunlit and shaded vegetation canopy is used though to keep the number of prognostic temperatures small (Fatichi et al., 2012a, b, c).

### 3.6.1   Canopy partition and scaling from leaf to canopy

It is necessary to scale processes from leaf to canopy level due to several non-linear interactions (de Pury and Farquhar, 1997; Wang and Leuning, 1998; Dai et al., 2004; Fatichi et al., 2012a, b, c). The sunlit $F_{sun}$ [−] and shaded $F_{shd}$ [−] canopy fraction is calculated assuming an exponential decay of direct beam radiation within the vegetation canopy (Dai et al., 2004; Ivanov et al., 2008b; Fatichi et al., 2012a, b, c):

$$F_{sun} = \frac{1}{LAI} \frac{1 - e^{(-K_{opt}LAI)}}{K_{opt}} , \tag{234}$$

$$F_{shd} = 1 - F_{sun} , \tag{235}$$

where $K_{opt}$ [−] is the light extinction parameter, and LAI [−] the leaf area index. The scaling factor for photosynthetic capacity $F_N$ [−] is calculated as in Fatichi et al. (2012a, b, c):

$$F_{N,sun} = \frac{1 - e^{-(K_N + K_{opt})LAI}}{K_N + K_{opt}} \ , \tag{236}$$

$$F_{N,shd} = \frac{1 - e^{-(K_N \, LAI)}}{K_N} - \frac{1 - e^{-(K_N + K_{opt})LAI}}{K_N + K_{opt}} \ , \tag{237}$$

where $K_N$ [−] is the canopy nitrogen decay coefficient. Subsequently, the maximum Rubisco capacity at 25°C for unit of leaf area [μmol $CO_2$ s$^{-1}$ m$^{-2}$ leaf] is calculated as (Fatichi et al., 2012a, b, c):

$$V_{max,sun} = V_{c,max}^T \, \frac{F_{N,sun}}{F_{sun}LAI} \ , \tag{238}$$

$$V_{max,shd} = V_{c,max}^T \, \frac{F_{N,shd}}{F_{shd}LAI} \ , \tag{239}$$

where $V_{c,max}^T$ [μmol $CO_2$ s$^{-1}$ m$^{-2}$] is a model input parameter and specifies the maximum Rubisco capacity at the top of the vegetation canopy at 25°C.

The results of the photosynthetic model at leaf level need to be scaled back to the canopy level for computing the net assimilation rate $\overline{A_{nC}}$ [μmol $CO_2$ s$^{-1}$ m$^{-2}$] and the leaf maintenance respiration $\overline{R_{dC}}$ [μmol $CO_2$ s$^{-1}$ m$^{-2}$] (Sect. 3.6.2 and 3.6.3) (Fatichi et al., 2012a, b, c).

$$\overline{A_{nC}} = A_{nC,sun} \, F_{sun}LAI + A_{nC,shd} \, F_{shd}LAI \ , \tag{240}$$

$$\overline{R_{dC}} = R_{dC,sun} \, F_{sun}LAI + R_{dC,shd} \, F_{shd}LAI \ , \tag{241}$$

The stomata resistances, $r_{s,sun}$ and $r_{s,shd}$ [s m$^{-1}$] (Sect. 3.6.2), are kept at the leaf scale as this is needed to caculate transpiration (Fatichi et al., 2012a, b, c).

### 3.6.2 Stomata conductance and stomata resistance

UT&C applies the biochemical model implemented in the ecohydrological model T&C (Fatichi et al., 2012a, b, c) to describe the coupling between photosynthesis and stomata resistance. The stomata resistance to water vapour $r_{s,H_2O}$ [m$^2$ s$^1$ μmol$^{-1}$ $CO_2$] is calculated as the inverse of the stomata conductance $g_{s,CO_2}$:

$$r_{s,H_2O} = \frac{1}{g_{s,CO_2}1.64} \ , \tag{242}$$

where 1.64 is the ratio of stomata resistance for $CO_2$ and stomata resistance for $H_2O$ ($r_{s,CO_2}/r_{s,H_2O} = 1.64$) (von Caemmerer and Farquhar, 1981). The following expression converts the resistance from biochemical units of [m$^2$ s$^1$ μmol$^{-1}$ $CO_2$] to hydrological units [s m$^{-1}$] (Sellers et al., 1996b):

$$r_s(s \, m^{-1}) = \frac{1}{0.0224} \frac{T_f \, P_{atm}}{(T + 273.15)P_{atm,0}} 10^6 r_{s,H_2O}(m^2 \, s \, \mu mol^{-1} CO_2) \ , \tag{243}$$

where

$P_{atm}$ = [Pa] is the atmospheric pressure.

$P_{atm,0}$ = 101325 [Pa] is the reference atmospheric pressure.

$T_f$ = 273.15 [K].

$T$ = [°C] is the leaf temperature.

$r_{s,H_2O}$ = [m$^2$ s µmol$^{-1}$ CO$_2$] is the resistance to convert.

Experiments have shown a relationship between stomata behaviour and net CO$_2$ assimilation rate $A_{nC}$, atmospheric vapor pressure deficit $\Delta e$, and intercellular CO$_2$ concentration $c_i$ (Ball et al., 1987; Leuning, 1995; Gao et al., 2002). UT&C calculates the stomata conductance $g_{s,CO_2}$ [µmolCO$_2$ m$^{-2}$ leaf s$^{-1}$] according to Leuning (1990, 1995) and as implemented by Fatichi et al. (2012a, b, c) as:

$$g_{s,CO_2} = g_{0,CO_2} + a\frac{A_{nC}}{(c_c - \Gamma^*)}f(\Delta e)\,P_{atm} \,, \tag{244}$$

$$f(\Delta e) = \left(\frac{1}{1 + \Delta e/\Delta_0}\right) \,, \tag{245}$$

where

$A_{nC}$ = [µmol CO$_2$ m$^{-2}$ s$^{-1}$] is net CO$_2$ assimilation rate at leaf scale.

$c_c$ = [Pa] is the leaf internal $CO_2$ concentration.

$\Gamma^*$ = [Pa] is the CO$_2$ compensation point.

$P_{atm}$ = [Pa] is the atmospheric pressure.

$g_{0,CO_2}$ = [µmol CO$_2$ m$^{-2}$ leaf s$^{-1}$] is the minimum stomatal conductance caused by cuticular conductance and imperfect stomatal closure when $A_{nC}$ is negative.

$\Delta e$ = [Pa] is the vapor pressure deficit.

$\Delta_0$ = [Pa] is an empirical coefficient that expresses the value of vapor pressure deficit at which $f(\Delta e = \Delta_0) = 0.5$.

$a$ = [−] is an empirical parameter connecting stomatal aperture and net assimilation.

The leaf internal $CO_2$ partial pressure $c_c$ is unknown a priori and an iterative approach is needed. Equation (246 is solved iteratively to calculate resistance between leaf chloroplasts and atmosphere (Fatichi et al., 2012a, b, c):

$$A_{nC} = \frac{c_a - c_c}{P_{atm}\left(1.64r_s + r_{mes} + 1.37r_b + r_a\right)} \,, \tag{246}$$

where

$A_{nC}$ = [µmol CO$_2$ m$^{-2}$ s$^{-1}$] is net CO$_2$ assimilation rate at leaf scale.

$c_c$ = [Pa] is the leaf internal $CO_2$ concentration.

$c_a$ = [Pa] is the atmospheric CO$_2$ concentration at the leaf surface.

$r_s$ = [m$^2$ s$^1$ µmol$^{-1}$ H$_2$O] is the stomata resistance. $r_{s,CO_2}/r_{s,H_2O} = 1.64$ (von Caemmerer and Farquhar, 1981).

$r_b$ = [m$^2$ s$^1$ µmol$^{-1}$ H$_2$O] is the leaf boundary resistance. $r_{b,CO_2}/r_{b,H_2O} = 1.37$ (von Caemmerer and Farquhar, 1981).

$r_{mes}$ = [m$^2$ s$^1$ µmol$^{-1}$ CO$_2$] is the mesophylic resistance (Warren, 2006).

$r_a$ = [m$^2$ s$^1$ µmol$^{-1}$ CO$_2$] is the aerodynamic resistance.

### 3.6.3 Biochemical model of photosynthesis

The biochemical model of photosynthesis (Fatichi et al., 2012a, b, c) calculates the net and gross photosynthetic assimilation rate, $A_{nC}$ and $A^*$ [$\mu$molCO$_2$ m$^{-2}$ s$^{-1}$], as a function of three limiting rates of enzyme kinectics. The RuBP-carboxylase limited carboxylation rate $J_c$ describes the amount and velocity of the carboxylating enzyme Rubisco. The maximum rate of photosynthetically active radiation captured by the leaf chlorophyll $J_e$ accounts for light limitations. The export-limited (for C$_3$ plants) and the PEP-carboxylase limited (for C$_4$ plants) rate of carboxylation $J_s$ describes the capacity of the leaf to use or export products of photosynthesis. The transition between the three rates $J_c$, $J_e$, and $J_s$ is not abrupt. The three processes are coupled with a continous smooth function (Fatichi et al., 2012a, b, c) which is described with two quadratic equations according to Collatz et al. (1991). The gross photosynthetic assimilation rate $A^*$ [$\mu$mol CO$_2$ m$^{-2}$ s$^{-1}$] is calculated solving both quadratic equations for their smaller roots:

$$\alpha_{ce} J_p^2 - J_p(J_c + J_e) + J_e J_c = 0 \ ,$$
$$\alpha_{ps}(A^*)^2 - A^*(J_p + J_s) + J_p J_s = 0 \ , \tag{247}$$

$J_p$ = [$\mu$mol CO$_2$ m$^{-2}$ s$^{-1}$] is the smoothed minimum of $J_c$ and $J_e$.

$A^*$ = [$\mu$mol CO$_2$ m$^{-2}$ s$^{-1}$] is the gross assimilation rate for unit leaf before accounting for soil moisture stress.

$\alpha_{ce}$ = is a coupling coefficients (Sellers et al., 1996a; Bonan et al., 2011) where $\alpha_{ce} = 0.98$ for C$_3$ species and $\alpha_{ce} = 0.80$ for C$_4$ species.

$\alpha_{ps}$ = is a coupling coefficients (Sellers et al., 1996a; Bonan et al., 2011) where $\alpha_{ps} = 0.95$.

Subsquently, the net assimilation rate at leaf scale $A_{nC}$ [$\mu$mol CO$_2$ m$^{-2}$ s$^{-1}$] is calculated as the difference between gross assimilation rate corrected for water stress $A_C$ and leaf maintenance respiration $R_{dC}$ (Fatichi et al., 2012a, b, c):

$$A_{nC} = A_C - R_{dC} \ , \tag{248}$$
$$A_C = \beta_S A^* \ , \tag{249}$$

where

$A_C$ = [$\mu$mol CO$_2$ m$^{-2}$ s$^{-1}$] is the gross assimilation rate.

$R_{dC}$ = [$\mu$mol CO$_2$ m$^{-2}$ s$^{-1}$] is the leaf maintenance respiration assumed to be equal to the leaf dark respiration, which is a coarse approximation for respiration during daytime (Villar et al., 1995; Atkin et al., 1997).

$\beta_S$ = [−] is a water stress factor limiting canopy photosynthesis based on leaf water potential $\Psi_L$ [MPa].

The leaf maintenance respiration $R_{dC}$ [$\mu$mol CO$_2$ m$^{-2}$ s$^{-1}$] is estimated as (Collatz et al., 1991, 1992; Bonan et al., 2011):

$$R_{dC} = 0.015 \, V_{c,max} \exp\left[\frac{H_a(T_v - T_{ref})}{(T_{ref} R T_v)}\right] \frac{1 + exp\left(\frac{T_{ref}\Delta S - H_d}{T_{ref} R}\right)}{1 + exp\left(\frac{T_v \Delta S - H_d}{T_v R}\right)} \quad \text{for } C_3 \ , \tag{250}$$

$$R_{dC} = 0.025 \, V_{c,max} \, 2.0^{0.1(T_v^C - 25)} \left[1 + e^{1.3(T_v^C - 55)}\right]^{-1} \quad \text{for } C_4 \ , \tag{251}$$

where

$V_{c,max} = [\mu mol\ CO_2\ s^{-1}\ m^{-2}]$ is the maximum Rubisco capacity.

$T_v \quad = [K]$ is the leaf temperature.

$T_v^C \quad = [°C]$ is the leaf temperature.

$T_{ref} \quad = 273.15\ [K]$.

$R \quad = 8.314\ [J\ mol^{-1}\ K^{-1}]$ is the universal gas constant.

$H_a \quad = 46.39\ [kJ\ mol^{-1}]$.

$H_d \quad = 150.65\ [kJ\ mol^{-1}]$.

$\Delta S \quad = 0.490\ [kJ\ mol^{-1}\ K^{-1}]$.

910      The water stress factor $\beta_S$, limiting canopy photosynthesis, is based on the leaf water potential $\Psi_L$ [MPa] and calculated as:

$$\beta_S = 1 - \frac{1}{1 + \exp(p_S \Psi_L + q_S)}\ , \tag{252}$$

where

$\Psi_L \quad = [MPa]$ is the leaf water potential.

$p_s \quad = f(\Psi_{S,00}, \Psi_{S,50}\ [MPa])$.

$q_S \quad = f(\Psi_{S,00}, \Psi_{S,50}\ [MPa])$.

$\Psi_{S,00} = [MPa]$ is the water potential threshold where stomata closure begins.

$\Psi_{S,50} = [MPa]$ is the water potential threshold where stomata closure reaches 50%.

     UT&C does not include plant hydraulics (Tuzet et al., 2003; Buckley et al., 2003; Katul et al., 2003; Bohrer et al., 2005;
915 Verbeeck et al., 2007; Vico and Porporato, 2008; Feddes et al., 2001; Sperry et al., 2003; Kirkham, 2005; Sack and Holbrook, 2006; Nobel, 2009) and the leaf water potential $\Psi_L$ is equal to the soil water potential $\Psi_{sR}$ experienced by the plant in the root zone. Note that the maximum Rubisco capacity at $25°C\ V_{c,max}$ [$\mu mol\ CO_2\ m^{-2}\ s^{-1}$] is an important parameter in the biochemical model and it is plant species specific.

RUBISCO LIMITED CARBOXYLATION RATE

920      The RuBP-carboxylase limited carboxylation rate is calculated as (Fatichi et al., 2012a, b, c):

$$J_c = V_m \left[ \frac{c_c - \Gamma^*}{c_c + K_c(1 + O_i/K_o)} \right] \quad \text{for } C_3\ , \tag{253}$$

$$J_c = V_m \qquad\qquad\qquad\qquad \text{for } C_4\ , \tag{254}$$

where

$c_c$ = [Pa] is the partial pressures of $CO_2$ in the leaf chloroplasts.

$O_i$ = [Pa] is the partial pressures of $O_2$ in the leaf chloroplasts.

$V_m$ = [μmol $CO_2$ s$^{-1}$ m$^{-2}$] is the temperature dependent Rubisco capacity at the leaf scale for C3 species $V_{m,C3}$, and C4 species $V_{m,C4}$.

$K_c$ = [Pa] is the temperature dependent Michaelis-Menten constants for $CO_2$.

$K_o$ = [Pa] is the temperature dependent Michaelis-Menten constants for $O_2$.

$\Gamma^*$ = [Pa] is the temperature dependent $CO_2$ compensation point.

925   The temperature dependence of the maximum catalytic Rubisco capacity for C3 species $V_{m,C3}$ [μmol $CO_2$ s$^{-1}$ m$^{-2}$] (Kattge and Knorr, 2007), and for C4 species $V_{m,C4}$ [μmol $CO_2$ s$^{-1}$ m$^{-2}$] (Sellers et al., 1996b; Dai et al., 2004; Bonan et al., 2011) is calculated as:

$$V_{m,C3} = V_{c,max} \exp\left[\frac{H_a(T_v - T_{ref})}{(T_{ref} R T_v)}\right] \frac{1 + exp\left(\frac{T_{ref}\Delta S - H_d}{T_{ref} R}\right)}{1 + exp\left(\frac{T_v \Delta S - H_d}{T_v R}\right)} \, , \tag{255}$$

$$V_{m,C4} = V_{c,max} \left[2.1^{0.1(T_v^C - 25)}\right] \left[\frac{1}{1 + \exp[0.3(T_v^C - 40)]}\right] \left[\frac{1}{1 + \exp(0.2(15 - T_v^C))}\right] \, , \tag{256}$$

930  The temperature dependence of the Michaelis-Menten constant for $CO_2$, $K_c$ [Pa] and $O_2$, $K_o$ [Pa], and the $CO_2$ compensation point $\Gamma^*$ [Pa] are calculated as (Bonan et al., 2011):

$$K_c = K_{c,25} \exp\left[\frac{79.43(T_v - T_{ref})}{(T_{ref} R T_v)}\right] \, , \tag{257}$$

$$K_o = K_{o,25} \exp\left[\frac{36.38(T_v - T_{ref})}{(T_{ref} R T_v)}\right] \, , \tag{258}$$

$$\Gamma^* = \Gamma_{25}^* \exp\left[\frac{37.83(T_v - T_{ref})}{(T_{ref} R T_v)}\right] \, , \tag{259}$$

935   where

$V_{c,max}$ = [μmol $CO_2$ m$^{-2}$ s$^{-1}$] is the maximum Rubisco capacity at 25 °C.

$H_a$ = [kJ mol$^{-1}$] is the species dependent activation energy with a typical range of $H_a = 45 - 95$ [kJ mol$^{-1}$]. A reference value of $H_a = 72$ [kJ mol$^{-1}$] is used if no paramter is provided (Kattge and Knorr, 2007).

$H_d$ = 200 [kJ mol$^{-1}$] is the constant deactivation energy describing the rate of decrease above the optimum temperature.

$\Delta S$ = [kJ mol$^{-1}$ K$^{-1}$] is the species dependent "entropy factor" with a typical range of $\Delta S = 0.625 - 0.665$ [kJ mol$^{-1}$ K$^{-1}$]. A reference value of $\Delta S = 0.649$ [kJ mol$^{-1}$ K$^{-1}$] is used if no paramter is provided (Kattge and Knorr, 2007).

$R$ = 8.314 [J mol$^{-1}$ K$^{-1}$] is the universal gas constant.

$T_{ref}$ = 273.15 [K].

$T_v$ = [K] is the leaf temperature.

$T_v^C$ = [°C] is the leaf temperature.

$K_{c,25}$ = 404.9 $10^{-6}$ $P_{atm}$ [Pa] is the reference value of the Michaelis-Menten constants for $CO_2$ at 25 °C (Bonan et al., 2011).

$K_{o,25}$ = 278.4 $10^{-3}$ $P_{atm}$ [Pa] is the reference value of the Michaelis-Menten constants for $O_2$ at 25 °C (Bonan et al., 2011).

## RATE LIMITED BY PHOTOSYNTHETIC ACTIVE RADIATION (PAR) CAPTURED BY LEAF CHLOROPHYLL

The maximum rate of photosynthetically active radiation captured by the leaf chlorophyll is calculated as (Farquhar et al., 1980; Collatz et al., 1991, 1992; Bonan et al., 2011; Fatichi et al., 2012a, b, c):

940
$$J_e = J \left[ \frac{c_c - \Gamma^*}{c_c + 2\Gamma^*} \right] \qquad \text{for } C_3 , \tag{260}$$

$$J_e = PPFD^* \qquad \text{for } C_4 , \tag{261}$$

where

$c_c$ = [Pa] is the partial pressures of $CO_2$ in the leaf chloroplasts.

$\Gamma^*$ = [Pa] is the temperature dependent $CO_2$ compensation point.

$PPFD^*$ = [μmol $CO_2$ s$^{-1}$ m$^{-2}$] is the effective photosynthetic photon flux density of photosystem II.

$J$ is the smaller root of the following quadratic equation:

945
$$\alpha_J J^2 - (PPFD^* + \frac{J_m}{4}) J + PPFD^* \frac{J_m}{4} = 0 , \tag{262}$$

with

$$PPFD^* = \epsilon\,\beta_Q\,PAR_{abs} \, , \tag{263}$$

$$PAR_{abs} = \frac{PAR_{abs,sun}}{F_{sun}LAI} \qquad \text{for sunlit leaves} \, , \tag{264}$$

$$PAR_{abs} = \frac{PAR_{abs,shd}}{F_{shd}LAI} \qquad \text{for shaded leaves} \, , \tag{265}$$

where

$J_m$     $= [\mu\text{mol equivalent s}^{-1}\,\text{m}^{-2}]$ is the temperature dependent electron transport capacity at leaf scale.

$\alpha_J$     $= 0.7\,[-]$ is a shape parameter (Bonan, 2002).

$\epsilon$     $= [\mu\text{mol CO}_2\,\mu\text{mol}^{-1}\,\text{photons}]$ is the intrinsic quantum efficiency depending on the photosynthesis pathway ($C_3$ or $C_4$). $\epsilon = 0.081\,[\mu\text{mol CO}_2\,\mu\text{mol}^{-1}\,\text{photons}]$ for $C_3$ plants, $\epsilon = 0.040\,[\mu\text{mol CO}_2\,\mu\text{mol}^{-1}\,\text{photons}]$ for $C_4$ plants (Farquhar et al., 1980; Collatz et al., 1991, 1992; Singsaas et al., 2001).

$\beta_Q$     $= 4.57\,[\mu\text{mol photons J}^{-1}]$ is a quanta-to-energy conversion factor between the measurement units (Dye, 2004).

$PAR_{abs}$ $= [\text{W m}^{-2}]$ is the absorbed photosynthetically active radiation at leaf scale.

$F_{sun}$     $= [-]$ is the fraction of sunlit leaves.

$F_{shd}$     $= [-]$ is the fraction of shaded leaves.

$LAI$     $= [-]$ is the leaf area index.

The maximum electron transport capacity $J_m$ $[\mu\text{mol equivalent s}^{-1}\,\text{m}^{-2}]$ as a function of temperature is calculated as (Kattge and Knorr, 2007):

$$J_m = J_{max}\exp\left[\frac{H_a(T_v - T_{ref})}{(T_{ref}\,RT_v)}\right]\frac{1 + exp\left(\frac{T_{ref}\Delta S - H_d}{T_{ref}\,R}\right)}{1 + exp\left(\frac{T_v\Delta S - H_d}{T_v\,R}\right)} \, , \tag{266}$$

$$J_{max} = r_{jv}\,V_{c,max} \, , \tag{267}$$

where

$J_{max}$    $= [\mu\text{mol equivalent s}^{-1}\,\text{m}^{-2}]$ is the maximum electron transport capacity at 25 °C.

$V_{c,max}$ $= [\mu\text{mol CO}_2\,\text{s}^{-1}\,\text{m}^{-2}]$ is the maximum Rubisco capacity.

$r_{jv}$     $= [\mu\text{mol equivalent }\mu\text{mol CO}_2^{-1}]$ is a scaling factor between $V_{c,max}$ and $J_{max}$ with a typical range $r_{jv} = 1.6 - 2.6$.

$H_a$     $= 50\,[\text{kJ mol}^{-1}]$ (Kattge and Knorr, 2007).

$H_d$     $= 200\,[\text{kJ mol}^{-1}]$ (Kattge and Knorr, 2007).

$\Delta S$     $= 0.646\,[\text{kJ mol}^{-1}\,\text{K}^{-1}]$ (Kattge and Knorr, 2007).

$R$     $= 8.314\,[\text{J mol}^{-1}\,\text{K}^{-1}]$ is the universal gas constant.

$T_{ref}$    $= 273.15\,[\text{K}]$.

$T_v$     $= [\text{K}]$ is the leaf temperature.

## PRODUCT EXPORT AND USAGE LIMITED RATE

The export-limited rate of carboxylation (for $C_3$ plants) and the PEP-carboxylase limited rate of carboxylation (for $C_4$ plants) are calculated as:

$$J_s = 3TPU \qquad\qquad \text{for } C_3 \ , \tag{268}$$

$$J_s = k_e \frac{c_c}{P_{atm}} \qquad\qquad \text{for } C_4 \ , \tag{269}$$

where

$TPU = [\text{μmol equivalent s}^{-1}\,\text{m}^{-2}]$ is the temperature dependent triose phosphate utilization at leaf scale.

$k_e \quad = [\text{μmol equivalent s}^{-1}\,\text{m}^{-2}]$ is the PEP Carboxylase coefficient.

$c_c \quad = [\text{Pa}]$ is the partial pressures of $CO_2$ in the leaf chloroplasts.

$P_{atm} = [\text{Pa}]$ is the atmospheric pressure.

The Triose Phosphate Utilization $TPU$ $[\text{μmol equivalent s}^{-1}\,\text{m}^{-2}]$ and the PEP Carboxylase coefficient $k_e$ $[\text{μmol equivalent s}^{-1}\,\text{m}^{-2}]$ are calculated as (Bonan et al., 2011):

$$TPU = TPU_{25} \exp\left[\frac{H_a(T_v - T_{ref})}{(T_{ref}\,RT_v)}\right] \frac{1 + exp\left(\frac{T_{ref}\Delta S - H_d}{T_{ref}\,R}\right)}{1 + exp\left(\frac{T_v \Delta S - H_d}{T_v\,R}\right)} \ , \tag{270}$$

$$TPU_{25} = 0.1182 V_{c,max} \ , \tag{271}$$

$$k_e = k_{e,25}\left[2.1^{0.1(T_v - 25)}\right] \ , \tag{272}$$

$$k_{e,25} = 20000 V_{c,max} \ , \tag{273}$$

where

$TPU_{25} = [\text{μmol equivalent s}^{-1}\,\text{m}^{-2}]$ is the triose phosphate utilization at 25 °C computed as a function of $V_{c,max}$.

$H_a \quad = 53.1 \ [\text{kJ mol}^{-1}]$.

$\Delta S \quad = 0.490 \ [\text{kJ mol}^{-1}\,\text{K}^{-1}]$.

$H_d \quad = 150.65 \ [\text{kJ mol}^{-1}]$.

$T_v \quad = [\text{°C}]$ is the leaf temperature.

$k_{e,25} \quad = [\text{μmol equivalent s}^{-1}\,\text{m}^{-2}]$ is the PEP Carboxylase coefficient at 25 °C.

## 4 Conductive heat flux

### 4.1 Conductive heat flux: Building envelope

The conductive heat flux into and out of the building envelope (wall and roof) is calculated with a numerical solution of the heat diffusion equation (Hu and Islam, 1995; Hillel, 1998; Núñez et al., 2010; Masson, 2000; Wang et al., 2011; Park and Lee,

2008):

$$\frac{\partial T_k}{\partial t} = k_k \frac{\partial^2 T_k}{\partial z^2} \ , \tag{274}$$

where $T_k$ [°C] is the temperature of wall or roof layer k, and $k_k = \lambda_k / cv_k$ [m$^2$ s$^{-1}$] the heat diffusivity of the wall or roof material. UT&C considers two physical layers for the vegetated roof and one physical layer for the impervious roof, and sunlit and shaded wall. The numerical solution is based on three nodes (two numerical layers) with the inner boundary condition equal to the interior building temperature $T_b$ and the outer boundary condition equal to the prognostic surface temperature $T_i$. The conductive heat flux of wall and roof layer 1 and 2, $G_1(t,z)$ and $G_2(t,z)$ [W m$^{-2}$], are calculated as:

$$G_1(t,z) = -\lambda_1 \frac{(T_{int}(t) - T_i(t))}{\Delta z_1} \ , \tag{275}$$

$$G_2(t,z) = -\lambda_2 \frac{(T_b(t) - T_{int}(t))}{\Delta z_2} \ , \tag{276}$$

where $\lambda_1$ and $\lambda_2$ [J K$^{-1}$ m$^{-1}$ s$^{-1}$] are the heat conductivity of layer 1 and 2, and $\Delta z_1$ and $\Delta z_2$ the thickness of layer 1 and 2. An internal wall and roof temperature $T_{int}$ is calculated to account for heat storage effects inside the wall or roof. The interior building air temperature $T_b$ is prescribed equal to the air temperature at atmospheric reference height if the air temperature is between a set minimum value $T_{b,min}$ and a set maximum value $T_{b,max}$. In the case of higher or lower air temperature, the interior building temperature $T_b$ is prescribed equal to $T_{b,min}$ or $T_{b,max}$ assuming that heating or cooling of building interior is occuring (de Munck et al., 2018).

## 4.2  Conductive heat flux: Ground

The conductive heat flux into and out of the ground is calculated applying the force restore method, which approximates the heat diffusion equation with a single ordinary differential equation as (Hu and Islam, 1995):

$$\frac{dT_g}{dt} = C_1 G - C_2 (T_g - T_d) \ , \tag{277}$$

where $T_g$ [K] is the ground surface temperature, and $T_d$ [K] the ground temperature at dampening depth $d$. $C_1$ [m$^2$ K J$^{-1}$] and $C_2$ [s$^{-1}$] are coefficients of the method. UT&C uses the Deardorff (1978) force restore method as implemented in the ecohydrological model T&C (Fatichi et al., 2012a, b, c):

$$G(t) = \frac{1}{C_1} \left[ C_2 [T_g(t) - T_d(t)] + \frac{T_g(t) - T_g(t-1)}{dt} \right] \ , \tag{278}$$

$$C_1 = 2/(cv_s d) = 2\sqrt{\pi/(\lambda_s cv_s \tau_{day})} \ , \tag{279}$$

$$C_2 = \omega_1 = \frac{2\pi}{\tau_{day}} \ , \tag{280}$$

where $\lambda_s$ [J K$^{-1}$ m$^{-1}$ s$^{-1}$] is the bulk ground heat conductivity, $cv_s$ [J K$^{-1}$ m$^{-3}$] the bulk ground volumetric heat capacity, and $\tau_{day} = 86400$ [s]. The dampening temperature $T_d$ is calculated as (Noilhan and Planton, 1989):

$$dT_d/dt = (T_g - T_d)/\tau_{day} \ , \tag{281}$$

## 4.3 Soil thermal properties

The soil volumetric heat capacity $cv_s$ and the soil thermal conductivity $\lambda_s$ are calculated as a function of soil type and soil water content according to de Vries (1963), Farouki (1981), and Oleson et al. (2004, 2013) as described in Fatichi et al. (2012a, b, c).

## 5 Anthropogenic heat flux

The current UT&C parametrization allows for a prescribed time series of anthropogenic heat flux, which is added to the canyon air at the canyon calculation height. The anthropogenic heat flux is a model input timeseries. Hence, anthropogenic heat emissions caused by air conditioning, car exhaust, industry, human metabolism, or any other additional source need to be estimated a priori, e.g. using existing approaches (Sailor and Lu, 2004; Sailor et al., 2015). The conductive anthropogenic heat flux caused by heating of building interiors is represented with a prescribed interior building temperature if air temperature falls below the set value $T_{b,min}$ (See Sect. 4.1). On the other hand, the conductive anthropogenic heat flux due to air conditioning of building interiors produces a negative anthropogenic heat effect, which could be counteracted by adding air conditioning heat emission input to the canyon air as described above. Future developments of UT&C could focus on the inclusion of anthropogenic heat emissions due to the air conditioning of buildings by adding the value of the total conductive heat flux into the building back into the urban canyon or above the roof (depending on location of airconditioning units), with an appropriate adjustement for efficiency.

## 6 Urban hydrological model

UT&C solves the urban water mass balance as:

$$\frac{dS}{dt} = P + Q_f - E - R \, , \tag{282}$$

where P $[\mathrm{mm\ h^{-1}}]$ is the incoming precipitation, $Q_f$ $[\mathrm{mm\ h^{-1}}]$ the anthropogenic water input, E $[\mathrm{mm\ h^{-1}}]$ the total evapotranspiration, R $[\mathrm{mm\ h^{-1}}]$ the total runoff plus deep leakage from the soil column, and $dS/dt$ $[\mathrm{mm\ h^{-1}}]$ the change of water storage S in the system. P and $Q_f$ are both model input timeseries, and E and R are calculated within UT&C as described in Sect. 2.2 to 2.2.5 and 6.3. The total water storage S consists of intercepted water, ponding water, and water stored in the soil column. The water mass balance is calculated individually for roof and canyon. It is assumed that the total roof runoff and the soil water leakage of green roofs is directed towards the sewer system and does not affect the canyon water budget anymore. It is further assumed that soil moisture changes slowly in comparison to energy fluxes to reduce the complexity of the system and to facilitate faster computation. Hence, the energy balance is solved first for a given time step t and the evapotranspiration is constrained by the water availability at the previous timestep (t-1). The obtained evapotranspiration $E_t$ $[\mathrm{kg\ m^{-2}\ s^{-1}}]$ is then used as an input to solve the water mass balance.

## 6.1 Interception and ponding

UT&C considers interception on vegetation canopy (Sect. 6.1.1), ponding on impervious surfaces (Sect. 6.1.2) and ponding on bare soil or soil underneath vegetation (Sect. 6.1.3). The interception and ponding storage dynamics are calculated according to a mass conservation equation as:

$$\frac{dIn}{dt} = P^* - D - E_{In} , \tag{283}$$

where $In$ [mm] is the intercepted or ponding water, $P^*$ [mm h$^{-1}$] the incoming water flux from precipitation and runon , D [mm h$^{-1}$] the canopy drainage or soil infiltration, and $E_{In}$ [mm h$^{-1}$] the evaporation from intercepted or ponding water. A finite difference approximation is used to solve Eq. (283) as suggested by Fatichi et al. (2012a, b, c) where the effects of evaporation and precipitation are considered first and the canopy drainage or infiltration are substracted subsequently:

$$In_t(t) = In(t - \Delta t) + P^*(t)\Delta t - E_{In}(t)\Delta t , \tag{284}$$

$$In(t) = In_t(t) - Dr(t)\Delta t , \tag{285}$$

where $\Delta t = 1$ [h] is the time step of the calculation.

### 6.1.1 Interception: Plant canopy

The canopy interception is calculated according to the Rutter model (Rutter et al., 1971, 1975; Mahfouf and Jacquemin, 1989; Eltahir and Bras, 1993; Ivanov et al., 2008b) as:

$$\frac{dIn}{dt} = P_{fol} - Dr - E_{In} , \tag{286}$$

The precipitation onto the canopy foilage $P_{fol}$ [mm h$^{-1}$] and the throughfall $P_{through}$ [mm h$^{-1}$] are calculated as a function of projected leaf area fraction onto the ground $C_{fol}$ as follows (Mahfouf and Jacquemin, 1989):

$$P_{fol} = P\, C_{fol} , \tag{287}$$

$$P_{through} = P\,(1 - C_{fol}) , \tag{288}$$

$$C_{fol} = 1 - e^{-\kappa(LAI+SAI)} ,, \tag{289}$$

where P [mm h$^{-1}$] is the incoming precipitation, LAI [$-$] and SAI [$-$] the leaf and stem area index, and $\kappa = 0.75$ (Ramírez and Senarath, 2000). $C_{fol} = [0 - 1]$ [m$^2$ obstructed area m$^{-2}$ VEG area] represents the projected leaf area onto the ground, which is active in the interception process.

The canopy drainage Dr [mm h$^{-1}$] is calculated as:

$$Dr = Dr_s + Dr_d , \tag{290}$$

where $Dr_s$ [mm h$^{-1}$] is the saturation excess drainage, and $Dr_d$ [mm h$^{-1}$] the canopy dripping. $Dr_s$ and $Dr_d$ are calculated as (Fatichi et al., 2012a, b, c):

$$Dr_s = \frac{(In_t - In^{Max})}{dt}(In > In^{Max}) \,, \tag{291}$$

$$Dr_d = K_c e^{g_c(In_t - In^{Max})} \,, \tag{292}$$

where $In^{Max}$ [mm] is the maximum interception capacity of the vegetation canopy, $K_c = 0.06$ [mm h$^{-1}$] the drainage rate coefficient (Rutter et al., 1971; Mahfouf and Jacquemin, 1989), and $g_c = 3.7$ [mm$^{-1}$] the exponential decay paramter (Rutter et al., 1971; Mahfouf and Jacquemin, 1989). The total intercepted water $In$ [mm] must always be smaller than the maximum interception capacity $In^{Max}$ (Fatichi et al., 2012a, b, c). The maximum interception capacity of the vegetation canopy $In^{Max}$ [mm] is calculated as (Dickinson et al., 1993):

$$In^{Max} = S_{p,In}(LAI + SAI) \,, \tag{293}$$

where $S_{p,In}$ [mm] is a model input parameter and a function of vegetation type.

The fraction of precipitation reaching the layer below the vegetation $P_{down}$ [mm] is calculated as:

$$P_{down} = P(1 - A_{veg}) + Dr A_{veg} \,, \tag{294}$$

where $A_{veg}$ is the vegetation canopy area in relation to the underlying ground area. It is assumed that the vegetated roof and canyon ground fraction $f_{veg}$ [−] are completely covered by vegetation leading to $A_{veg} = 1$. The impervious, bare and vegetated ground cover fraction underneath trees are homogeneously distributed leading to $A_{veg,tree} = 4r_{tree}$.

### 6.1.2 Ponding: Impervious surface

Ponding on impervious surfaces is calculated according to a water mass budget as:

$$\frac{dIn}{dt} = P_{imp} - Lk - E_{In} \,, \tag{295}$$

The incoming water flux to the impervious roof fraction $P_{r,imp}$ and the impervious ground fraction $P_{g,imp}$ are calculated as follows:

$$P_{r,imp} = P + q_{roof} \,, \tag{296}$$

$$P_{g,imp} = P_{down} + q_{ground} \,, \tag{297}$$

where $P_{down}$ [mm h$^{-1}$] is the precipitation plus dripping reaching the ground level within the canyon accounting for tree canopy interception, and $q_{roof}$ and $q_{ground}$ are the roof and ground runon which represent the runoff fluxes that did not leave the system in the previous time step (Sect. 6.3).

The leakage of the impervious roof fraction $Lk_r$ [mm h$^{-1}$] is zero whereas the leakage of the impervious ground fraction $Lk_g$ [mm h$^{-1}$] is modelled with a prescribed hydraulic conductivity $K_{g,imp}$, typically a small value corresponding to asphalt or other pavements which is a model input parameter.

The maximum storage capacity of the impervious roof $In_{r,imp}^{M}$ [mm] and ground $In_{g,imp}^{M}$ [mm] is a model input parameter and it depends on the roof and ground cover roughness and micro-depressions. Ponding water exceeding the maximum interception capacity is leaving the system as runoff or can remain in the system and becomes runon in the following time step (Sect. 6.3).

### 6.1.3 Ponding: Soil surface

Ponding and water logging on bare soil surfaces is calculated with the water budget equation:

$$\frac{dIn}{dt} = P_{soil} - I_{f\ soil} - E_{In} \,, \tag{298}$$

where $P_{soil}$ [mm h$^{-1}$] is the incoming water flux to the soil, $I_{f\ soil}$ [mm h$^{-1}$] the soil infiltration rate (Sect. 6.2.2), and $E_{In}$ [mm h$^{-1}$] the evaporation from ponding water on the soil. The incoming water flux to the roof $P_{r,soil}$ and ground $P_{g,soil}$ soil fractions is calculated as follows:

$$P_{r,soil} = P_{down} + q_{roof}(t-1) \,, \tag{299}$$

$$P_{g,bare,soil} = P_{down,tree} + q_{ground}(t-1) \,, \tag{300}$$

$$P_{g,veg,soil} = P_{down,tree,veg} + q_{ground}(t-1) \,, \tag{301}$$

where $P_{down}$ [mm h$^{-1}$] is the precipitation reaching the soil level underneath the roof vegetation canopy accounting for canopy interception (Sect. 6.1.1), $P_{down,tree}$ [mm h$^{-1}$] is the precipitation reaching the canyon ground accounting for tree canopy interception, $P_{down,tree,veg}$ [mm h$^{-1}$] is the precipitation reaching the soil level underneath the ground vegetation canopy accounting for both tree and ground vegetation canopy interception. Finally, $q_{roof}(t-1)$ and $q_{ground}(t-1)$ are the roof and ground runon, i.e., the ponding water remaining in the system from the previous time step (Sect. 6.3).

### 6.2 Vadose zone dynamics

The urban soil and its vertical and horizontal $\theta(z,x)$ soil moisture profile directly influence water and energy fluxes in the urban environment. UT&C divides the urban soil into three soil columns beneath the impervious, bare, and vegetated ground cover fractions and one soil column for the vegetated roof fraction (Fig. 8). Soil underneath buildings is not considered in the current model formulation. The first two soil layers of the impervious ground soil column are assumed largely impermeable and do not participate in the water exchanges.

### 6.2.1 Vertical and horizontal soil moisture profile

The soil moisture and soil water content is calculated according to the 1D-Richards equation (Richards, 1931) describing the flow of water in variably saturated soils subjected to capillary and gravity forces in the vertical direction z (positive downward) as:

$$\frac{\partial \theta}{\partial t} = \frac{\partial}{\partial z}\left[K_v(\theta)\frac{\partial \Psi_S(\theta)}{\partial z} + K_v(\theta)\right] - S \,, \tag{302}$$

where $\theta$ [$-$] is the soil water content, $K_v(\theta)$ [mm h$^{-1}$] the vertical hydraulic conductivity as a function of soil moisture, and $\Psi_S(\theta)$ [mm] the soil water potential. The sink term $S$ [h$^{-1}$] accounts for lateral fluxes, soil evaporation, and root water uptake for transpiration.

The 1D-Richards equation is first solved in vertical direction for each soil column (impervious, bare, vegetated) using a finite volume approach with the method of lines (Lee et al., 2004), discretizing the spatial domain and reducing the partial differential equation to a system of ordinary differential equations in time as described by Fatichi et al. (2012a, b, c). Each soil column is subdivided into $j = 1, ..., n$ layers with varying layer thickness $d_{z,j}$ [mm]. Soil layer depth z is increasing downwards (Fig. 8) and the top soil layer is soil layer 1. For each soil layer, the ordinary differential equation describing the change in soil moisture over time can be written as (Fatichi et al., 2012a, b, c):

$$d_{z,j}\frac{d\theta_j}{dt} = (q_{j-1} - q_j) + (Q_{l,in,j} - Q_{l,out,j}) - T_H\, r_{H_j} - T_L\, r_{L_j} - E_g \;, \tag{303}$$

where $q_{j-1}$ and $q_j$ [mm h$^{-1}$] are the vertical fluxes in and out of soil layer j, and $Q_{l,in,j}$ and $Q_{l,out,j}$ [mm h$^{-1}$] are the lateral fluxes in and out of soil layer j from and into the adjacent soil columns. The soil evaporation $E_g$ [mm h$^{-1}$] is assumed to be only present in the first ($j = 1$) soil layer of the bare and vegetated soil column.

The transpirative sinks of high and low vegetation, $T_H$ and $T_L$ [mm h$^{-1}$], are weighted according to their root biomass fraction in each soil layer, $r_{H_j}$ and $r_{L_j}$ [$-$]. In the absence of trees or ground vegetation, $T_H$ and $T_L$ are zero. The calculation of root biomass fraction in each soil layer, $r_{H_j}$ and $r_{L_j}$ [$-$], is described in Sect. 7.1 and 7.2.

The vertical water flow associated with soil layer j is calculated as:

$$q_j = \overline{K_{v,j}}\left(1 + \frac{\Psi_{S,j} - \Psi_{S,j+1}}{Dz_{j+1}}\right) \;, \tag{304}$$

where $\Psi_{S,j}$ [mm] is the soil water potential of layer $j$, $\overline{K_{v,j}}$ [mm h$^{-1}$] the vertical unsaturated hydraulic conductivity arithmetically averaged between soil layers j and j+1, and $Dz_{j+1}$ [mm] the distance between the center of soil layer j and j+1. The vertical inflow to the first soil layer is the infiltration $q_0 = I_f$ [mm h$^{-1}$] as calculated in Sect. 6.2.2. The outflow of the last soil layer is the deep leakage $q_n = L_{kb}$ [mm h$^{-1}$]. It is possible that soil layers become saturated for example when an impermeable bottom is defined. In this case, a shallow water table depth is calculated and the excess water is transported to the soil layers above. This mechanism can lead to a saturated zone within the soil column (Fatichi et al., 2012a, b, c).

The lateral water inflow to soil layer j in soil column k from the adjacent soil column i, $Q_{l,in,j,i\to k}$ [mm h$^{-1}$], with k and i denoting vegetated, bare, or impervious soil column, is calculated as:

$$Q_{l,in,j,i\to k} = a_r\left[K_{v,j,\overline{ik}}\left(\frac{\Psi_{S,j,i} - \Psi_{S,j,k}}{Dy}\right)\right]\left(\frac{d_{z,j}}{f_k\,W_{can}}\right) \;, \tag{305}$$

where $a_r = K_h/K_v$ [$-$] is an anisotropy factor accounting for the difference in horizontal, $K_h$, and vertical hydraulic conductivity, $K_v$ (Garrote and Bras, 1995; Assouline and Or, 2006), $K_{v,j,\overline{ik}}$ [mm h$^{-1}$] is the arithmetic average of the vertical hydraulic conductivity of soil layer j in soil column i and k, and $\Psi_{S,j,k}$ and $\Psi_{S,j,i}$ [mm] are the soil water potential of layer $j$ in soil column k and i, respectively. $Dy = 1000$ [mm] is a selected characteristic length scale on which soil moisture differences will affect the unsaturated lateral water exchange and it is a model input parameter. The factor $d_{z,j}/(f_k\,W_{can})$ rescales the
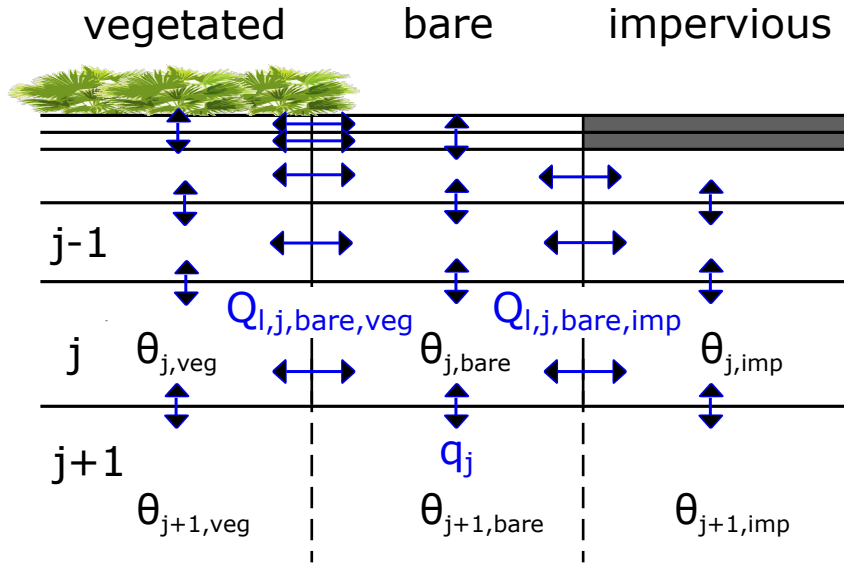
**Figure 8.** Soil layer (j) and soil column (vegetated, bare, and impervious) discretization. $Q_{l,j,bare,veg}$ and $Q_{l,j,bare,imp}$ denote the lateral water fluxes between bare and vegetated soil column and bare and impervious soil column in layer j and $q_j$ the vertical water flux between soil layers.

horizontal water flux over the layer depth $d_{z,j}$ [mm] to the vertical water flux over the column width where $f_k$ [−] is the ground cover fraction of column k and $W_{can}$ [mm] the total canyon width. Note that the scaling factors of the lateral soil water fluxes vary depending on the extent of the origin and destination soil columns to garantuee mass conservation.

The soil moisture profile is numerically resolved in a mesh with n vertical layers and i = 1, 2, or 3 columns (Fig. 8) with width specified by the ground cover fractions (impervious, bare and vegetated) and roof cover fraction. A typical vertical soil layer parametrization includes n=10-30 ground layers and n=1-5 roof layers. The vertical mesh has a higher resolution near the surface and coarser resolution near the bottom with soil layer depths varying from 10 to 500 [mm] (Fatichi et al., 2012a, b, c).

The first two soil layers of the impervious soil column are considered impervious and do not interact with the vertical and lateral soil water transport. A small infiltration capacity can be prescribed for the impervious soil column and the infiltrated water will be directly added to the third soil layer. The lateral soil water exchange is calculated among all ground soil columns resulting in 3! lateral fluxes. No lateral soil water exchange is calculated for the vegetated roof fraction.

### 6.2.2 Infiltration

The actual infiltration into the bare and vegetated soil column is calculated as the minimum between infiltration capacity $I_f^C$ [mm h$^{-1}$] and water availability at the soil surface $q_{ins}$ [mm h$^{-1}$] (Fatichi et al., 2012a, b, c):

$$I_f = \min\left(q_{ins}, I_f^C\right),$$ (306)

The infiltration capacity $I_f^C$, as the upper limit to infiltration, is calculated as a soil hydraulic conductivity applying a Dirichlet boundary condition at the soil surface which assumes a soil water potential of zero (Fatichi et al., 2012a, b, c) and using the actual water potential of the first soil layer. The hydraulic conductivity is calculated from the water potential with the pedotransfer functions described in Sect. 6.4. UT&C does not yet account for soil crust mechanisms and soil surface sealing.

Similarly, a maximum impervious infiltration capacity $I_{f,imp}^C$ [mm h$^{-1}$] is prescribed for the impervious soil column. $I_{f,imp}^C$ is typically very small when compared to the permeability of natural surfaces.

## 6.3 Runoff and runon

Runoff $R$ [mm h$^{-1}$] is generated as infiltration excess runoff (Hortonian runoff) when the available water at the ground surface exceeds the maximum infiltration capacity $I_f^C$ [mm h$^{-1}$] and the maximum allowed ponding depth over bare and vegetated surfaces $In^{Max}$ [mm h$^{-1}$] is overcome (Fatichi et al., 2012a, b, c). Runoff can further be generated as saturation excess runoff when a soil column becomes saturated and the shallow water table reaches the surface as described in Sect. 6.2.1.

The total roof and ground runoff are calculated as the area weighted average of the runoff generated by each surface fraction:

$$R_r = \sum f_{r,i} R_{r,i} \,, \tag{307}$$

$$R_g = \sum f_{g,i} R_{g,i} \,, \tag{308}$$

where $f_{r,i}$ and $f_{g,i}$ [−] are the roof and ground cover fractions, and $R_{r,i}$, and $R_{g,i}$ [mm h$^{-1}$] are the roof and ground runoff of each surface fraction. It is assumed that roof runoff does not interact with the ground but rather enters into a sewer system.

A fraction of the total roof and ground runoff can be kept in the system and becomes runon in the next time step $R_{on}(t+1)$ [mm h$^{-1}$]:

$$R_{on}(t+1) = \lambda_{R_{on}} \, R_i \,, \tag{309}$$

where $\lambda_{R_{on}} = [0-1]$ [−] is the fraction of runoff kept in the system and and $R_i$ [mm h$^{-1}$] is the total roof or ground runoff. The runon is distributed homogeneously over either the roof or ground and is put back into the system at the next time step. A runon fraction larger than zero ($\lambda_{R_{on}} > 0$) can account for microdepressions and surface exchanges between the various surfaces in the urban environment before the water reaches the sewer system. For example, it can account for runoff from impervious area that is redirected to infiltrate in vegetated areas in the roof or as for example in bioswales.

## 6.4 Soil hydraulic properties

UT&C can either use the van Genuchten (1980) or the Saxton and Rawls (2006) parameterization to calculate the soil hydraulic conductivity $K(\theta)$ [mm h$^{-1}$] and the soil water retention curve $\Psi_s = f(\theta)$ [MPa] which are a function of soil moisture content $\theta$ [mm$^3$ mm$^{-3}$]. Soil hydraulic properties are calculated according to the soil composition specified as fraction of clay, sand, and organic material in the soil. The hydraulic conductivity at field capacity is set to 0.2 [mm h$^{-1}$] and the soil water potential at residual water content to -10 [MPa]. Further description on the calculation of soil hydraulic properties can be found in Fatichi et al. (2012a, b, c).

## 7 Plant water and biophysical relations

### 7.1 Horizontal root distribution

UT&C assumes that ground and roof vegetation can only access the soil moisture of the vegetated ground and roof fraction. Two possible horizontal tree root distributions are implemented that specify the abilty of the tree to reach different soil columns: (1) the trees have even access to the impervious, bare, and vegetation ground columns, and (2a) the trees have only access to the vegetated and bare ground columns, if the tree canopy is smaller than the combined vegetated and bare ground area, or (2b) the trees fully accesses the vegetated and bare soil columns and parts of the impervious soil column if the tree canopy is bigger than the combined vegetated and bare ground area.

### 7.2 Vertical root distribution and root soil moisture access

The fraction of root biomass within each soil layer $r_j$ $[-]$ with $j = 1...n_s$, $n_s$ being the last soil layer accessed by the roots, is calculated assuming a vertical root biomass profile (Fatichi et al., 2012a, b, c). Four different root biomass profiles can be specified in UT&C: (1) an exponential root profile (Arora and Boer, 2005; Ivanov et al., 2008a), (2) a linear dose response root profile (Schenk and Jackson, 2002; Collins and Bras, 2007), (3) a constant root profile, and (4) a linear dose response profile with tap roots (Fatichi et al., 2012a, b, c). The described root profiles are specified by the rooting depth containing 50 % and 95 % of the fine root biomass $Z_{R,50}$ and $Z_{R,95}$ [mm], and by the maximum rooting depth $Z_{R,max}$ [mm]. $Z_{R,50}$, $Z_{R,95}$, and $Z_{R,max}$ are model input parameters. Note that the maximum rooting depth $Z_{R,max}$ and the rooting depth containing 95 % of the fine roots $Z_{R,95}$ need to be smaller than the total soil depth as the soil profile is not resolved underneath (Fatichi et al., 2012a, b, c). The detailed description of the root biomass fraction calculation can be found in Fatichi et al. (2012a, b, c).

The average water content available to the roots of a given plant type $\theta_R$ $[-]$ is calculated according to Fatichi et al. (2012a, b, c) as:

$$\theta_R = \sum_{j=1}^{n_s} r_j \theta_j \ , \tag{310}$$

where $r_j$ $[-]$ is the fraction of root biomass in soil layer j, $\theta_j$ $[-]$ the soil moisture of soil layer j, and $n_s$ the total number of soil layers. The average water content available to the roots $\theta_R$ $[-]$ is used to calculate the soil water potential felt by the plant roots $\Psi_{sR}$ [MPa] and the resulting water stress $\beta$ $[-]$ (Sect. 3.6.3).

### 7.3 Plant hydraulics

Plant hydraulics is currently not implemented in UT&C. It is assumed that leaf water potential $\Psi_L$ [MPa] and xylem water potential $\Psi_X$ [MPa] are equal to the soil water potential felt by the plant $\Psi_{sR}$ [MPa] (Fatichi et al., 2012a, b, c).

## 7.4 Plant water uptake

The plant-water uptake $J_{sx}$ [mm h$^{-1}$] is assumed to be equal to the transpirative flux $T$ [mm h$^{-1}$] since there is no plant hydraulic component implemented in UT&C (Sect. 7.3). The plant water uptake and transpirative flux can be limited by the soil water availability and maximum root-water uptake capacity $RWU_{max}$ [mm h$^{-1}$] and are calculated as:

$$J_{sx} = T = min(T_{\text{“pot”}}, soil\ water, RWU_{max}) \,, \tag{311}$$

The plant-water uptake $J_{sx}$ is distributed within the different soil layers according to the root biomass fractions $r_j$ [−]. The soil-to-root conductance in each soil layer j $g_{sr,j}$ [mmol H$_2$0 s$^{-1}$ MPa$^{-1}$ m$^{-2}$ ground] parameterizes the hydraulic resistance between soil and root and is calculated as (Newman, 1969; Deckmyn et al., 2008; Fatichi et al., 2012a, b, c):

$$g_{sr,j} = \kappa K_v(\theta_j) R_{L,j} 2\pi \log\left[\frac{r_{cyl}}{r_{root}}\right] \,, \tag{312}$$

where $\kappa = 5.66 \cdot 10^9$ is an unit conversion factor, $K_v(\theta_j)$ [m s$^{-1}$] the unsaturated hydraulic conductivity as a function of soil water content in layer j, $R_{L,j} = r_j R_L$ [m root m$^{-2}$ ground] the root length density in a given soil layer for a given vegetation type, $r_{root} = 0.5$ mm the average radius of fine roots, and $r_{cyl} = 2.0$ mm the average radius to which roots have soil access. The root length density $R_L$ [m root m$^{-2}$ ground] is a model input parameter.

The maximum root-water uptake capacity in each soil layer $RWU_{max,j}$ [mm h$^{-1}$] is calculated with the soil-to-root conductance $g_{sr,j}$ [mmol H$_2$0 s$^{-1}$ MPa$^{-1}$ m$^{-2}$ ground] as described in Fatichi et al. (2012a, b, c):

$$RWU_{max,j} = \tilde{\kappa} g_{sr,j} |\Psi_{s,j} - \Psi_{min}| \,, \tag{313}$$

where $\tilde{\kappa} = 0.0648$ is a unit conversion factor (Fatichi et al., 2012a, b, c), $\Psi_{s,j}$ [MPa] the soil water potential in soil layer j, and $\Psi_{min} = min(\Psi_{X,50}, \Psi_{L,50})$ [MPa] the minimum water potential experienced by the leaf $\Psi_{L,50}$ [MPa] or xylem $\Psi_{X,50}$ [MPa] before a 50 % reduction of hydraulic conductivty occurs. $\Psi_{min}$ represents a lower limit for plant water extraction. Furthermore, low values of soil-to-root conductance prevent plant water uptake.

## 8 Anthropogenic water

UT&C accounts for prescribed timeseries of anthropogenic water $Q_f$ [mm h$^{-1}$] to the vegetated roof, bare ground, and vegetated ground. The anthropogenic water can either be added above the vegetation canopy or on the soil underneath to represent sprinkler and hose irrigation or drip irrigation.

## 9 Model input parameters

The following tables summarize the model input parameters used in the model performance assessment for Singapore, Melbourne and Phoenix. Specifically, they specify the urban geometry, radiation and conductive heat flux parameters (Table 1), vegetation parameters (Table 2), soil, interception and runoff parameters (Table 3), location parameters, as well as anthropogenic heat forcings (Table 4), and irrigation time series (Table 5).

**Table 1.** Urban Geometry, radiation, and conductive heat flux parameters used for the model validation in Singapore (SG), Melbourne (MB), and Phoenix (PH).

| Parameter | Description | SG | MB | PH |
|---|---|---|---|---|
| $H_{can}$ | Height of urban canyon (m) | 9.86[1,2] | 6.4[4,5] | 4.5[7] |
| $W_{can}$ | Ground width of urban canyon (m) | 16.16[1,2,3]* | 15.2[4,5]* | 11.3[7]* |
| $W_{roof}$ | Roof width of urban canyon (m) | 10.33[1,2,3]* | 12.2[4,5]* | 4[7]* |
| $H_{tree}$ | Tree height (m) | 7.26[1,2] | 4.2 | 4[7] |
| $R_{tree}$ | Tree radius (=1/4 $f_{g,tree}$ *$W_{can}$) (m) | 0.73[1,2,3]* | 1.5[4,5]* | 0.19[7]* |
| $D_{tree}$ | Distance of wall to tree trunk (m) | 3[a] | 2[a] | 2[a] |
| $N_{tree}$ | Absence (0) or presence (1) of trees (−) | 1[1,2] | 1[6] | 1[7] |
| $f_{r,imp}$ | Fraction of impervious roof (−) [+] | 1[a] | 1[a] | 1[a] |
| $f_{r,veg}$ | Fraction of vegetated roof (−) [+] | 0[a] | 0[a] | 0[a] |
| $f_{g,imp}$ | Fraction of impervious ground (−) [+] | 0.75[1,2] | 0.53[4,5] | 0.32[7] |
| $f_{g,bare}$ | Fraction of bare ground (−) [+] | 0[1,2] | 0.02[4,5] | 0.53[7] |
| $f_{g,veg}$ | Fraction of vegetated ground (−) [+] | 0.25[1,2] | 0.45[4,5] | 0.15[7] |
| $\alpha_r$ | Albedo roof [imp, veg] (−) | [0.2[8], -] | [0.15[6], -] | [0.16[10], -] |
| $\alpha_g$ | Albedo ground [imp, bare, veg] (−) | [0.08[8], 0.2[a], 0.27[8]] | [0.1[6], 0.2[a], 0.27] | [0.15[9], 0.2[a], 0.27] |
| $\alpha_w$ | Albedo wall (−) | 0.5[8] | 0.3[6] | 0.5[8] |
| $\alpha_t$ | Albedo tree canopy (−) | 0.27[8] | 0.27 | 0.27 |
| $\epsilon_r$ | Emissivity roof [imp, veg] (−) | [0.9[8], -] | [0.92[6], -] | [0.95[9], -] |
| $\epsilon_g$ | Emissivity ground [imp, bare, veg] (−) | [0.94[8], 0.95[a], 0.97[8]] | [0.92[6], 0.973[5], 0.97[8]] | [0.95[9], 0.98[11], 0.97[8]] |
| $\epsilon_w$ | Emissivity wall (−) | 0.9[8] | 0.88[6] | 0.95[9] |
| $\epsilon_t$ | Emissivity tree canopy (−) | 0.97[8] | 0.97[8] | 0.97[8] |
| $\lambda_{r,imp}$ | Thermal conductivity of impervious roof (W K$^{-1}$ m$^{-1}$) | 0.406[3]* | 0.773[5]* | 0.6[9] |
| $\lambda_{g,imp}$ | Thermal conductivity of impervious ground (W K$^{-1}$ m$^{-1}$) | 1.552[3]* | 2.682[5]* | 1.2[9] |
| $\lambda_w$ | Thermal conductivity of wall (W K$^{-1}$ m$^{-1}$) | 0.75[3]* | 0.342[5]* | 1.3[9] |
| $Cv_{r,imp}$ | Volumetric heat capacity of impervious roof (MJ K$^{-1}$ m$^{-3}$) | 0.577[3]* | 0.813[5]* | 1.9[9] |
| $Cv_{g,imp}$ | Volumetric heat capacity of impervious ground (MJ K$^{-1}$ m$^{-3}$) | 1.552[3]* | 1.3413[5]* | 1.1[9] |
| $Cv_w$ | Volumetric heat capacity of wall (MJ K$^{-1}$ m$^{-3}$) | 1.357[3]* | 0.9035[5]* | 1.5[9] |
| $dz_r$ | Thickness of roof layers [1, 2] (m) | [0.106, 0.106][8]* | [0.057, 0.057][5]* | [0.075, 0.075][a] |
| $dz_w$ | Thickness of wall layers [1, 2] (m) | [0.098, 0.098][8]* | [0.074, 0.074][5]* | [0.075, 0.075][a] |

* Calculated from literature values, [a] Assumption, [1] Velasco et al. (2013), [2] Roth et al. (2016), [3] Demuzere et al. (2017), [4] Coutts et al. (2007a, b), [5] Grimmond et al. (2011), [6] Nice et al. (2018), [7] Chow et al. (2014), [8] Harshan et al. (2017), [9] Song and Wang (2015), [10] Yang et al. (2015), [11] Park and Lee (2008); [+] land cover fractions reported in literature were rescaled by the canyon and roof fraction so that $f_{r,imp}+f_{r,veg}$ = 1 and $f_{g,imp}+f_{g,bare}+f_{g,veg}$ = 1.

**Table 2.** Vegetation parameters* used for the model validation in Singapore (SG), Melbourne (MB), and Phoenix (PH). Seperate parameters for roof vegetation [$r_{veg}$], ground vegetation [$g_{veg}$], and trees [$_{tree}$] are specified for each location in this respective order.

| Parameter | Description | SG [$r_{veg}, g_{veg, tree}$] | MB [$r_{veg}, g_{veg, tree}$] | PH [$r_{veg}, g_{veg, tree}$] |
|---|---|---|---|---|
| $h_c$ | Canopy height (m) | [-, 0.05, 7.26] | [-, 0.1, 4.2] | [-, 0.1, 4] |
| $d_{leaf}$ | Leaf dimension (cm) | [-, 2, 5] | [-, 2, 3] | [-, 0.8, 1.5] |
| $LAI$ | Leaf area index ($-$) | [-, 2.5, 3$^{(2)}$] | [-, 3, 3] | [-, 1.5, 1.8] |
| $SAI$ | Stem area index ($-$) | [-, 0.001, 0.2] | [-, 0.001, 0.1] | [-, 0.001, 0.1] |
| $S_{LAI}$ | Specific leaf area ($\mathrm{m^2\,LAI\,g\,C^{-1}}$) | [-, 0.025, 0.02] | [-, 0.016, 0.009] | [-, 0.022, 0.015] |
| $K_{opt}$ | Canopy light extinction coefficient ($-$) | [-, 0.5, 0.5] | [-, 0.5, 0.5] | [-, 0.5, 0.5] |
| $VCASE_{root}$ | Vertical root profile (1, 2, 3, 4) | [-, 1, 1] | [-, 1, 1] | [-, 1, 1] |
| $HCASE_{root}$ | Type of root profile of tree (1, 2) | 2 | 2 | 2 |
| $ZR_{50}$ | Root depth, $50^{th}$ percentile (mm) | [-, -, -] | [-, -, -] | [-, -, -] |
| $ZR_{95}$ | Root depth, $95^{th}$ percentile of vegetation (mm) | [-, 300, 1500$^{(1)}$] | [-, 200, 1000] | [-, 250, 1000] |
| $RI_{root}$ | Root length index (m root m$^{-2}$ PFT) | [-, 4000, 2200] | [-, 4500, 5000] | [-, 2000, 1200] |
| $\psi_{Sto_{00}}$ | Soil water potential at the beginning of stomatal closure (MPa) | [-, -0.5, -0.9] | [-, -0.6, -0.7] | [-, -0.5, -0.9] |
| $\psi_{Sto_{50}}$ | Soil water potential at 50 % stomatal closure (MPa) | [-, -1.6, -1.7] | [-, -2, -1.5] | [-, -3, -2] |
| $\psi_{L50}$ | Water potential at 50 % of leaf hydraulic conductivity (MPa) | [-, -2, -2.8] | [-, -2.5, -2.5] | [-, -2.5, -1.2] |
| $\psi_{X50}$ | Water potential at 50 % of xylem hydraulic conductivity and limit for water extraction from soil (MPa) | [-, -5.5, -4.5] | [-, -9.5, -9] | [-, -3.5, -4] |
| $\phi_p$ | Photosynthesis pathway ($C_3$, $C_4$, or $CAM$) | [-, 4, 3] | [-, 3, 3] | [-, 3, 3] |
| $K_N$ | Canopy nitrogen decay coefficient ($-$) | [-, 0.3, 0.4] | [-, 0.3, 0.15] | [-, 0.2, 0.25] |
| $V_{c,max}$ | Maximum Rubisco capacity at 25 °C leaf scale ($\mathrm{\mu mol\,CO_2\,m^{-2}\,s^{-1}}$) | [-, 54, 49] | [-, 54, 45] | [-, 58, 45] |
| $g_{0,CO_2}$ | Minimum/cuticular stomatal conductance ($\mathrm{mol\,CO_2\,m^{-2}\,leaf\,s^{-1}}$) | [-, 0.01, 0.01] | [-, 0.01, 0.01] | [-, 0.01, 0.01] |
| $a_1$ | Empirical parameter linking net assimilaton $A_{nC}$ to stomatal conductance $g_{s,CO_2}$ ($-$) | [-, 5, 9] | [-, 7, 8] | [-, 6, 9] |
| $r_{jv}$ | Scaling factor between $J_{max}$ and $V_{c,max}$ ($\mathrm{\mu mol\,equivalent\,\mu mol^{-1}\,CO_2}$) | [-, 2.1, 2.2] | [-, 2.1, 2.0] | [-, 2.2, 2.0] |
| $\epsilon_{FI}$ | Intrinsec quantum efficency ($\mathrm{\mu mol\,CO_2\,\mu mol^{-1}\,photons}$) | [-, 0.04, 0.081] | [-, 0.081, 0.081] | [-, 0.081, 0.081] |
| $\Delta_{0,r}$ | Empirical coefficient that expresses the value of vapor pressure deficit at which $f(\Delta e) = 0.5$ (Pa) | [-, 2000, 2000] | [-, 1000, 1200] | [-, 2000, 2000] |

* (Fatichi and Pappas, 2017), $^{(1)}$ Harshan et al. (2017), $^{(2)}$ Liu et al. (2017)

**Table 3.** Soil, interception, and runoff parameters used for the model validation in Singapore (SG), Melbourne (MB), and Phoenix (PH).

| Parameter | Description | SG | MB | PH |
|---|---|---|---|---|
| $Z_{s,r}$ | Roof soil layer discretization (mm) | - | - | - |
| $Z_{s,g}$ | Ground soil layer discretization (mm) | [0 ... 2000] | [0 ... 2000] | [0 ... 2000] |
| $F_{r,soil}$ | Roof soil composition [$f_{clay}$, $f_{sand}$, $f_{organic}$] $(-)$ | - | - | - |
| $F_{g,soil}$ | Ground soil composition [$f_{clay}$, $f_{sand}$, $f_{organic}$] $(-)$ | [0.20, 0.40, 0.025] | [0.20, 0.40, 0.025] | [0.20, 0.40, 0.025] |
| $K_{imp}$ | Hydraulic conductivity of impervous surface [$_{roof}$, $_{ground}$] (mm h$^{-1}$) | [-, 0.001] | [-, 0.001] | [-, 0.001] |
| $K_{bot}$ | Hydraulic conductivity of at the bottom of the last soil layer [$_{roof}$, $_{ground}$] (mm h$^{-1}$) | [-, free drainage] | [-, free drainage] | [-, free drainage] |
| $SPAR$ | Soil parameter type, 1-VanGenuchten or 2-Saxton-Rawls [$_{roof}$, $_{ground}$] $(-)$ | [-, 2] | [-, 2] | [-, 2] |
| $In_{imp}^{max}$ | Maximum interception capacity of impervious surfaces [$_{roof}$, $_{ground}$] (mm) | [0.25, 0.5] | [0.25, 0.5] | [0.25, 0.5] |
| $In_{soil}^{max}$ | Maximum interception capacity on top of soil [$_{r,veg}$, $_{g,bare}$, $_{g,veg}$] (mm) | [-, 10, 10] | [-, 10, 10] | [-, 10, 10] |
| $S_{P,In}^{max}$ | Specific water retained by vegetation surface [$_{r,veg}$, $_{g,veg}$, $_{tree}$] (mm m$^2$ PFT area m$^{-2}$ leaf area) | [-, 0.2, 0.1] | [-, 0.2, 0.1] | [-, 0.2, 0.1] |
| $\lambda_r$ | Percentage of runoff that leaves the system [$_{roof}$, $_{ground}$] $(-)$ | [1, 0.5] | [1, 0.5] | [1, 0.5] |

**Table 4.** Location and measurement parameters, and anthropogenic heat used for the model validation in Singapore (SG), Melbourne (MB), and Phoenix (PH).

| Parameter | Description | SG | MB | PH |
|---|---|---|---|---|
| $\phi_{data}$ | Latitude (positive north) (°) | 1.31[1,2] | -37.81[6] | 33.48[8] |
| $\lambda_{data}$ | Longitude (positive east) (°) | 103.91[1,2] | 144.88[6] | -112.14[8] |
| $\theta_{canyon}$ | Canyon orientation [direction 1, direction 2] (°) | [78, 157][10] | [98, 189][10] | [90, 180][10] |
| $\Delta_{GMT}$ | difference of LT with Greenwich Meridian Time (h) | 8[2] | 10 | -7 |
| $Z_{atm}$ | Atmospheric forcing/reference height (m) | 23.7[3,4,5] | 40[6,7] | 22.1[8] |
| $T_{b,min}$ | Minimum interior building temperature (°C) | 20 | 18 | 18 |
| $T_{b,max}$ | Maximum interior building temperature (°C) | 25 | 27 | 28 |
| $Q_{f,roof}$ | Anthropogenic heat input on top of roof (W m$^{-1}$) | 0 | 0 | 0 |
| $Q_{f,can}$ | Anthropogenic heat input within canyon (W m$^{-1}$) | 11[2] | 0 | 23.25[9] |

[1] Velasco et al. (2013), [2] Roth et al. (2016), [3] Demuzere et al. (2017), [4] Harshan et al. (2017), [5] Liu et al. (2017), [6] Coutts et al. (2007a, b), [7] Grimmond et al. (2011), [8] Chow et al. (2014), [9] average calculated from values reported by Chow et al. (2014), [10] estimated from GoogleEarth.

**Table 5.** Timeseries of urban irrigation applied during model performance assessment of UT&C in Singapore, Melbourne, and Phoenix. In short, no irrigation is applied in Singapore, while plants receive irrigation during summer and autumn time in Melbourne, and there is hose irrigation year-round with higher values during summer time in Phoenix (Volo et al., 2014).

| | Time (h) | Vegetated roof $(mm\ h^{-1})$ | Bare ground $(mm\ h^{-1})$ | Vegetated ground $(mm\ h^{-1})$ |
|---|---|---|---|---|
| **Singapore** | | | | |
| $1^{st}$ of January - $31^{st}$ of December | 00:00-23:00 | - | 0 | 0 |
| **Melbourne** | | | | |
| $15^{th}$ of November - $29^{th}$ of February | 00:00-23:00 | - | 0 | 0.125 |
| $1^{st}$ of March - $15^{th}$ of April | 00:00-23:00 | - | 0 | 0.083 |
| $16^{th}$ of April - $14^{th}$ of November | 00:00-23:00 | - | 0 | 0 |
| **Phoenix** | | | | |
| January | 06:00 - 17:00 | - | 0 | 0.0365 |
| February | 06:00 - 17:00 | - | 0 | 0.0437 |
| March | 06:00 - 17:00 | - | 0 | 0.1313 |
| April | 06:00 - 17:00 | - | 0 | 0.4375 |
| May | 06:00 - 17:00 | - | 0 | 1.0646 |
| June | 06:00 - 17:00 | - | 0 | 1.1812 |
| July | 06:00 - 17:00 | - | 0 | 1.2396 |
| August | 06:00 - 17:00 | - | 0 | 0.2625 |
| September | 06:00 - 17:00 | - | 0 | 0.1604 |
| October | 06:00 - 17:00 | - | 0 | 0.1167 |
| November | 06:00 - 17:00 | - | 0 | 0.0729 |
| December | 06:00 - 17:00 | - | 0 | 0.0219 |

## 10 Additional Figures and model performance results

The following Tables 6 and 7 provide additional model performance results for the total time periods as well as daytime and nighttime fluxes. The following figures show the validation of shortwave radiation (Fig. 9), and longwave radiation (Fig. 10) in Singapore, Melbourne, and Phoenix as an addition to the validation of net all wave radiation presented in the main article. Figure 12 and 13 show the sensitivity of evapotranspiration and the energy fluxes to the change in vegetated ground cover ($\lambda_{G,veg}$), leaf area index (LAI), and maximum Rubisco capacity ($V_{c,max}$) in Singapore as an addition to the sensitivity of 2 m air temperature, 2 m humidity and the water fluxes presented in the main article.

**Table 6.** Coefficient of determination ($R^2$), mean bias error (MBE), root mean square error (RMSE), systematic root mean square error ($\text{RMSE}_s$), unsystematic root mean square error ($\text{RMSE}_u$), and mean absolute error (MAE) of the UT&C model performance assessment in Singapore, Melbourne and Phoenix split in daytime and nighttime values for the radiative fluxes. The validation period specifies the total UT&C simulation period in hours (h) and the percentage of time with available eddy-covariance measurements for model performance assessment.

| | $R^2$ | MBE | RMSE | $\text{RMSE}_s$ | $\text{RMSE}_u$ | MAE | Validation period |
|---|---|---|---|---|---|---|---|
| | $(-)$ | $(\text{W m}^{-2})$ | $(\text{W m}^{-2})$ | $(\text{W m}^{-2})$ | $(\text{W m}^{-2})$ | $(\text{W m}^{-2})$ | % of (h) |
| $S\uparrow$ (Singapore), full period, daytime | 0.97 | -5.5 | 9.7 | 7.6 | 6 | 6.6 | 84 % of 4015 h |
| $S\uparrow$ (Singapore), dry period, daytime | 0.97 | -13.1 | 16.3 | 15.1 | 6.1 | 13.3 | 99 % of 330 h |
| $S\uparrow$ (Melbourne), full period, daytime | 0.99 | -12.5 | 16.3 | 15.9 | 3.4 | 12.8 | 65 % of 5747 h |
| $S\uparrow$ (Phoenix), full period, daytime | 0.98 | -5.9 | 10.7 | 8.8 | 6.1 | 8.1 | 98 % of 4539 h |
| $L\uparrow$ (Singapore), full period | 0.93 | 8.3 | 23.3 | 20.4 | 11.4 | 17.3 | 86 % of 8760 h |
| $L\uparrow$ (Singapore), full period, daytime | 0.93 | 28.2 | 33.4 | 31.6 | 10.6 | 28.4 | 84 % of 4015 h |
| $L\uparrow$ (Singapore), full period, nighttime | 0.79 | -8.3 | 9.3 | 8.4 | 3.9 | 8.6 | 88 % of 4015 h |
| $L\uparrow$ (Singapore), dry period | 0.98 | 8.9 | 23.8 | 22.8 | 6.9 | 18.2 | 99 % of 720 h |
| $L\uparrow$ (Singapore), dry period, daytime | 0.98 | 29.7 | 33.8 | 33.1 | 7 | 29.7 | 99 % of 330 h |
| $L\uparrow$ (Singapore), dry period, nighttime | 0.94 | -9 | 9.4 | 9.1 | 2 | 9 | 100 % of 330 h |
| $L\uparrow$ (Melbourne), full period | 0.94 | 7.8 | 14.8 | 8.6 | 12 | 11.7 | 62 % of 11376 h |
| $L\uparrow$ (Melbourne), full period, daytime | 0.95 | 15.2 | 18.8 | 15.5 | 10.7 | 16 | 64 % of 5747 h |
| $L\uparrow$ (Melbourne), full period, nighttime | 0.91 | -0.1 | 8.6 | 6.1 | 6 | 7 | 61 % of 5629 h |
| $L\uparrow$ (Phoenix), full period | 0.98 | 4.9 | 11.5 | 5.4 | 10.2 | 9.2 | 98 % of 9144 h |
| $L\uparrow$ (Phoenix), full period, daytime | 0.98 | 8.2 | 13.5 | 8.6 | 10.5 | 11.2 | 98 % of 4539 h |
| $L\uparrow$ (Phoenix), full period, nighttime | 0.99 | 1.6 | 9.1 | 8 | 4.3 | 7.3 | 98 % of 4605 h |
| $R_n$ (Singapore), full period | >0.99 | -4.9 | 20.8 | 19 | 8.4 | 16.4 | 84 % of 8760 h |
| $R_n$ (Singapore), full period, daytime | >0.99 | -22.8 | 28 | 26.2 | 10 | 23.4 | 84 % of 4015 h |
| $R_n$ (Singapore), full period, nighttime | 0.91 | 11.3 | 12.2 | 11.8 | 3.1 | 11.4 | 84 % of 4015 h |
| $R_n$ (Singapore), dry period | >0.99 | -2.3 | 17 | 15.2 | 7.5 | 14.3 | 93 % of 720 h |
| $R_n$ (Singapore), dry period, daytime | >0.99 | -16.6 | 21.1 | 19 | 9.2 | 17.6 | 99 % of 330 h |
| $R_n$ (Singapore), dry period, nighttime | 0.87 | 12.1 | 12.4 | 12.2 | 2.4 | 12.1 | 87 % of 330 h |
| $R_n$ (Melbourne), full period | >0.99 | -0.6 | 9.5 | 1.5 | 9.4 | 7.5 | 62 % of 11376 h |
| $R_n$ (Melbourne), full period, daytime | >0.99 | -2.7 | 9.4 | 3 | 8.9 | 7.5 | 64 % of 5747 h |
| $R_n$ (Melbourne), full period, nighttime | 0.94 | 1.7 | 9.6 | 6.9 | 6.6 | 7.5 | 61 % of 5629 h |
| $R_n$ (Phoenix), full period | >0.99 | -2.1 | 12.5 | 2.1 | 12.3 | 9.7 | 98 % of 9144 h |
| $R_n$ (Phoenix), full period, daytime | >0.99 | -2.3 | 15 | 2.3 | 14.8 | 11.9 | 98 % of 4539 h |
| $R_n$ (Phoenix), full period, nighttime | 0.8 | -1.9 | 9.4 | 4.3 | 8.3 | 7.4 | 98 % of 4605 h |

**Table 7.** Same as Table 6 for sensible ($H$) and latent ($\lambda E$) heat fluxes.

| | $R^2$ | MBE | RMSE | $RMSE_s$ | $RMSE_u$ | MAE | Validation period |
|---|---|---|---|---|---|---|---|
| | $(-)$ | $(\mathrm{W\ m^{-2}})$ | $(\mathrm{W\ m^{-2}})$ | $(\mathrm{W\ m^{-2}})$ | $(\mathrm{W\ m^{-2}})$ | $(\mathrm{W\ m^{-2}})$ | % of (h) |
| $H$ (Singapore), full period | 0.93 | -3.3 | 25.6 | 3.3 | 25.3 | 15.4 | 82 % of 8760 h |
| $H$ (Singapore), full period, daytime | 0.87 | -3.3 | 37 | 3.3 | 36.8 | 26.6 | 80 % of 4015 h |
| $H$ (Singapore), full period, nighttime | 0.35 | -3 | 8.2 | 7.5 | 3.2 | 5.9 | 84 % of 4015 h |
| $H$ (Singapore), dry period | 0.95 | -8.1 | 30 | 8.2 | 28.9 | 20.4 | 99 % of 720 h |
| $H$ (Singapore), dry period, daytime | 0.89 | -10.5 | 43.1 | 13.8 | 40.8 | 35.2 | 98 % of 330 h |
| $H$ (Singapore), dry period, nighttime | 0.62 | -5.2 | 8.9 | 8.4 | 3 | 7.2 | 100 % of 330 h |
| $H$ (Melbourne), full period | 0.9 | 14.4 | 36.6 | 17.2 | 32.3 | 23.6 | 93 % of 11376 h |
| $H$ (Melbourne), full period, daytime | 0.86 | 25.5 | 49.8 | 26.3 | 42.3 | 37.2 | 93 % of 5747 h |
| $H$ (Melbourne), full period, nighttime | 0.48 | 2.9 | 13.1 | 8.2 | 10.2 | 9.7 | 92 % of 5629 h |
| $H$ (Phoenix), full period | 0.92 | 10.9 | 27.4 | 11.6 | 24.9 | 20.7 | 78 % of 9144 h |
| $H$ (Phoenix), full period, daytime | 0.88 | 7.6 | 33.8 | 8.2 | 32.8 | 26.3 | 77 % of 4539 h |
| $H$ (Phoenix), full period, nighttime | 0.1 | 14 | 19.2 | 15.6 | 11.2 | 15.1 | 78 % of 4605 h |
| $\lambda E$ (Singapore), full period | 0.58 | -0.6 | 28.7 | 13.8 | 25.2 | 15.9 | 81 % of 8760 h |
| $\lambda E$ (Singapore), full period, daytime | 0.27 | 1.4 | 39.8 | 27 | 29.3 | 26.7 | 80 % of 4015 h |
| $\lambda E$ (Singapore), full period, nighttime | 0.25 | -2.1 | 12.9 | 11.7 | 5.5 | 6.2 | 81 % of 4015 h |
| $\lambda E$ (Singapore), dry period | 0.67 | 2.5 | 16.2 | 7 | 14.7 | 10.5 | 97 % of 720 h |
| $\lambda E$ (Singapore), dry period, daytime | 0.24 | 4.8 | 22.5 | 18 | 13.5 | 17.2 | 98 % of 330 h |
| $\lambda E$ (Singapore), dry period, nighttime | 0.03 | 0.2 | 6.2 | 5.8 | 2.2 | 3.9 | 95 % of 330 h |
| $\lambda E$ (Melbourne), full period | 0.62 | 1.9 | 26.8 | 9.4 | 25.1 | 16.8 | 93 % of 11376 h |
| $\lambda E$ (Melbourne), full period, daytime | 0.48 | 3.5 | 34.3 | 14.9 | 30.9 | 23.5 | 93 % of 5747 h |
| $\lambda E$ (Melbourne), full period, nighttime | 0.15 | 0.2 | 15.6 | 11.6 | 10.5 | 10 | 92 % of 5629 h |
| $\lambda E$ (Phoenix), full period | 0.5 | 4.1 | 19.5 | 11.3 | 16 | 11.5 | 78 % of 9144 h |
| $\lambda E$ (Phoenix), full period, daytime | 0.3 | 7.1 | 25.2 | 19.5 | 15.9 | 17.8 | 77 % of 4539 h |
| $\lambda E$ (Phoenix), full period, nighttime | 0.16 | 1.2 | 11.7 | 10.1 | 5.8 | 5.3 | 78 % of 4605 h |
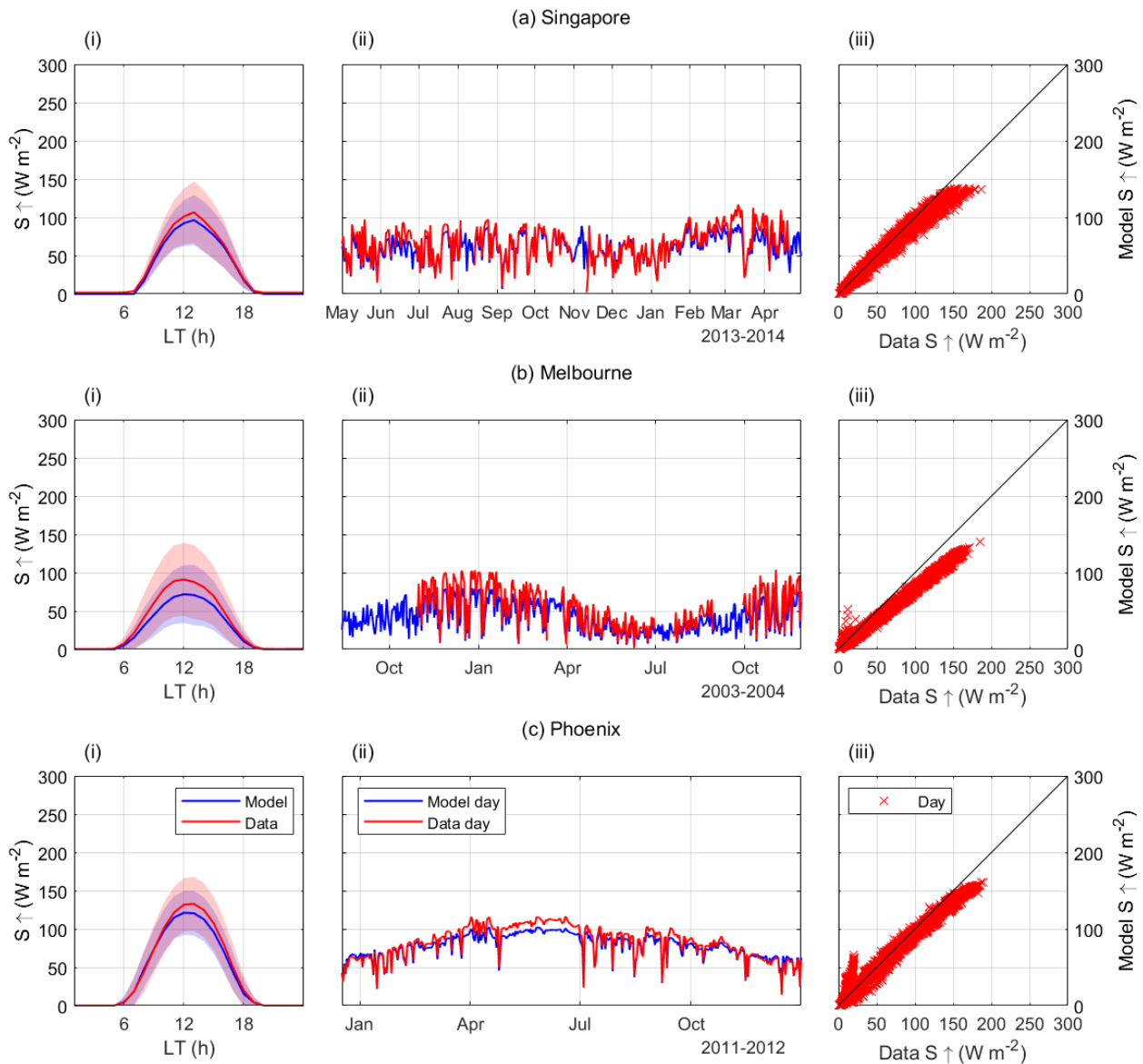
**Figure 9.** Comparison of modelled and measured outgoing shortwave radiation $K\uparrow$ for the validation sites in a) Singapore, b) Melbourne, and c) Phoenix. (i): Mean daily cycle (lines) +/-1 standard deviation (shaded area). (ii): Time series of mean daytime fluxes. (iii): Correlation of hourly daytime measurements and simulations.
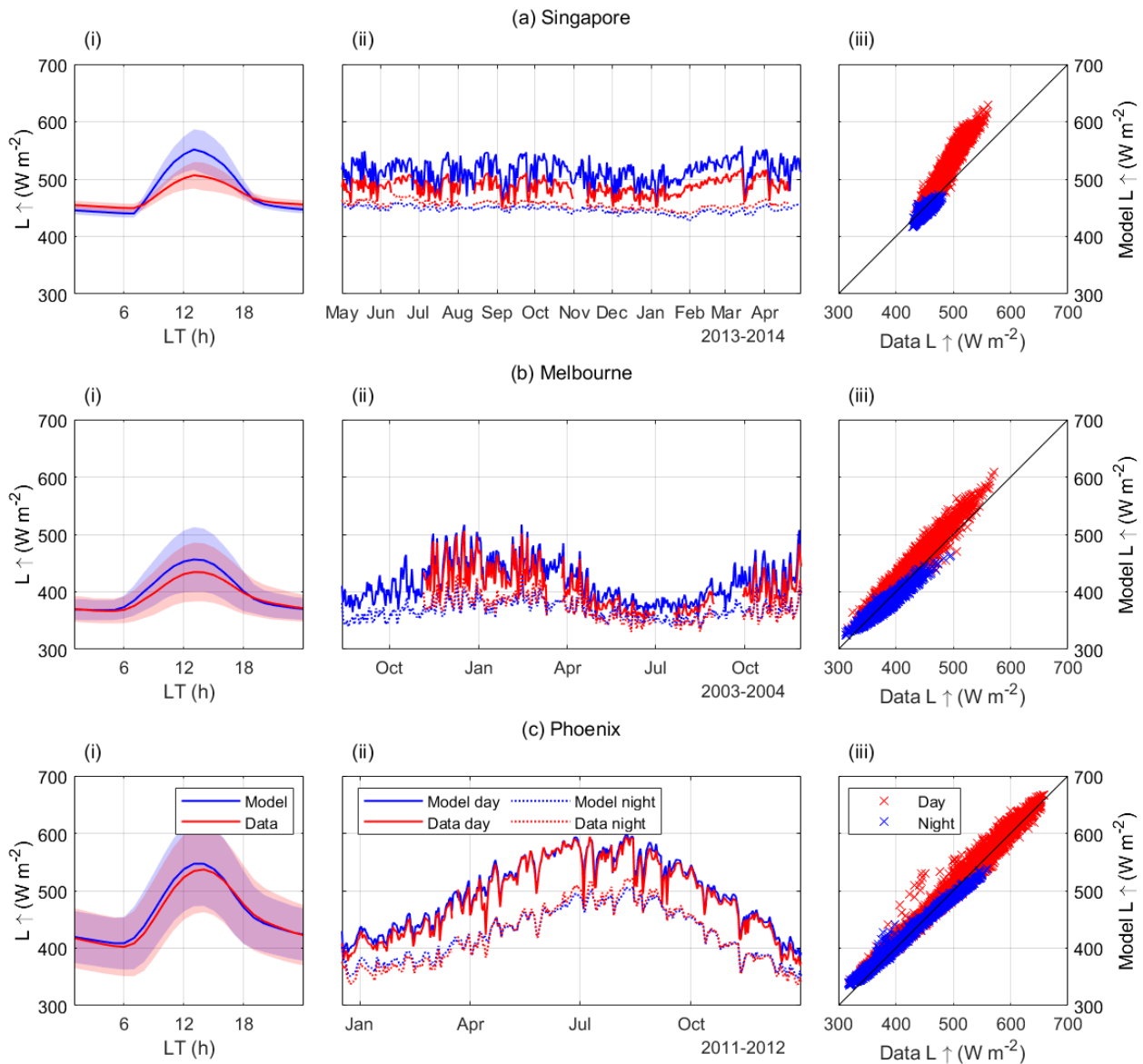
**Figure 10.** Comparison of modelled and measured outgoing longwave radiation $L\uparrow$ for the validation sites in a) Singapore, b) Melbourne, and c) Phoenix. (i): Mean daily cycle (lines) +/-1 standard deviation (shaded area). (ii): Time series of mean daytime (solid lines) and nighttime (dashed lines) fluxes. (iii): Correlation of hourly daytime/nighttime measurements and simulations.
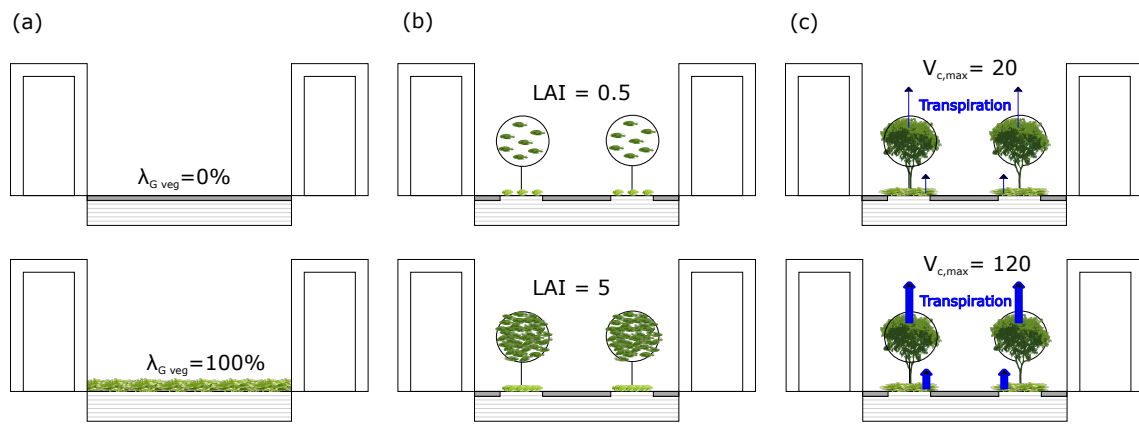
**Figure 11.** Geometric set-up of the urban scene in Telok Kurau Singapore for the sensitivity analysis of the vegetated ground fraction ($\lambda_{G,veg}$), LAI and maximum Rubisco capacity ($V_{c,max}$). $\lambda_{G,veg}$ is varied between 0 and 100 % (0 and 1), LAI between 0.5 and 5, and $V_{c,max}$ between 20 and 120 µmol $CO_2$ s$^{-1}$m$^{-2}$. The urban scene is defined by the parameter set of Telok Kurau (Sect. 9 of TRM).
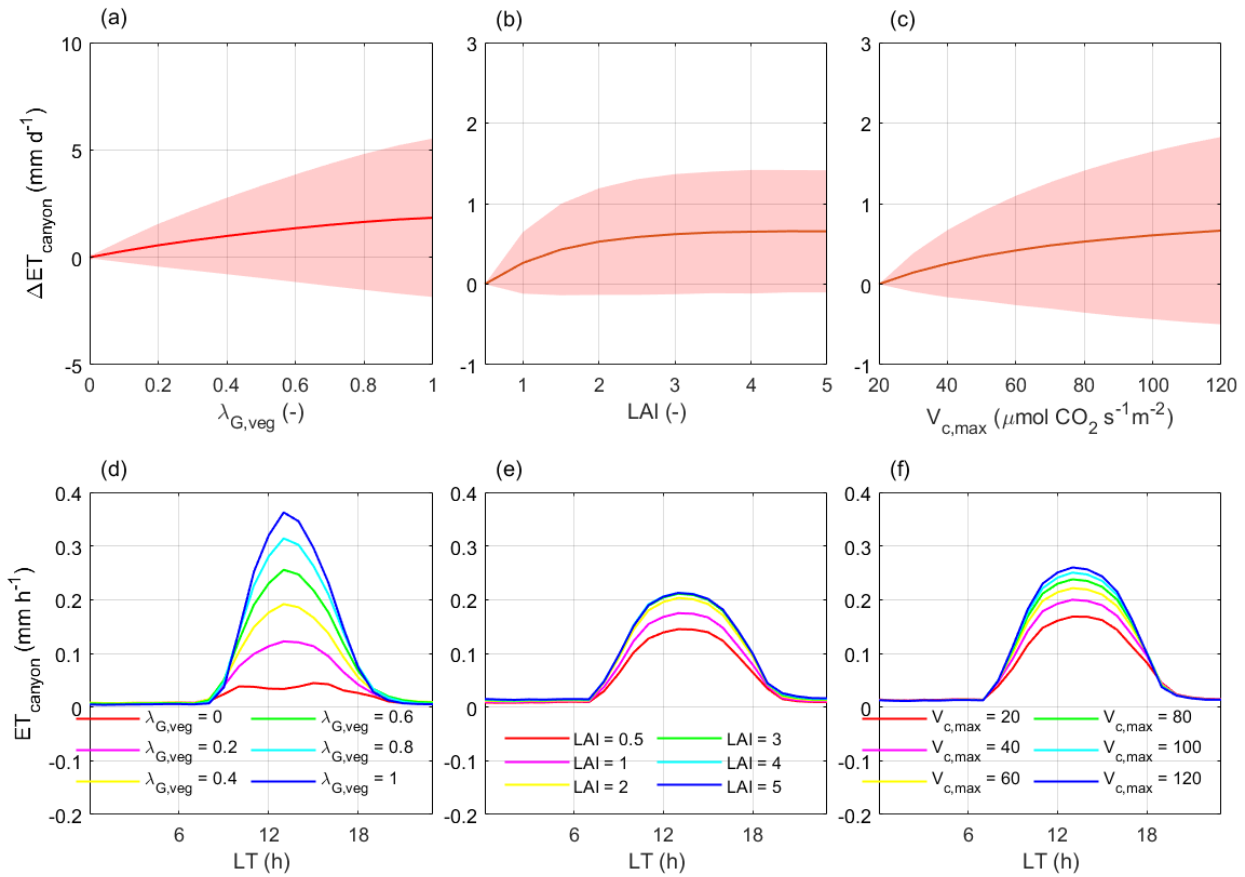
**Figure 12.** Sensitivity analysis of canyon evapotranspiration ($ET_{canyon}$) caused by the change in vegetated ground cover fraction ($\lambda_{veg}$), leaf area index (LAI), and maximum Rubisco capacity ($V_{c,max}$) in Telok Kurau Singapore. (a), (b), and (c): Long term mean evapotranspiration change with respect to the baseline case of no-vegetation (solid line) +/-1 standard deviation (shaded area). (d), (e), and (f): Long term mean daily cycle of evapotranspiration. $\lambda_{veg}$ is increased from 0 to 1, LAI is increased from 0.5 to 5, $V_{c,max}$ is increased from 20 to 120.
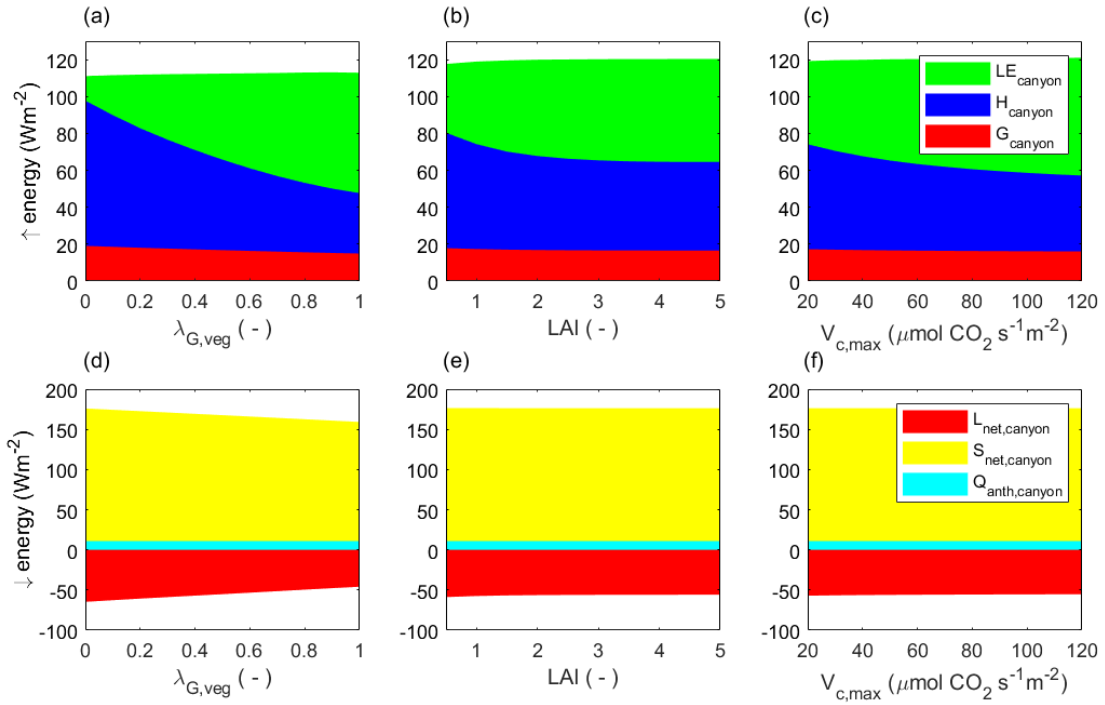
**Figure 13.** Energy balance components of the urban canyon ($LE_{canyon}$: Latent heat, $H_{canyon}$: Sensible heat, $G_{canyon}$: Conductive heat flux) as a function of (a) vegetated ground cover fraction ($\lambda_{G,veg}$), (b) leaf area index (LAI), and (c) maximum Rubisco capacity ($V_{c,max}$) in Telok Kurau Singapore. Absorbed longwave radiation ($L_{net,canyon}$), absorbed shortwave radiation ($S_{net,canyon}$), and anthropogenic heat flux ($Q_{anth,canyon}$) in the urban canyon as a function of (d) vegetated ground cover fraction ($\lambda_{G,veg}$), (e) leaf area index (LAI), and (f) maximum Rubisco capacity ($V_{c,max}$) in Telok Kurau Singapore. The overall conductive heat flux $G_{canyon}$ comprises ground heat fluxes as well as conductive fluxes into buildings which in Singapore often have airconditioned interiors resulting in an overall positive $G_{canyon}$ .

*Code and data availability.* The development of UT&C, model validation, and graphs presented in this paper were conducted in Matlab R2018b. The exact version of UT&C used to produce the results used in this paper is archived on Zenodo (Meili and Fatichi, 2019). The original source code for the ecohydrological model Tethys-Chloris was obtained from the author (Fatichi et al., 2012a, b) while the building and tree shading calculations are based on the code of Ryu et al. (2016). The tower based eddy covariance measurements used for model validation were obtained from the authors in Telok Kurau Singapore (Velasco et al., 2013; Roth et al., 2016), in Preston Melbourne (Coutts et al., 2007a, b; Nice et al., 2018), and from the Global Institute of Sustainability, Arizona State University (ASU) in Maryvale Phoenix (Chow et al., 2014; Chow, 2017).

*Author contributions.* NM, and SF designed the study, developed the code, conducted the analysis and wrote the manuscript with inputs from GM. MR, EV, AC, WC collected and shared their eddy-covariance measurements for the purpose of model validation. EBZ shared the code presented in Ryu et al. (2016). All authors gave commments and contributed to the final version of the manuscript.

*Competing interests.* The authors declare that they have no conflict of interest.

*Acknowledgements.* The research was conducted at the Future Cities Laboratory at the Singapore-ETH Centre, which was established collaboratively between ETH Zurich and Singapore's National Research Foundation (FI370074016) under its Campus for Research Excellence and Technological Enterprise programme. GM was supported by the "The Branco Weiss Fellowship - Society in Science" administered by ETH Zurich. EV acknowledges a research fellowship granted by the Centre for Urban Greenery and Ecology of Singapore's National Parks Board.

## References

1275

Abdella, K. and McFarlane, N. A.: Parameterization of the surface-layer exchange coefficients for atmospheric models, Boundary-Layer Meteorology, 80, 223–248, 1996.

Arora, V. K. and Boer, G. J.: A parameterization of leaf phenology for the terrestrial ecosystem component of climate models, Global Change Biology, 11, 39–59, 2005.

1280 Arya, S. P.: Introduction to Micrometeorology, Academic Press, 2nd edn., 2001.

Assouline, S. and Or, D.: Anisotropy factor of saturated and unsaturated soils, Water Resour. Res., 42, W12 403, doi:10.1029/2006WR005001, 2006.

Atkin, O. K., Westbeek, M. H. M., Cambridge, M. L., Lambers, H., and Pons, T. L.: Leaf respiration in light and darkness. A comparison of slow- and fast-growing Poa species, Plant Physiology, 113, 961–965, 1997.

1285 Ball, J. T., Woodrow, I. E., and Berry, J. A.: A model predicting stomatal conductance and its contribution to the control of photosynthesis under different environmental conditions, in: Progress in photosynthesis research, edited by Biggins, pp. 221–224, Martinus Nijhoff, Netherlands, 1987.

Beljaars, A. C. M.: The parametrization of surface fluxes in large-scale models under free convection, Q. J . R. Meteorol. Soc., 121, 255–270, 1994.

1290 Bertoldi, G., Rigon, R., Tamanini, D., and Zanotti, F.: GEOtop version 0.875: Technical description and programs guide, Tech. Rep. dica-06-001, University of Trento E-Prints, 2006.

Bohrer, G., Mourad, H., Laursen, T. A., Drewry, D., Avissar, R., Poggi, D., Oren, R., and Katul, G. G.: Finite element tree crown hydrodynamics model (FETCH) using porous media flow within branching elements: A new representation of tree hydrodynamics, Water Resources Research, 41, doi:10.1029/2005WR004181, 2005.

1295 Bonan, G.: Ecological Climatology: Concept and Applications, Cambridge Univ. Press, New York, 2002.

Bonan, G. B., Lawrence, P. J., Oleson, K. W., Levis, S., Jung, M., Reichstein, M., Lawrence, D. M., and Swenson, S. C.: Improving canopy processes in the Community Land Model version 4 (CLM4) using global flux fields empirically inferred from FLUXNET data, Journal of Geophysical Research, 116, doi:10.1029/2010JG001593, 2011.

Brutsaert, W.: Evaporation into the atmosphere, D. Reidel, 1982.

1300 Brutsaert, W.: Hydrology. An Introduction, Cambridge University Press, Cambridge, UK, 2005.

Buckley, T. N., Mott, K. A., and Farquhar, G. D.: A hydromechanical and biochemical model of stomatal conductance, Plant, Cell and Environment, 26, 1767–1785, 2003.

Choudhury, B. J. and Monteith, J. L.: A four-layer model for the heat budget of homogeneous land surfaces, Quarterly Journal of the Royal Meteorological Society, 114, 378–398, 1988.

1305 Chow, W.: Eddy covariance data measured at the CAP LTER flux tower located in the west Phoenix, AZ neighborhood of Maryvale from 2011-12-16 through 2012-12-31. Environmental Data Initiative., https://doi.org/10.6073/pasta/fed17d67583eda16c439216ca40b0669, 2017.

Chow, W. T. L., Volo, T. J., Vivoni, E. R., Darrel, G., and Ruddell, B. L.: Seasonal dynamics of a suburban energy balance in Phoenix , Arizona, International Journal of Climatology, 34, 3863–3880, https://doi.org/10.1002/joc.3947, 2014.

1310 Collatz, G. J., Ball, J. T., Grivet, C., and Berry, J. A.: Physiological and environmental regulation of stomatal conductance, photosynthesis and transpiration-A model that includes a laminar boundary-layer, Agricultural and Forest Meteorology, 54, 107–136, 1991.

Collatz, G. J., Ribas-Carbo, M., and Berry, J. A.: Coupled photosynthesis-stomatal conductance model for leaves of C4 plants, Australian Journal of Plant Physiology, 19, 519–538, 1992.

Collins, D. B. G. and Bras, R. L.: Plant rooting strategies in water-limited ecosystems, Water Resources Research, 43, doi:10.1029/2006WR005541, 2007.

Coutts, A. M., Beringer, J., and Tapper, N. J.: Characteristics influencing the variability of urban CO2 fluxes in Melbourne, Australia, Atmospheric Environment, 41, 51–62, https://doi.org/10.1016/j.atmosenv.2006.08.030, 2007a.

Coutts, A. M., Beringer, J., and Tapper, N. J.: Impact of increasing urban density on local climate: Spatial and temporal variations in the surface energy balance in Melbourne, Australia, Journal of Applied Meteorology and Climatology, 46, 477–493, https://doi.org/10.1175/JAM2462.1, 2007b.

Dai, Y., Dickinson, R. E., and Wang, Y.-P.: A two-big-leaf model for canopy temperature, photosynthesis, and stomatal conductance, Journal of Climate, 17, 2281–2299, 2004.

de Munck, C., Lemonsu, A., Masson, V., Le Bras, J., and Bonhomme, M.: Evaluating the impacts of greening scenarios on thermal comfort and energy and water consumptions for adapting Paris city to climate change, Urban Climate, 23, 260–286, https://doi.org/10.1016/j.uclim.2017.01.003, 2018.

de Pury, D. G. G. and Farquhar, G. D.: Simple scaling of photosynthesis from leaves to canopies without the errors of big-leaf models, Plant, Cell and Environment, 20, 537–557, 1997.

de Vries, D. A.: Thermal Properties of Soils, in: Physics of the Plant Environment, edited by van Wijk, W., North-Holland, Amsterdam, 1963.

Deardorff, J. W.: Efficient prediction of ground surface temperature and moisture with inclusion of a layer of vegetation, Journal of Geophysical Research, 83, 1889–1903, 1978.

Deckmyn, G., Verbeeck, H., de Beeck, M. O., Vansteenkiste, D., Steppe, K., and Ceulemans, R.: ANAFORE: A stand-scale process-based forest model that includes wood tissue development and labile carbon storage in trees, Ecological Modelling, 215, 345–368, doi:10.1016/j.ecolmodel.2008.04.007, 2008.

Demuzere, M., Harshan, S., Jaervi, L., Roth, M., Grimmond, C. S. B., Masson, V., Oleson, K. W., Velasco, E., and Wouters, H.: Impact of urban canopy models and external parameters on the modelled urban energy balance in a tropical city, Quarterly, https://doi.org/10.1002/qj.3028, 2017.

Dickinson, R. E., Henderson-Sellers, A., and Kennedy, P. J.: Biosphere-atmosphere transfer scheme (BATS) version 1E as coupled to the NCAR Community Climate Model, Tech. Rep. NCAR/TN-387+STR, Natl. Cent. for Atmos. Res., Boulder, Colorado, 1993.

Dye, D. G.: Spectral composition and quanta-to-energy ratio of diffuse photosynthetically active radiation under diverse cloud conditions, Journal of Geophysical Research, 109, doi:10.1029/2003JD004251, 2004.

Eltahir, E. A. B. and Bras, R. L.: A Description of rainfall interception over large-areas, Journal of Climate, 6, 1002–1008, 1993.

Farouki, O. T.: The thermal properties of soils in cold regions, Cold Regions Science and Technology, 5, 67–75, 1981.

Farquhar, G. D., Caemmerer, S. V., and Berry, J. A.: A biochemical model of photosynthetic $CO_2$ assimilation in leaves of C3 species, Planta, 149, 78–90, 1980.

Fatichi, S. and Pappas, C.: Constrained variability of modeled T:ET ratio across biomes, Geophysical Research Letters, 44, 6795–6803, https://doi.org/10.1002/2017GL074041, 2017.

Fatichi, S., Ivanov, V. Y., and Caporali, E.: A mechanistic ecohydrological model to investigate complex interactions in cold and warm water-controlled environments : 1 . Theoretical framework and plot-scale analysis, Journal of Advances in Modeling Earth Systems, 4, 1–31, https://doi.org/10.1029/2011MS000086, 2012a.

Fatichi, S., Ivanov, V. Y., and Caporali, E.: A mechanistic ecohydrological model to investigate complex interactions in cold and warm water-controlled environments : 2 . Spatiotemporal analyses, Journal of Advances in Modeling Earth Systems, 4, 1–22, https://doi.org/10.1029/2011MS000087, 2012b.

Fatichi, S., Ivanov, V. Y., and Caporali, E.: Supplementary Material : A mechanistic ecohydrological model to investigate complex interactions in cold and warm water-controlled environments . 1 . Theoretical Framework, Journal of Advances in Modeling Earth Systems, pp. 1–73, 2012c.

Feddes, R. A., Hoff, H., Bruen, M., Dawson, T., de Rosnay, P., Dirmeyer, P., Jackson, R. B., Kabat, P., Kleidon, A., Lilly, A., and Pitmank, A. J.: Modeling Root Water Uptake in Hydrological and Climate Models, Bulletin of the American Meteorological Society, 82, 2797–2809, 2001.

Frank, A., Heidemann, W., and Spindler, K.: Modeling of the surface-to-surface radiation exchange using a Monte Carlo method, Journal of Physics: Conference Series, 745, https://doi.org/10.1088/1742-6596/745/3/032143, 2016.

Gao, Q., Xhao, P., Zeng, X., Cai, X., and Shen, W.: A model of stomatal conductance to quantify the relationship between leaf transpiration, microclimate, and soil water stress, Plant, Cell and Environment, 25, 1373–1381, 2002.

Garrote, L. and Bras, R. L.: A distributed model for real-time flood casting using digital elevation models, Journal of Hydrology, 167, 279–306, 1995.

Grimmond, C. S. B., Blackett, M., Best, M. J., Baik, J., Belcher, S. E., Beringer, J., Bohnenstengel, S. I., Calmet, I., Chen, F., Coutts, A., Dandou, A., Fortuniak, K., Gouvea, M. L., Hamdi, R., Hendry, M., Kanda, M., Kawai, T., Kawamoto, Y., Kondo, H., Krayenhoff, E. S., Lee, S., Loridan, T., Martilli, A., Masson, V., Miao, S., Oleson, K., Ooka, R., Pigeon, G., Porson, A., Ryu, Y., Salamanca, F., Steeneveld, G. J., and Tombrou, M.: Initial results from Phase 2 of the international urban energy balance model comparison, International Journal of Climatology, 272, 244–272, https://doi.org/10.1002/joc.2227, 2011.

Guan, D., Zhang, Y., and Zhu, T.: A wind-tunnel study of windbreak drag, Agricultural and Forest Meteorology, 118, 75–84, https://doi.org/10.1016/S0168-1923(03)00069-8, 2003.

Guan, D.-x., Zhu, T.-y., and Han, S.-j.: Wind tunnel experiment of drag of isolated tree models in surface boundary layer, Journal of Forestry Research, 11, 156–160, https://doi.org/10.1007/bf02855516, 2000.

Haghighi, E., Shahraeeni, E., Lehmann, P., and Or, D.: Evaporation rates across a convective air boundary layer are dominated by diffusion, Water Resour. Res., 49, 1602–1610, doi:10.1002/wrcr.20166, 2013.

Harman, I. A. N. N.: Radiative exchange in an urban street canyon, Boundary-Layer Meteorology, 110, 301–316, 2003.

Harshan, S., Roth, M., Velasco, E., and Demuzere, M.: Evaluation of an urban land surface scheme over a tropical suburban neighborhood, Theoretical and Applied Climatology, pp. 1–20, https://doi.org/10.1007/s00704-017-2221-7, 2017.

Hillel, D.: Environmental Soil Physics: Fundamentals, Applications, and Environmental Considerations, Academic Press, London, UK, 1998.

Hoff, S. J. and Janni, K. a.: Monte Carlo Technique for the Determination of Thermal Radiation Shape Factors, American Society of Agricultural Engineers, 32, 1023–1028, https://doi.org/10.13031/2013.31108, 1989.

Hu, Z. and Islam, S.: Prediction of ground surface temperature and soil moisture content by the force restore-method, Water Resources Research, 31, 2531–2539, 1995.

1385    Ivanov, V. Y., Bras, R. L., and Vivoni, E. R.: Vegetation-hydrology dynamics in complex terrain of semiarid areas: 1. A mechanistic approach to modeling dynamic feedbacks, Water Resources Research, 44, doi:10.1029/2006WR005588, 2008a.

Ivanov, V. Y., Bras, R. L., and Vivoni, E. R.: Vegetation-hydrology dynamics in complex terrain of semiarid areas: 1. A mechanistic approach to modeling dynamic feedbacks, Water Resources Research, 44, doi:10.1029/2006WR005588, 2008b.

Jones, H. G.: Plants and Microclimate, Cambridge University Press, New York, 1983.

1390    Kattge, J. and Knorr, W.: Temperature acclimation in a biochemical model of photosynthesis: a reanalysis of data from 36 species, Plant, Cell and Environment, 30, 1176–1190, doi: 10.1111/j.1365-3040.2007.01690.x, 2007.

Katul, G. G., Leuning, R., and Oren, R.: Relationship between plant hydraulic and biochemical properties derived from a steady-state coupled water and carbon transport model, Plant, Cell and Environment, 26, 339–350, 2003.

Kent, C. W., Grimmond, S., and Gatey, D.: Aerodynamic roughness parameters in cities: Inclusion of vegetation, Journal of Wind Engineering

1395    and Industrial Aerodynamics, 169, 168–176, https://doi.org/10.1016/j.jweia.2017.07.016, http://dx.doi.org/10.1016/j.jweia.2017.07.016, 2017.

Kirkham, M. B.: Principles of soil and plant water relations, Elsevier Academic Press, 2005.

Kondo, J. and Ishida, S.: Sensible Heat Flux from the Earth's Surface under Natural Convective Conditions, Journal of the Atmospheric Sciences, 54, 498–509, 1997.

1400    Kot, S. C. and Song, Y.: An improvement of the Louis scheme for the surface layer in an atmopsheric modelling system, Boundary-Layer Meteorology, 88, 239–254, 1998.

Kusaka, H., Kondo, H., and Kikegawa, Y.: A simple single-layer urban canopy model for atmospheric models: Comparison with multi-layer and slab models, Boundary-Layer Meteorology, 101, 329–358, 2001.

Lee, H. S., Matthews, C. J., Braddock, R. D., Sander, G. C., and Gandola, F.: A MATLAB method of lines template for transport equations,

1405    Environmental Modelling & Software, 19, 603–614, doi:10.1016/j.envsoft.2003.08.017, 2004.

Leuning, R.: Modelling stomatal behaviour and photosynthesis of Eucalyptus grandis, Australian Journal of Plant Physiology, 17, 159–175, 1990.

Leuning, R.: A critical appraisal of a combined stomatal- photosynthesis model for C3 plants, Plant, Cell and Environment, 18, 357–364, 1995.

1410    Leuning, R., Kelliher, F. M., Pury, D. G. G., and Schulze, E.-D.: Leaf nitrogen, photosynthesis, conductance and transpiration: Scaling from leaves to canopies, Plant, Cell and Environment, pp. 1183–1200, 1995.

Liu, X., Li, X.-x., Harshan, S., Roth, M., and Velasco, E.: Evaluation of an urban canopy model in a tropical city : the role of tree evapotranspiration Evaluation of an urban canopy model in a tropical city : the role of tree evapotranspiration, Environmental Research Letters, 12, 2017.

1415    Maass, J., Vose, J., Swank, W., and Martínez-Yrízar, A.: Seasonal changes of leaf area index (LAI) in a tropical deciduous forest in west Mexico, Forest Ecology and Management, 74, 171–180, http://www.sciencedirect.com/science/article/pii/037811279403485F, 1995.

Macdonald, R. W., Griffiths, R. F., and Hall, D. J.: An improved method for the estimation of surface roughness of obstacle arrays, Atmospheric Environment, 32, 1857–1864, 1998.

Mahat, V., Tarboton, D. G., and Molotch, N. P.: Testing above- and below-canopy representations of turbulent fluxes in an energy balance

1420    snowmelt model, Water Resources Research, 49, 1107–1122, doi:10.1002/wrcr.20073, 2013.

Mahfouf, J.-F. and Jacquemin, B.: A study of rainfall interception using a land surface parameterization for mesoscale meteorological models, Journal of Applied Meteorology, 28, 1282–1302, 1989.

Mascart, P., Noilhan, J., and Giordani, H.: A Modified Parameterization of Flux-Profile Relationships in the Surface Layer using Different Roughness LengthValues for Heat and Momentum, Boundary-Layer Meteorology, 72, 331–334, 1995.

Masson, V.: A physically-based scheme for the urban energy budget in atmospheric models, Boundary-Layer Meteorology, 94, 357–397, 2000.

Meili, N. and Fatichi, S.: Urban Tethys-Chloris (UT&C v1.0), https://doi.org/10.5281/zenodo.3377122, 2019.

Monin, A. S. and Obukhov, A. M.: Dimensionless Characteristics of Turbulence in the Surface Layer of the Atmosphere, Trudy Geofiz. Inst. Akad. Nauk. SSSR, 24, 163–187, (In Russian), 1954.

Monteith, J. L.: Principles of Environmental Physics, Edward Arnold, London, 1973.

Mualem, Y.: A new model for predicting the hydraulic conductivity of unsaturated porous media, Water Resour. Res, 12, 513–522, doi:10.1029/WR012i003p00513, 1976.

Newman, E. I.: Resistance to water flow in soil and plant. I. Soil resistance in relation to amounts of root: theoretical estimate, J. Appl. Ecol., 6, 1–12, 1969.

Nice, K. A., Coutts, A. M., and Tapper, N. J.: Development of the VTUF-3D v1.0 urban micro-climate model to support assessment of urban vegetation influences on human thermal comfort, Urban Climate, pp. 1–25, https://doi.org/10.1016/j.uclim.2017.12.008, http://linkinghub. elsevier.com/retrieve/pii/S2212095517301141, 2018.

Nobel, P. S.: Physicochemical and Environmental Plant Physiology, Elsevier Academic Press, 2009.

Noilhan, J. and Mafhouf, J.-F.: The ISBA land surface parameterisation scheme, Global and Planetary Change, 13, 145–159, 1996.

Noilhan, J. and Planton, S.: A simple parameterization of land surface processes for meteorological models, Monthly Weather Review, 117, 536–549, 1989.

Núñez, C. M., Varas, E. A., and Meza, F. J.: Modelling soil heat flux, Theoretical Applied Climatology, 100, 251–260, doi:10.1007/s00704-009-0185-y, 2010.

Oleson, K. W., Dai, Y., Bonan, G., Bosilovich, M., Dickinson, R., Dirmeyer, P., Hoffman, F., Houser, P., Levis, S., Niu, G. Y., Thornton, P., Vertenstein, M., Yang, Z. L., and Zeng, X.: Technical Description of the Community Land Model (CLM), Tech. Rep. NCAR/TN-461+STR, Natl. Cent. for Atmos. Res., Boulder, Colorado, 2004.

Oleson, K. W., Bonan, G. B., Feddema, J., Vertenstein, M., and Grimmond, C. S. B.: An Urban Parameterization for a Global Climate Model . Part I : Formulation and, Journal of Applied Meteorology and Climatology, 47, 1038–1060, https://doi.org/10.1175/2007JAMC1597.1, 2007.

Oleson, K. W., Lawrence, D. M., Bonan, G. B., Drewniak, B., Huang, M., Kowen, C. D., Levis, S., Li, F., Riley, W. J., Subin, Z. M., Swenson, S. C., and Thornton, P. E.: Technical Description of version 4.5 of the Community Land Model (CLM), Tech. Rep. NCAR/TN-503+STR, Natl. Cent. for Atmos. Res., Boulder, Colorado, 2013.

Park, S.-h. and Lee, S.-u.: A Vegetated Urban Canopy Model for Meteorological and Environmental Modelling, Boundary-Layer Meteorology, 126, 73–102, https://doi.org/10.1007/s10546-007-9221-6, 2008.

Philip, J. R.: Evaporation, and moisture and heat fields in the soil, Journal of Meteorology, 14, 354–366, 1957.

Ramírez, J. A. and Senarath, S. U. S.: A Statistical-Dynamical Parameterization of Interception and Land Surface-Atmosphere Interactions, Journal of Climate, 13, 4050–4063, 2000.

Richards, L. A.: Capillary conduction of liquids through porous mediums, Physics, 1, 318–333, 1931.

Roth, M., Jansson, C., and Velasco, E.: Multi-year energy balance and carbon dioxide fluxes over a residential neighbourhood in a tropical city, International Journal of Climatology, https://doi.org/10.1002/joc.4873, 2016.

Rowley, F. B. and Eckley, W. A.: Surface coefficients as affected by wind direction, ASHREA Trans., 39, 33–46, 1932.

Rowley, F. B., Algren, A. B., and Blackshaw, J.: Surface conductance as affected by air velocity, temperature and character of surface, ASHREA Trans., 36, 429–446, 1930.

Rutter, A. J., Kershaw, K. A., Robins, P. C., and Morton, A. J.: A predictive model of rainfall interception in forests. 1. Derivation of the model from observation in a plantation of Corsican pine, Agricultural Meteorology, 9, 367–384, 1971.

Rutter, A. J., Morton, A. J., and Robins, P. C.: A predictive model of rainfall interception in forests. 2. Generalization of model and comparison with observations in some coniferous and hardwood stands, The Journal of Applied Ecology, 12, 367–380, 1975.

Ryu, Y.-H., Baik, J.-J., and Lee, S.-H.: A New Single-Layer Urban Canopy Model for Use in Mesoscale Atmospheric Models, Journal of Applied Meteorology and Climatology, 50, 1773–1794, https://doi.org/10.1175/2011JAMC2665.1, 2011.

Ryu, Y.-H., Bou-Zeid, E., Wang, Z.-H., and Smith, J. A.: Realistic Representation of Trees in an Urban Canopy Model, Boundary-Layer Meteorology, 159, 193–220, https://doi.org/10.1007/s10546-015-0120-y, 2016.

Sack, L. and Holbrook, N. M.: Leaf hydraulics, Annual Review of Plant Biology, 57, 361–381, 2006.

Sailor, D. J. and Lu, L.: A top-down methodology for developing diurnal and seasonal anthropogenic heating profiles for urban areas, Atmospheric Environment, 38, 2737–2748, https://doi.org/10.1016/j.atmosenv.2004.01.034, 2004.

Sailor, D. J., Georgescu, M., Milne, J. M., and Hart, M. A.: Development of a national anthropogenic heating database with an extrapolation for international cities, Atmospheric Environment, 118, 7–18, https://doi.org/10.1016/j.atmosenv.2015.07.016, http://dx.doi.org/10.1016/j.atmosenv.2015.07.016, 2015.

Saxton, K. E. and Rawls, W. J.: Soil Water Characteristic Estimates by Texture and Organic Matter for Hydrologic Solutions, Soil Science Society of America Journal, 70, 1569–1578, doi:10.2136/sssaj2005.0117, 2006.

Schenk, H. J. and Jackson, R. B.: The global biogeography of roots, Ecological Monography, 72, 311–328, 2002.

Sellers, P. J., Los, S. O., Tucker, C. J., Justice, C. O., Dazlich, D. A., Collatz, G. J., and Randall, D. A.: A revised land surface parameterization (SiB2) for atmospheric GCMs. 2. The generation of global fields of terrestrial biophysical parameters from satellite data, Journal of Climate, 9, 706–737, 1996a.

Sellers, P. J., Randall, D. A., Collatz, G. J., Berry, J. A., Field, C. B., Dazlich, D. A., Zhang, C., Collelo, G. D., and Bounoua, L.: A revised land surface parameterization (SiB2) for atmospheric GCMs. 1. Model formulation, Journal of Climate, 9, 674–705, 1996b.

Sellers, P. J., Dickinson, R. E., Randall, D. A., Betts, A. K., Hall, F. G., Berry, J. A., Collatz, G. J., Denning, A. S., Mooney, H. A., Nobre, C. A., Sato, N., Field, C. B., and Henderson-Sellers, A.: Modeling the Exchanges of Energy, Water and Carbon Between Continents and the Atmosphere, Science, 275, 502–509, 1997.

Shahraeeni, E., Lehmann, P., and Or, D.: Coupling of evaporative fluxes from drying porous surfaces with air boundary layer-Characteristics of evaporation from discrete pores, Water Resour. Res., 48, W09 525, doi:10.1029/2012WR011857, 2012.

Shuttleworth, W. J.: Terrestrial hydrometeorology, John Wiley & Sons, Ltd, 2012.

Shuttleworth, W. J. and Gurney, R. J.: The theoretical relationship between foliage temperature and canopy resistance in sparse crops, Quarterly Journal of the Royal Meteorological Society, 116, 497–519, 1990.

Singsaas, E. L., Ort, D. R., and Delucia, E. H.: Variation in measured values of photosynthetic quantum yield in ecophysiological studies, Oecologia, 128, 15–23, 2001.

Song, J. and Wang, Z. H.: Interfacing the Urban Land–Atmosphere System Through Coupled Urban Canopy and Atmospheric Models, Boundary-Layer Meteorology, 154, 427–448, https://doi.org/10.1007/s10546-014-9980-9, 2015.

Sparrow, E. and Cess, R. D.: Radiation Heat Transfer, Chapters 3-4, Appendices A & B, Thermal Science Series, Brooks/Cole, 1970.

Sperry, J. S., Stiller, V., and Hacke, U. G.: Xylem Hydraulics and the Soil-Plant-Atmosphere Continuum: Opportunities and Unresolved Issues, Agronomy Journal, 95, 1362–1370, 2003.

Su, Z.: The Surface Energy Balance System (SEBS) for estimation of turbulent heat fluxes, Hydrology and Earth System Sciences, 6, 85–99, 2002.

Tuzet, A., Perrier, A., and Leuning, R.: A coupled model of stomatal conductance, photosynthesis and transpiration, Plant, Cell and Environment, 26, 1097–1116, 2003.

van den Hurk, B. J. J. M. and Holtslag, A. A. M.: On the bulk parameterization of surface fluxes for various conditions and parameter ranges, Boundary-Layer Meteorology, 82, 119–134, 1997.

van Genuchten, M. T.: A closed-form equation for predicting the hydraulic conductivity of unsaturated soils, Soil Science Society of America Journal, 44, 892–898, 1980.

Velasco, E., Roth, M., Tan, S. H., Quak, M., Nabarro, S. D. A., and Norford, L.: The role of vegetation in the CO 2 flux from a tropical urban neighbourhood, Atmospheric Chemistry and Physics, 13, 10 185–10 202, https://doi.org/10.5194/acp-13-10185-2013, 2013.

Verbeeck, H., Steppe, K., Nadezhdina, N., DeBeeck, M. O., , Deckmyn, G., Meiresonne, L., Lemeur, R., Čermák, J., Ceulemans, R., and Janssens, I. A.: Stored water use and transpiration in Scots pine: a modeling analysis with ANAFORE, Tree Physiology, 27, 1671–1685, 2007.

Vico, G. and Porporato, A.: Modelling C3 and C4 photosynthesis under water-stressed conditions, Plant Soil, 313, 187–203, doi:10.1007/s11104-008-9691-4, 2008.

Villar, R., Held, A. A., and Merino, J.: Dark leaf respiration in light and darkness of an evergreen and a deciduous plant species, Plant Physiology, 107, 421–427, 1995.

Viterbo, P. and Beljaars, A. C. M.: An improved land surface parameterization scheme in the ECMWF model and its validation, Journal of Climate, 8, 2716–2748, 1995.

Volo, T. J., Vivoni, E. R., Martin, C. A., Earl, S., and Ruddell, B. L.: Modelling soil moisture, water partitioning, and plant water stress under irrigated conditions in desert Urban areas, Ecohydrology, 7, 1297–1313, https://doi.org/10.1002/eco.1457, 2014.

von Caemmerer, S. and Farquhar, G. D.: Some relationships between the biochemistry of photosynthesis and the gas exchange of leaves, Planta, 153, 376–387, 1981.

Wang, Y.-P. and Leuning, R.: A two-leaf model for canopy conductance, photosynthesis and portioning of available energy I: Model description and comparison with a multi-layered model, Agricultural and Forest Meteorology, 91, 89–111, 1998.

Wang, Z.-h.: Geometric effect of radiative heat exchange in concave structure with application to heating of steel I-sections in fire, International Journal of Heat and Mass Transfer, 53, 997–1003, https://doi.org/10.1016/j.ijheatmasstransfer.2009.11.013, http://dx.doi.org/10.1016/j.ijheatmasstransfer.2009.11.013, 2010.

Wang, Z.-h.: Monte Carlo simulations of radiative heat exchange in a street canyon with trees, SOLAR ENERGY, 110, 704–713, https://doi.org/10.1016/j.solener.2014.10.012, http://dx.doi.org/10.1016/j.solener.2014.10.012, 2014.

Wang, Z.-h., Bou-Zeid, E., and Smith, J. A.: A Spatially-Analytical Scheme for Surface Temperatures and Conductive Heat Fluxes in Urban Canopy Models, Boundary-Layer Meteorology, 138, 171–193, https://doi.org/10.1007/s10546-010-9552-6, 2011.

Wang, Z.-h., Bou-zeid, E., and Smith, J. A.: A coupled energy transport and hydrological model for urban canopies evaluated using a wireless sensor network, Quarterly Journal of the Royal Meteorological Society, 139, 1643–1657, https://doi.org/10.1002/qj.2032, 2013.

Warren, C. R.: Why does photosynthesis decrease with needle age in Pinus pinaster?, Trees, 20, 157–164, doi: 10.1007/s00468-005-0021-7, 2006.

Wieringa, J.: Representative roughness parameters for homogeneous terrain, Boundary-Layer Meteorology, 63, 323–363, 1993.

Yang, J., Wang, Z. H., Chen, F., Miao, S., Tewari, M., Voogt, J. A., and Myint, S.: Enhancing Hydrologic Modelling in the Coupled Weather Research and Forecasting–Urban Modelling System, Boundary-Layer Meteorology, 155, 87–109, https://doi.org/10.1007/s10546-014-9991-6, 2015.

1540